University of Alberta

Application of continuous wavelet analysis to hyperspectral data for the characterization of vegetation

by

Tao Cheng

A thesis submitted to the Faculty of Graduate Studies and Research
in partial fulfillment of the requirements for the degree of

Doctor of Philosophy

Department of Earth and Atmospheric Sciences

Fall 2010
Edmonton, Alberta

Examining Committee

Benoit Rivard, Earth and Atmospheric Sciences

Arturo Sánchez-Azofeifa, Earth and Atmospheric Sciences

Arie Croitoru, Earth and Atmospheric Sciences

Herb Yang, Computing Science

Stéphane Jacquemoud, Space and Planetary Geophysics, Université Paris Diderot

ABSTRACT

This thesis explores the application of continuous wavelet analysis (CWA) to hyperspectral data for the characterization of vegetation at the leaf level. The first study dealt with the spectral detection of green attack damage (pre-visual stress) due to mountain pine beetle (*Dendroctonus ponderosae* Hopkins) infestation that occurs on lodgepole pines at an early stage, in contrast to considerable research on the remote detection of red attack damage. A new methodology was developed to separate healthy pine trees from beetle infested trees, based on the CWA of hyperspectral measurements for pine needles. This pilot study showed that a decline in water content occurred for the pine trees at the green attack stage and the spectral response to that physiological change could be detected using a few features in the wavelet domain. The second topic addressed the application of CWA to the determination of leaf water content from remotely sensed reflectance. Unlike most previous studies involving a limited number of species, this study examined a wide range of tropical forest species with the aim to determine reliable and effective wavelet features (coefficients) sensitive to changes in leaf gravimetric water content (GWC). Of those significant wavelet features extracted, some related to the absorption of leaf water while more related to the absorption of dry matter. An evaluation of the wavelet features as compared with published water indices indicated their great potential for the estimation of leaf GWC. Lastly, the third study tested the wavelet-based methodology developed in the second study using a leaf spectral database generated by the PROSPECT radiative transfer model. The ability of PROSPECT

to simulate leaf reflectance measured for the tropical data set was first assessed. Then the performance of the aforementioned methodology was evaluated in terms of the consistency of wavelet features extracted across data sets. This work demonstrated the effectiveness of the wavelet-based methodology and the robustness and reliability of recurrent wavelet features for the estimation of leaf GWC across a wide range of species.

ACKNOWLEDGEMENTS

I am very grateful to my supervisor Dr. Benoit Rivard who provides continuous support and plenty of critical inputs to the work during the course of my PhD degree. I also appreciate the insightful discussions through which he inspires my thinking but never interfere with my decision on what to do next. He always encourages me to explore my own research interests and helps to keep me on the right track. I enjoy being a part of his research team that is highly experienced in hyperspectral data analysis.

I would like to thank Dr. Arturo Sánchez-Azofeifa who inspires me to explore science problems at University of Alberta and to bring my research into the context of ecology and environmental science through the interesting group meetings. I am thankful to him along with Dr. Rivard for having me involved with the mountain pine beetle project from which I gained experience on field work and saw how remote sensing could be used to solve a practical problem. He also supported my research by providing the field datasets used in Chapter Three and Chapter Four.

Among the professors with CEOS, I am grateful to Dr. Arie Croitoru and Dr. John Gamon for their useful comments on my candidacy exam. I really enjoyed Dr. Croitoru's EAS522 course that drove me to get started with programming for image processing in Matlab. Dr. Gamon encouraged me to learn more about plant physiology. A few people at the university who generously helped to read through my thesis and provided useful comments on language editing are Dr. Paula Brook (Chapter Three), Dr. Patricia Rempel (Chapters One & Five) and Donnette Thayer (Chapter Three).

Thanks to a few people for their help with the field work. Mei Mei Chong was very helpful for coordinating several field campaigns and assisting in data collection in the field. She also trained me to measure chlorophyll in the laboratory. Dr. Janusz Zwiazek, along with Dr. Monica Calvo-Polanco who co-authored the paper version of Chapter Two, helped me with designing the girdling

experiment and collecting girdled samples. I am also thankful to Ms. Alena Prolova for field work assistance and Ms. Nicola Laberge for assistance with field and laboratory data collection.

I am thankful to Drs. Jilu Feng and Derek Rogge for their discussions about hyperspectral data processing and IDL coding, especially to Dr. Feng for sharing the knowledge about wavelet analysis. Ms. Yingduan Huang and her husband gave me a lot of help with living in Edmonton. I thank this couple for sharing with me so many overseas living experiences. Thanks to other members in EOSL for keeping the lab a good academic environment.

Special thanks to my wife, Ms. Qiqi Qu for experiencing the student life with me and making it so interesting. Her love is great support to my PhD studies. Thank you to my parents who always encourage me to pursue my interest and to make decisions on my own. Thank you to my brothers with whom I had so much fun in the countryside. We are supportive to each other all the time. Thanks should also be extended to my parents-in-law for their generous support. I cannot imagine how far I could go on the academic path without the constant support from all family members.

Lastly, I would like to acknowledge the funding agencies including Alberta Sustainable Resource Development (Chapter Two), the National Science & Engineering Research Council of Canada (NSERC) through the Discovery Grant (Chapter Three), and the National Science Foundation (Chapter Three). Part of this work (Chapters Three and Four) was funded with the support of the Inter American Institute for Global Change Research via their Collaborative Network Program, specifically Tropi-Dry (CRN2-021) via a grant from the U.S. National Science Foundation (GEO-0452325). The J Gordin Kaplan Graduate Student Award is acknowledged for supporting the travel to IGARSS 2010 in Honolulu, Hawaii.

TABLE OF CONTENTS

LIST OF TABLES

LIST OF FIGURES

LIST OF SYMBOLS AND ABBREVIATIONS

AIC	Akaike's information criterion
C_{a+b}	Leaf chlorophyll $a+b$ concentration
C_m	Leaf dry matter content
C_w	Leaf equivalent water thickness
CWA	Continuous wavelet analysis
CWT	Continuous wavelet transform
DMC	Dry matter content
DMSO	Dimethyl sulphoxide
DOG	Derivative of Gaussian
DW	Dry weight
DWT	Discrete wavelet transform
EWT	Equivalent water thickness
FS	Fort Sherman
FW	Fresh weight
GA-PLS	Genetic algorithms partial least squares
GWC	Gravimetric water content
LAI	Leaf area index
LOPEX	Leaf optical properties experiment
LWC_D	Leaf water content as percent of dry mass
LWC_F	Leaf water content as percent of fresh mass
MPB	Mountain pine beetle
MSI	Moisture stress index
N	Leaf structure parameter
NDWI	Normalized difference water index
NIR	Near infrared
PLS	Partial least squares

PNM	Parque Natural Metropolitano
PROSPECT	A model of leaf optical properties spectra
RMSE	Root mean square error
RWC	Relative water content
SMLR	Stepwise multiple linear regression
STRI	Smithsonian Tropical Research Institute
SWIR	Shortwave infrared
VIS	Visible
WI	Water index

CHAPTER 1 – INTRODUCTION

1.1. Background

As a key component of the earth system, vegetation influences the energy and mass exchange with the atmosphere and soil, particularly the cycling of carbon, water and nutrient in terrestrial ecosystems. Remote sensing, precisely imaging spectroscopy, offers an effective way to detect the spatial variations in chemical constituents of vegetation canopies such as pigment, water, nitrogen and carbon constituents at broad spatial scales and their relations with biodiversity and the Earth's climate system (Asner & Vitousek, 2005; Ollinger et al., 2008; Ustin et al., 2004). Over the last few decades, imaging spectrometer data acquired from aircraft or spacecraft have become increasingly available for developing remote sensing techniques to estimate canopy chemistry in various forest ecosystems. (Coops et al., 2003; Martin & Aber, 1997; Peterson et al., 1988; Townsend et al., 2003; Wessman et al., 1988). Following these successful estimations at the landscape level, the spatial distribution of ecosystem chemical composition over large portions of the globe may be revealed in the near future by a few new hyperspectral satellite missions such as HyspIRI and EnMAP (Kokaly et al., 2009).

Compared to imaging spectrometers that remotely measure the reflectance of plant canopies in hundreds of narrow and contiguous spectral bands (Goetz et al., 1985), laboratory spectrometers are able to measure the reflectance of leaves in thousands of spectral bands in a laboratory setting. The reflectance measurements from the former are more complex than those from the latter due to the impact of such factors as canopy structural variation and viewing geometry (Clark et al., 2005; Roberts et al., 2004). Therefore, the application of imaging spectroscopy to plant canopies could benefit from the advancement of laboratory research in which leaf chemical properties are more accurately estimated from higher quality spectroscopic data measured in more controlled conditions.

Previous laboratory studies on the determination of leaf chemistry have contributed significantly to our understanding of leaf spectral responses associated with changes in chemical concentrations (Asner & Martin, 2008; Curran, 1989; Curran et al., 2001; Kokaly, 2001; Kokaly & Clark, 1999). In addition, quantitative chemical information derived from leaf reflectance is of importance for the detection of vegetation stresses caused by the insufficient availability of such foliar chemicals as water, nitrogen, and total chlorophyll in plant physiological processes (Pu et al., 2008; Strachan et al., 2002; Zarco-Tejada et al., 2002).

The reflectance spectra for different types of vegetation (400-2500 nm) are similar in shape because vegetation reflectance is mainly influenced by the spectral absorptions of common chemical components weighted by their concentrations (Curran, 1989; Kokaly & Clark, 1999). Due to the spectral absorptions by multiple chemicals, it is difficult to uniquely relate the reflectance at a wavelength to the concentration of a single chemical constituent in leaves. One solution to that problem is to utilize more than one wavelength to enhance the absorption features being examined and suppress the spectral variability caused by factors irrelevant to leaf chemistry (e.g., illumination variation).

In order to resolve the absorption of a leaf chemical constituent with multiple wavelengths, many studies use stepwise multiple linear regression (SMLR) to build calibration equations by selecting a small number of wavelengths that separately correlate with concentrations of each of such constituents as water, nitrogen, lignin, cellulose (Card et al., 1988; Curran et al., 1992; Gross et al., 1996). Two spectral preprocessing techniques have often been applied prior to the regression: derivative analysis and continuum removal. Derivative analysis, performed by means of applying the first or second derivative to reflectance spectra, has been widely used to emphasize subtle absorption features of leaf chemicals due to its lower sensitivity to illumination intensity and leaf internal structural variability (Curran et al., 1992; Danson et al., 1992; Johnson & Billow, 1996; Peñuelas et al., 1994). This approach does not provide a

flexible way to extract meaningful information on absorption features of various widths at a time (Bruce & Li, 2001). In addition, the sensitivity of derivative spectra to noise in reflectance spectra poses a problem for the effectiveness of second- or higher-order derivatives. Continuum removal is a spectral analysis tool specifically designed to isolate absorption features of interest from the continuum of reflectance spectra. The use of continuum-removed spectra enables us to build direct relationships between concentrations of chemical constituents and absorption characteristics (Curran et al., 2001; Kokaly, 2001; Kokaly & Clark, 1999). However, the shape of continuum-removed spectra is non-deterministic because it is subject to the analyst's definition of the absorption region of interest and to the choice of an algorithm to approximate the continuum (Rivard et al., 2008).

To avoid the direct use of reflectance or derivative reflectance, one can use spectral indices that are band ratios of spectral reflectance at a small number of wavelengths. However, spectral indices are often empirically developed through correlation between chemical concentrations and leaf spectral properties for a few species that are close in geographic location or taxonomy (Blackburn, 1998; Eitel et al., 2006; Peñuelas et al., 1997). Those empirical relationships tend to become weaker when spectral indices are applied to a data set that exhibits much diversity in species composition and substantial variation in leaf spectral properties. Thus, further investigations are required to develop more robust relationships to reduce the spectral variation irrespective of leaf chemical properties by incorporating more informative wavelengths (Datt, 1999a; Datt, 1999b; le Maire et al., 2004; Sims & Gamon, 2002). Recently, continuous wavelet analysis (CWA) has emerged as a promising tool in laboratory spectroscopy for deriving chemical properties from leaf reflectance spectra (Blackburn & Ferwerda, 2008; Ferwerda & Jones, 2006). CWA enables us to decompose a reflectance spectrum into a number of scale components each of which is directly comparable to a reflectance spectrum and therefore readily linked to the absorption features. The multi-scale representation of a reflectance spectrum facilitates the characterization of absorption features of different widths at various

scales. These characteristics of CWA offer a valuable opportunity to gain new insights into the spectral responses associated with changes in leaf chemical constituents.

1.2. Thesis goal and objectives

The main goal of this thesis is to investigate the application of CWA to the characterization of vegetation using hyperspectral data. The objectives are: 1) to develop methodologies based on continuous wavelet analysis of reflectance spectra for two specific applications: the early detection of beetle attack damage and the estimation of leaf water content across a variety of tropical species, and 2) to evaluate the generality of the methodology developed for the estimation of leaf water content using a modeling approach. Specifically, the first objective addresses how to use spectral signatures of pine needles to detect the insufficiency of water and chlorophyll as a physiological response to beetle infestation, and what spectral features are the most sensitive to changes in leaf water content. The second objective addresses the use of a simulated data set generated by a leaf radiative transfer model (PROSPECT) to test the wavelet-based methodology developed using a laboratory-measured data set. This research focuses on understanding the fundamentals of leaf-level spectral variations in relation to changes in concentrations of leaf water and chlorophyll through the use of CWA. It is therefore expected to be extended to canopy or landscape level in the future. Those methodologies, although specifically developed for the early detection of beetle attack damage and estimation of leaf water content in this thesis, should also assist in the stress detection and in the retrieval of any leaf biochemical constituent in other vegetation studies that use reflectance spectroscopy as a main tool.

1.3. Thesis outline

This thesis is based on the compilation of three standalone papers published or submitted to peer-reviewed journals. Following the introduction, the three chapters deal with the application of continuous wavelet analysis to reflectance spectra coupled with leaf trait data (total chlorophyll and water) for characterizing vegetation conditions.

The main goal of Chapter 2 is to search for spectral signals that relate to the early detection of the effect of mountain pine beetle (*Dendroctonus ponderosae* Hopkins) infestation on the spectral response of lodgepole pines. To detect the pre-visual beetle attack damage, two research questions were addressed: 1) do infested trees undergo water stress, chlorophyll stress, or both? 2) if any of these stresses occurs, is the stress detectable using spectral reflectance? Several field campaigns were conducted to collect measurements of needle spectral reflectance, total chlorophyll concentration, and water content from healthy pine trees and infested trees that were at the green attack stage. Statistical analysis was performed on chlorophyll and water data to achieve a good understanding of the physiological mechanism of the green attack damage and provide guidance for subsequent spectral analysis. To detect the potential stress in the spectral domain, a novel method was developed to spectrally distinguish healthy trees from infested trees using CWA of reflectance spectra. This study, *Continuous wavelet analysis for the detection of green attack damage due to mountain pine beetle infestation* (Cheng et al., 2010), was published in *Remote Sensing of Environment, 114*, 899-910.

As Chapter 2 concludes that the water content of needles is a physiological indicator of the green attack damage, Chapter 3 focuses on determining the most reliable spectral information that relates to the water content in a leaf. Measurements of leaf reflectance and gravimetric water content (GWC) for 47 tropical forest species in Panama were collected from 265 leaf samples to represent the wide ranges of water content and spectral variability (Castro et al., 2006; Sánchez-Azofeifa et al., 2009). Using CWA, an effective method was developed to determine the most significant wavelet features that are sensitive to

changes in leaf GWC across a variety of species. The performance of the wavelet features extracted using this new method was evaluated and compared with that of common spectral indices for the estimation of leaf GWC. In addition, the significance of those wavelet features was interpreted with reference to absorption features in leaf reflectance spectra.

In Chapter 4, I test the wavelet-based methodology developed in Chapter 3 using the leaf reflectance spectra simulated by the PROSPECT radiative transfer model. Input parameters for simulations with PROSPECT were defined based on the measurements of the tropical leaf data set used in Chapter 3. Two experiments were conducted, each with different simulation conditions. One was designed for assessing the ability of PROSPECT to simulate the measured reflectance in the tropical leaf data set. The other was used to evaluate the performance of the wavelet-based methodology for the estimation of leaf GWC from simulated spectra. The wavelet features derived from the simulated spectra were compared with common water indices in terms of the predictive capabilities. More importantly, these wavelet features were compared to those from the measured spectra to determine the robust wavelet features sensitive to changes in leaf GWC across data sets. This research in conjunction with the study in Chapter 3 provides a new insight into explaining the spectral variations caused by changes in leaf GWC through the use of CWA.

Lastly, I close this thesis by summarizing the conclusions presented in the three chapters above and describing the directions of future research.

1.4. References

Asner, G. P., & Martin, R. E. (2008). Spectral and chemical analysis of tropical forests: Scaling from leaf to canopy levels. *Remote Sensing of Environment, 112*, 3958-3970.

Asner, G. P., & Vitousek, P. M. (2005). Remote analysis of biological invasion and biogeochemical change. *Proceedings of the National Academy of Sciences of the United States of America, 102*, 4383-4386.

Blackburn, G. A. (1998). Spectral indices for estimating photosynthetic pigment concentrations: A test using senescent tree leaves. *International Journal of Remote Sensing, 19*, 657-675.

Blackburn, G. A., & Ferwerda, J. G. (2008). Retrieval of chlorophyll concentration from leaf reflectance spectra using wavelet analysis. *Remote Sensing of Environment, 112*, 1614-1632.

Bruce, L. M., & Li, J. (2001). Wavelets for computationally efficient hyperspectral derivative analysis. *IEEE Transactions on Geoscience and Remote Sensing, 39*, 1540-1546.

Card, D. H., Peterson, D. L., Matson, P. A., & Aber, J. D. (1988). Prediction of leaf chemistry by the use of visible and near infrared reflectance spectroscopy. *Remote Sensing of Environment, 26*, 123-147.

Cheng, T., Rivard, B., Sánchez-Azofeifa, G. A., Feng, J. & Calvo-Polanco, M. (2010). Continuous wavelet analysis for the detection of green attack damage due to mountain pine beetle infestation. *Remote Sensing of Environment, 114*, 899-910.

Clark, M. L., Roberts, D. A., & Clark, D. B. (2005). Hyperspectral discrimination of tropical rain forest tree species at leaf to crown scales. *Remote Sensing of Environment, 96*, 375-398.

Coops, N. C., Smith, M. -L., Martin, M. E., & Ollinger, S. V. (2003). Prediction of eucalypt foliage nitrogen content from satellite-derived hyperspectral data. *IEEE Transactions on Geoscience and Remote Sensing, 41*, 1338-1346.

Curran, P. J. (1989). Remote sensing of foliar chemistry. *Remote Sensing of Environment, 30*, 271-278.

Curran, P. J., Dungan, J. L., Macler, B. A., Plummer, S. E., & Peterson, D. L. (1992). Reflectance spectroscopy of fresh whole leaves for the estimation of chemical concentration. *Remote Sensing of Environment, 39*, 153-166.

Curran, P. J., Dungan, J. L., & Peterson, D. L. (2001). Estimating the foliar biochemical concentration of leaves with reflectance spectrometry: Testing the Kokaly and Clark methodologies. *Remote Sensing of Environment, 76*, 349-359.

Danson, F. M., Steven, M. D., Malthus, T. J., & Clark, J. A. (1992). High-spectral resolution data for determining leaf water content. *International Journal of Remote Sensing, 13*, 461-470.

Datt, B. (1999a). Remote sensing of water content in eucalyptus leaves. *Australian Journal of Botany, 47*, 909-923.

Datt, B. (1999b). Visible/near infrared reflectance and chlorophyll content in eucalyptus leaves. *International Journal of Remote Sensing, 20*, 2741-2759.

Eitel, J. U. H., Gessler, P. E., Smith, A. M. S., & Robberecht, R. (2006). Suitability of existing and novel spectral indices to remotely detect water stress in populus spp. *Forest Ecology and Management, 229*, 170-182.

Ferwerda, J. G., & Jones, S. (2006). Continuous wavelet transformations for hyperspectral feature detection. *Proceedings of the 12th International Symposium on Spatial Data Handling*, 12-14 July, University of Vienna, Austria.

Goetz, A. F. H., Vane, G., Solomon, J. E., & Rock, B. N. (1985). Imaging spectrometry for earth remote sensing. *Science, 228*, 1147-1153.

Grossman, Y. L., Ustin, S. L., Jacquemoud, S., Sanderson, E. W., Schmuck, G., & Verdebout, J. (1996). Critique of stepwise multiple linear regression for the extraction of leaf biochemistry information from leaf reflectance data. *Remote Sensing of Environment, 56*, 182-193.

Johnson, L. F., & Billow, C. R. (1996). Spectrometric estimation of total nitrogen concentration in douglas-fir foliage. *International Journal of Remote Sensing, 17*, 489-500.

Kokaly, R. F. (2001). Investigating a physical basis for spectroscopic estimates of leaf nitrogen concentration. *Remote Sensing of Environment, 75*, 153-161.

Kokaly, R. F., Asner, G. P., Ollinger, S. V., Martin, M. E., & Wessman, C. A. (2009). Characterizing canopy biochemistry from imaging spectroscopy and its application to ecosystem studies. *Remote Sensing of Environment, 113*, S78-S91.

Kokaly, R. F., & Clark, R. N. (1999). Spectroscopic determination of leaf biochemistry using band-depth analysis of absorption features and stepwise multiple linear regression. *Remote Sensing of Environment, 67*, 267-287.

le Maire, G., François, C., & Dufrêne, E. (2004). Towards universal broad leaf chlorophyll indices using PROSPECT simulated database and hyperspectral reflectance measurements. *Remote Sensing of Environment, 89*, 1-28.

Martin, M. E., & Aber, J. D. (1997). High spectral resolution remote sensing of forest canopy lignin, nitrogen, and ecosystem processes. *Ecological Applications*, 431-443.

Ollinger, S. V., Richardson, A. D., Martin, M. E., Hollinger, D. Y., Frolking, S. E., Reich, P. B., Plorde, L. C., Katul, G. G., Munger, J. W., Oren, R., Smith, M. –L., Paw U, K. T., Bolstad, P. V., Cook, B. D., Day, M. C., Martin, T. A., Monson, R. K. & Schmid, H. P. (2008). Canopy nitrogen, carbon assimilation, and albedo in temperate and boreal forests: Functional relations and potential climate feedbacks. *Proceedings of the National Academy of Sciences of the United States of America, 105*, 19336-19341.

Penuelas, J., Gamon, J. A., Fredeen, A. L., Merino, J., & Field, C. B. (1994). Reflectance indices associated with physiological changes in nitrogen- and water-limited sunflower leaves. *Remote Sensing of Environment, 48*, 135-146.

Peñuelas, J., Piñol, J., Ogaya, R., & Filella, I. (1997). Estimation of plant water concentration by the reflectance water index WI (R900/R970). *International Journal of Remote Sensing, 18*, 2869-2875.

Peterson, D. L., Aber, J. D., Matson, P. A., Card, D. H., Swanberg, N., Wessman, C., Spanner, M. (1988). Remote sensing of forest canopy and leaf biochemical contents. *Remote Sensing of Environment, 24*, 85-108.

Pu, R., Kelly, M., Chen, Q., & Gong, P. (2008). Spectroscopic determination of health levels of coast live oak (*Quercus agrifolia*) leaves. *Geocarto International, 23*, 3-20.

Rivard, B., Feng, J., Gallie, A., & Sánchez-Azofeifa, A. (2008). Continuous wavelets for the improved use of spectral libraries and hyperspectral data. *Remote Sensing of Environment, 112*, 2850-2862.

Roberts, D. A., Ustin, S. L., Ogunjemiyo, S., Greenberg, J., Bobrowski, S. Z., Chen, J., & Hinckley, T. M. (2004). Spectral and structural measures of northwest forest vegetation at leaf to landscape scales. *Ecosystems, 7*, 545-562.

Sims, D. A., & Gamon, J. A. (2002). Relationships between leaf pigment content and spectral reflectance across a wide range of species, leaf structures and developmental stages. *Remote Sensing of Environment, 81,* 337-354.

Smith, M. L., Ollinger, S. V., Martin, M. E., Aber, J. D., Hallett, R. A., & Goodale, C. L. (2002). Direct estimation of aboveground forest productivity through hyperspectral remote sensing of canopy nitrogen. *Ecological Applications, 12*, 1286-1302.

Strachan, I. B., Pattey, E., & Boisvert, J. B. (2002). Impact of nitrogen and environmental conditions on corn as detected by hyperspectral reflectance. *Remote Sensing of Environment, 80*, 213-224.

Townsend, P. A., Foster, J. R., Chastain Jr., R. A., & Currie, W. S. (2003). Application of imaging spectroscopy to mapping canopy nitrogen in the forest of the central Appalachian mountains using hyperion and AVIRIS. *IEEE Transactions on Geoscience and Remote Sensing, 41,* 1347-1354.

Ustin, S. L., Roberts, D. A., Gamon, J. A., Asner, G. P., & Green, R. O. (2004). Using imaging spectroscopy to study ecosystem processes and properties. *Bioscience, 54*, 523-534.

Vogelmann, J. E., Rock, B. N., & Moss, D. M. (1993). Red edge spectral measurements from sugar maple leaves. *International Journal of Remote Sensing, 14*, 1563-1575.

Wessman, C. A., Aber, J. D., Peterson, D. L., & Melillo, J. M. (1988). Remote sensing of canopy chemistry and nitrogen cycling in temperate forest ecosystems. *Nature, 335*, 154-156.

Zarco-Tejada, P. J., Miller, J. R., Mohammed, G. H., Noland, T. L., & Sampson, P. H. (2002). Vegetation stress detection through chlorophyll a + b estimation and fluorescence effects on hyperspectral imagery. *Journal of Environmental Quality, 31*, 1433-1441.

CHAPTER 2 – CONTINUOUS WAVELET ANALYSIS FOR THE DETECTION OF GREEN ATTACK DAMAGE DUE TO MOUNTAIN PINE BEETLE INFESTATION[1]

2.1. Introduction

The mountain pine beetle (*Dendroctonus ponderosae* Hopkins) is a native insect of the pine forests of western Northern America, and significant outbreaks of its population periodically occur in these stands (Safranyik et al., 1974; Taylor et al., 2006). In Canada, the beetle population at epidemic levels has been primarily recorded in British Columbia where the cumulative area of beetle outbreak was 130,000 km^2 by the end of 2006 (Westfall, 2007). However, forest monitoring indicated an increasing presence of mountain pine beetle and a spread from west-central Alberta to southwestern and northwestern Alberta since 1992, consistent with the expansion of mountain pine beetle outbreak areas in British Columbia (Alberta Sustainable Resource Development, 2007). During great outbreaks, beetle populations are capable to cause mortality of mature trees over many thousands of hectares (Safranyik & Carroll, 2006). The beetle-killed trees have an environmental impact by reducing forest carbon uptake and increasing future emissions (Kurz et al. 2008)) but they also represent a large economic loss to the forest industry. Recent research demonstrated that the current outbreak of mountain pine beetle in western Canada even affected forest carbon dynamics over large areas and contributed significantly to global climate change (Kurz et al., 2008).

---

[1] A version of this paper has been published: Cheng, T., Rivard, B., Sánchez-Azofeifa, G. A., Feng, J. & Calvo-Polanco, M. (2010). Continuous wavelet analysis for the detection of green attack damage due to mountain pine beetle infestation. *Remote Sensing of Environment, 114*, 899-910. Reprinted with permission from Elsevier.

Author contributions: Dr. Rivard and Dr. Sánchez-Azofeifa helped design the whole study, discussed the results, and provided editing comments on the manuscript. Dr. Feng was partly involved with discussion about data processing using continuous wavelet analysis. Dr. Calvo-Polanco helped with site selection and data collection for the girdling experiment. I collected spectral measurements in the field, did water content and chlorophyll concentration measurements in the laboratory, wrote the codes for data processing, processed the data, interpreted the results, and composed the manuscript.

The principal hosts killed by mountain pine beetle in western Canada are mature pine trees of which the lodgepole pine (*Pinus contorta* Dougl. Ex Loud. Var *latifolia* Engelm.) is extensively studied (Safranyik & Carroll, 2006). The beetle usually starts attacking the healthy trees by colonizing the hosts during late July through mid August. The trees bear green foliage during the early stage of attack also referred to as green attack. Subsequently, the damage is transitioned to red attack with the crown fading to uniform yellow to red and to brown by late summer of the following year (Amman, 1982; Henigman et al., 1999).

To meet the information needs of the extent and damage level of the mountain pine beetle infestation, remotely sensed data have been extensively utilized over large areas (Wulder et al., 2006). In particular, a number of successful studies have focused on the detection of red attack damage using multispectral satellite imagery at a range of spatial resolutions (Coops et al., 2006a; Coops et al., 2006b; Franklin et al., 2003; Skakun et al., 2003; White et al., 2005; White et al., 2006). Franklin et al. (2003) used stratified Landsat TM imagery to identify red-attack stands from non-attack forest stands with an overall classification accuracy of 73%. White et al (2005) used IKONOS imagery to detect red attack at sites with different intensities of infestation. They obtained accuracies of 71% and 92% for stands that respectively contained 1-5% and 5-20% trees with red attack. Using QuickBird imagery, Coops et al (2006a) generated a ratio of red to green reflectance to distinguish red-attack and non-attacked pixels and found a significant relationship between the number of red attack pixels and red attacked crowns observed in the field (r^2=0.48, p<0.001, standard error=2.8 crowns). In this case the identification of red-attack crowns is viable because the spatial resolution of Ikonos (4m) and QuickBird (2.5m) multispectral imagery are consistent with the size of individual tree crowns. The spectral resolution of these data is however insufficient to capture the spectral response of trees to the biophysical phenomena (e.g., water stress) caused by beetle attack. White et al (2007) recently examined six moisture indices derived from EO-1 Hyperion hyperspectral imagery and established a significant relationship between the Moisture Stress Index and levels of red attack (r^2=0.51,

p=0.0001). Their study suggests that hyperspectral data may provide a means to detect the signals from red attacked stands with low densities of infestation.

Studies investigating the spectral detection of green attack are sparse in the literature. Using foliage reflectance data acquired from 360-1050 nm, Ahern (1988) determined that the most promising spectral bands for the detection of green attack were located near the green peak, red edge and near-infrared shoulder. A red-shift of the red edge position was also observed in the spectra of trees under green attack. Runesson (1991) investigated the detection of green attack based on in-situ spectroscopy and digital airborne data and found that the separation between healthy and attacked tree canopies was poor. In contrast to the previous study, the analysis of foliage reflectance spectra demonstrated a blue-shift of the red edge for attacked trees.

The studies by Ahern (1988) and Runesson (1991) paid particular attention to the examination of pigment-driven spectral variations in the visible and near infrared regions. Changes in leaf water content and ensuing changes in leaf spectral reflectance were not investigated or were undetected because spectral data beyond 1100nm were unavailable. Declines in sapwood moisture content resulting from beetle attack have been documented (Reid, 1961; Yamaoka et al., 1990) and consequently moisture stress may result in non-visual symptoms that are detectable with spectral data particularly if data are acquired between 1000-2500 nm where water absorption features in vegetation are well documented.

This study examines the spectral properties (350-2500 nm) and total chlorophyll and water content characteristics of needles obtained from infested and control (healthy) lodgepole pine trees to assess the detection of pre-visual symptoms. As a baseline, I also examine these properties for healthy trees and trees girdled to induce a water stress. The literature provides a number of spectral indices for the detection of pigment and water variability in leaves (Blackburn, 1998; Gamon et al., 1992; Gao, 1996; Hunt & Rock, 1989; Peñuelas et al., 1993, 1997; Rock et al., 1986; Sims & Gamon, 2002) but these employ only a limited number of spectral bands. Alternatively wavelet analysis has shown promise for the analysis of hyperspectral data (Blackburn, 2007; Blackburn & Ferwerda,

2008; Ferwerda & Jones, 2006; Kalacska et al., 2007; Koger et al., 2003; Pu & Gong, 2004; Rivard et al. 2008; Zhang et al., 2006). Wavelet analysis has the merit of decomposing the reflectance spectra into components of different scales (or frequencies) thus facilitating the detection of subtle signals. The aim of this study was to focus on the detection of green attack induced by mountain pine beetle utilizing leaf-level reflectance spectra analysed with a continuous wavelet transform. Specifically the study compared the responses of healthy control trees to infested and girdled trees and investigated the feasibility of separating these two groups using an appropriate set of spectral features (at particular scales and wavelength positions).

2.2. Data collection

2.2.1. Study sites

To assess the spectral detection of green attack for pine needles, two sites located northwest of Edmonton, Alberta, Canada were investigated (Fig. 2-1). The first site, located near Swan Hills, served for the girdling experiment to simulate the injury of sapwood tissues by a beetle attack. The second site, located near Grande Prairie, consisted of trees that were infested by mountain pine beetle (MPB).

Lodgepole pine (*Pinus contorta* Dougl. ex Loud. var. *latifolia* Engelm.) dominates the forests at the two sites. The trees investigated were approximately 20 years old, 8 meter tall, and displaying a diameter at breast height of 15 cm. At each site a number of control and treatment pine tree pairs were sampled. The sites with girdled trees and MPB infested trees encompass 16 and 15 tree pairs, respectively. Trees showing pitch tubes and bearing green foliage at the beginning of the sampling period were chosen to comprise the infested samples. The selected lodgepole pine trees received extensive sunlight occurring along clearings. Each healthy tree used as control was located within 5 meters of the treatment tree to facilitate comparison between control and treatment samples.

The girdling treatment was implemented in May 2007 to simulate the effect of MPB infestation where fungus transmitted by the beetle infects the sapwood and plugs the water-conducting xylem elements (tracheids) effectively preventing them from conducting water (Solheim, 1995; Yamaoka et al., 1990). An incision with a saw was made around the trunk of the tree approximately 50 cm above the ground and 5 cm into the sapwood. In doing so I aimed to interrupt the continuity of xylem tracheids in the tree and interrupt the flow of xylem sap into the crown. This treatment has been previously used to induce water-deficit stress in trees (Brix & Mitchell, 1985; Kent et al., 2004; Riggs & Running, 1991; Running, 1980). All treatment and control pairs at the girdling site were densely distributed along two roads at two subset sites two kilometers apart. Field measurements were acquired at this site on June 18th and August 30th of 2007.

Infested trees at the second site were attacked by mountain pine beetle in the summer of 2007 and all tree pairs occurred within an area of 1.5 km^2 along a main road. Field measurements were acquired in 2008 on June 5th, July 13th, August 14th, September 20th and October 14th. All tree samples were bearing green needles on June 5th and two trees showing discoloration of foliage on subsequent dates were excluded from sampling. The final number of trees available for analysis at each date is shown in Table 2-1.

2.2.2. Sampling of needles

A pole pruner was used in the early afternoon to collect one sunlit branch from each tree. Needles were then collected throughout the branch excluding new shoots. Reflectance spectra were either immediately acquired or the branch samples were packed with ice bags and transported to a nearby indoor laboratory where they were measured. Within minutes of each spectral measurement, approximately one third of the needles were wrapped in moistened paper towels and sealed with foil paper in a cooler with ice (Foley et al., 2006). The samples were then kept at -18^{o}C for subsequent leaf biochemical analysis.

2.2.3. Measurement of reflectance

An optically thick layer of needles extracted from a given branch was arranged on a panel coated with spectrally flat black paint (maximum reflectance of 9.8% at 400 nm). The FieldSpec® FR spectroradiometer (ASD Inc., Boulder, CO, USA) was then used to measure the reflectance of needle samples from 350 to 2500 nm. The instrument is characterized by a resolution of 3 nm at 700 nm, 10 nm at 1500 nm, and 10 nm at 2100 nm. The FieldSpec® FR fiberoptic cable utilized to collect light reflected from a sample was coupled to a high intensity reflectance probe attachment which is equipped with an internal artificial light source thus providing measurements independent of solar illumination conditions. The probe attachment was placed on the optically thick layer of needles and it encompassed an approximate field of view of 2.5cm in diameter. The probe was in contact with the needle layer and excluded external light. Reflectance was determined by standardizing one sample spectrum to that of a white Spectralon reference panel (99% reflectance). Each measurement (e.g. sample and reference) were recorded as an average of twenty scans in order to minimize instrument noise.

2.2.4. Measurement of pigment and water content

For each sample, two bundles of two needles were placed in a 15 ml centrifuge tube and pigments were extracted by adding 10 ml of dimethyl sulphoxide (DMSO) to the tube and placing the tube in a 65 ℃ water bath in the dark for more than 5 hours. The extract was transferred to a 4.5 ml cuvette and the absorbance at 664 nm, 646 nm and 470 nm was measured with a Smart® Spectro spectrophotometer (LaMotte, Chestertown, MD, USA). A blank sample was measured for calibration once for each wavelength. The concentrations of chlorophyll a, chlorophyll b and total carotenoids in μg/g were determined using the coefficients and equations derived by Wellburn (1994).

The remaining needles for each sample were weighted to determine fresh weight (FW). Dry weight (DW) was then determined by weighing after oven

drying at 80 ℃ for 24 hours. The water content of the needles as a percent of dry mass was given by:

$$H_2O\% = ((FW-DW) / DW) \times 100 \quad (2\text{-}1)$$

2.3. Methodology

2.3.1. Continuous wavelet transform

Wavelet analysis is a powerful signal processing tool (Mallat, 1999) which has been used successfully in medical sciences (Addison, 2005), geophysics (Farge, 1992; Torrence & Compo, 1998) and remote sensing image processing (Núñez et al., 1999; Simhadri et al., 1998) to extract information from various scales. Past studies include spectral smoothing and noise removal (Schmidt & Skidmore, 2004), discrimination of weeds from crop (Koger et al., 2003), tree stress detection (Kempeneers et al., 2005), tropical tree species identification (Zhang et al., 2006), forest leaf area index (LAI) and crown closure mapping (Pu & Gong, 2004), and retrieval of foliar pigment content (Blackburn, 2007; Blackburn & Ferwerda, 2008).

Recent studies (Bruce & Li, 2001; Bruce et al., 2001, 2002, 2006; Li & Bruce, 2004) have demonstrated the merits of using wavelet deconvolution for the analysis of hyperspectral data because such data exhibit non-stationarity, that is, spectral signals can vary in both amplitude (e.g. feature depth) and scale (e.g. feature width). Wavelet analysis can be implemented as a continuous wavelet transform (CWT) or a discrete wavelet transform (DWT). Most of the studies listed above exploited the DWT as a method for feature reduction but a substantial drawback is the inherent difficulty in interpreting the output coefficients. The CWT can decompose a signal at a continuum of positions rather than at dyadic positions and thus the outputs from the CWT are directly comparable to the original spectrum and are more easily interpretable. Recently, Rivard et al. (2008) provided an examination of CWT to highlight key spectral features in mineral spectra. Therefore, CWT was used in this study to examine its

potential to extract spectral information of various scales for leaf reflectance spectra.

The wavelet transform uses a mother wavelet basis function to convert a hyperspectral reflectance spectrum $f(\lambda)$ (λ=1, 2,..., n, n is the number of wavebands and n=2151 herein) into sets of coefficients. The wavelets $\psi_{a,b}(\lambda)$ are produced by scaling (dilating) and shifting (translating) the mother wavelet $\psi(\lambda)$ (Bruce et al., 2001):

$$\psi_{a,b}(\lambda) = \frac{1}{\sqrt{a}}\psi(\frac{\lambda - b}{a}) \qquad (2\text{-}2)$$

where a and b are positive real numbers for CWT. a represents the scaling factor defining the width of the wavelet and b is the shifting factor determining the position. The output of CWT is given by:

$$W_f(a,b) = \left\langle f, \psi_{a,b} \right\rangle = \int_{-\infty}^{+\infty} f(\lambda)\psi_{a,b}(\lambda)d\lambda \qquad (2\text{-}3).$$

Given any specific scale a_i (i=1, 2, ..., m, m is the maximum scale available), the continuous wavelets can be shifted through any waveband and the CWT of a reflectance spectrum generates a $1 \times n$ vector of wavelet coefficients. The CWT coefficients ($W_f(a_i,b_j)$, i=1, 2, ..., m, j=1,2,..., n) constitute a 2-dimensional scalogram (i.e. a $m \times n$ matrix) where one dimension is scale and the other is wavelength (or waveband). The value of each element of the scalogram represents the *wavelet power* which measures the correlation between the scaled and shifted mother wavelet and a segment of the reflectance spectrum and reflects the similarity of the local spectral shape to a particular wavelet basis. Low scale components of the scalogram capture absorption features of fine spectral details and high scale components emulate the overall continuum of the reflectance spectrum.

Leaf reflectance spectra contain specific absorption features from 350 to 2500 nm caused by the presence of pigments, water and dry matter. The shape of the absorption features is similar to Gaussian or quasi-Gaussian function,

therefore, the second derivative of Gaussian (DOG) also known as the Mexican Hat was used as the mother wavelet basis (Torrence & Compo, 1998) (Fig. 2). Since the wavelet decomposition at a continuum of possible scales (*i=1, 2, ..., m.*) would be computationally expensive and lead to a large data volume, the dimensions of the scalogram was reduced by decomposing the reflectance spectra at dyadic scales 2^1, 2^2, 2^3, ..., and 2^{10} which are proportional to the effective length of the wavelet compressed or stretched at that scale. Note that those scales are labelled as scales 1, 2, 3, …, and 10 in the following and still comparable to the scales described in published studies by Blackburn & Ferwerda (2008) and Rivard et al. (2008). The maximum scale available for the data of this study is 2^{11}=2048 but this scale was discarded due to the low information content. All CWT operations were accomplished in the IDL 6.3 Wavelet Toolkit (ITT Visual Information Solutions, Boulder, CO, USA).

2.3.2. Statistical analysis of leaf pigment and water properties

The linear correlation coefficient between leaf pigment and water content was examined for each dataset listed in Table 2-1. For each biochemical property, a paired *t*-test was then performed on each dataset to evaluate the separability of control and treatment (girdled and infested) samples. The resulting *p*-values were used to determine the statistical significance of the observed separability (Zar, 1996). The datasets displaying control and treatment samples with distinct leaf properties were then retained for subsequent wavelet analysis examining the correlation between spectral and chemical properties.

2.3.3. Correlation scalograms

The continuous wavelet analysis converts each 1-D reflectance spectrum to a 2-D wavelet power dataset which can be visualized as a scalogram with dimensions of wavelength and scale and power represented as amplitude. In this study, correlation scalograms (Fig. 2-3) were used to determine the wavelet power features that most strongly correlate with the leaf properties investigated (Cocchi

et al., 2003). Each correlation scalogram reports the squared correlation coefficient (R^2), ranging in value from 0 to 1, at each wavelength and scale. R^2 is obtained for the linear correlation established between wavelet power and an independent variable across all measurements of a given dataset (e.g. combined control and treatment). To build the correlation scalogram the control and treatment (e.g. girdled or infested) data were combined to achieve a larger sample size. In doing so, there were concerns that the dependence of control and treatment samples might violate the statistical assumption of randomization for observations within a sample. The dependence between the wavelet power and water content of control and treatment samples was examined and no significant correlation was observed.

In this study, the independent variables examined include the concentration of total chlorophyll, leaf water content, and class ID, the latter being used to identify features that distinguish the control and treatment samples. Fig. 2-3 provides an example correlation scalogram for the leaf water content and spectra of August 14 2008. Areas of the scalogram highlighted in blue on Fig. 2-3 display the most significant correlation and were selected as described in the next section. Scalogram outputs from the wavelet analysis were computed for 10 scales and thus are not convenient for visualization. To facilitate the visual inspection of scalograms, values at each scale were replicated or interpolated resulting in resized scalograms (100×2151) that have a 10 times vertical exaggeration. The interpolated scalograms were resampled with a cubic convolution providing a smoother appearance that was used strictly for visualization of features (Fig. 2-3A). The replicated scalograms (Fig. 2-3B) have a rough appearance preserving the original data and were used for determining the location of features selected as described in the next section.

2.3.4. Feature selection using correlation scalograms

Each element of a correlation scalogram represents a feature characterized by a R^2 value, wavelength and scale. The selection of the most informative features for a given independent variable involved two steps: 1) retaining features

where the correlations are statistically significant (p<0.05), and 2) sorting these features in descending order of R^2 value to retain those encompassing the top 1% of R^2 values (Fig. 2-4). These feature sets are highlighted in blue on Figs. 2-3, 2-6 and 2-7.

Fig. 2-5 provides a structured and labelled representation of the scalogram list for the girdled and infestation datasets. A total of 21 correlation scalograms were examined to produce 21 individual feature sets. Note that once a feature set was defined for a given independent variable and spectral dataset, the intersection of two feature sets could be established as a crossover feature set. For example, from the intersection of feature sets by class ID and water for August 14, 2008 one can examine if features that allow separation of control and infested samples by class ID are consistent with features that correlate with water content for these samples.

2.4. Results

2.4.1. Leaf pigment and water properties

A summary of correlations between laboratory-measured leaf properties is provided in Table 2-2. A weak correlation between total chlorophyll and water content is observed for the girdled and control datasets. As expected, a strong correlation is seen between total chlorophyll and carotenoid content for all datasets. Therefore, the leaf carotenoid data were excluded from the following analysis.

The results of the two-tailed paired student's *t*-tests are summarized in Table 2-3. Significant differences in water content are observed for the control and treatment samples of the two girdled datasets (Jun18-2007 and Aug30-2007) and two of the five infested datasets (Jul13-2008 and Aug14-2008). Significant differences in chlorophyll content are only observed for the two girdled datasets. For these four datasets, one-tailed *t*-tests (H_0: control = treatment; H_A: control > treatment) resulted in the same significance and stronger statistical power (one-tailed test not shown). The distinct chlorophyll and water content for the control

and treatment samples of the two girdled datasets suggests that girdled trees suffered water and chlorophyll stress induced by the mechanical injury. However, the trees infested by mountain pine beetle show evidence of a water deficit but no significant reduction in chlorophyll. The absence of significant difference in water content between control and infested samples in June likely results from the lack of time for tree to develop a response. The lack of a response for September and October remains unexplained. Subsequent analysis of leaf pigment, water, and spectral properties were conducted on the two girdled datasets and the two infested datasets where control and treatment samples were separable based on leaf water content.

2.4.2. Continuous wavelet analysis of the girdled datasets

The correlation scalograms produced with the Jun18-2007 dataset are displayed in Fig. 2-6A~E. Fig. 2-6A highlights features strongly sensitive to chlorophyll concentration that are observed in the visible (VIS) (530-740 nm) and in the shortwave-infrared (SWIR) (1990-2120 nm) regions at scales of 1 to 7. The discrimination by class ID (Fig. 2-6B) highlights features found in the SWIR (1550-2150 nm) at scales of 2 to 5 that distinguish the control and treatment samples. Leaf water content was strongly correlated with a few features in the near-infrared (NIR) (950-1230 nm) (Fig. 2-6C) and in the SWIR (1500-2400 nm) at scales of 2 to 5. The intersection of features observed for class ID with those of chlorophyll (Fig. 2-6D) and water (Fig. 2-6E) respectively results in features near 1990-2010 nm at scales of 4 to 5 and near 1560-2150 nm at scales of 3 to 5. These findings suggest that the significant differences in total chlorophyll and water between the two groups of samples derived from *t*-tests (Table 2-3) are detected in the CWT representation of spectral data. Scales of 4 and 5 are in general the most frequently selected. The location of features is listed in Table 2-4.

Fig. 2-6F~J shows the resultant correlation scalograms produced for the Aug30-2007 dataset. Generally, the locations of features selected are similar to those of Jun18-2007 but there are more features at low scales. In the case of water (Fig. 2-6F) several narrow feature regions are observed in the visible region that

are absent in the June dataset. The features are generally concordant with broader feature regions observed for chlorophyll (Fig. 2-6H) and likely result from the significant correlation between leaf water content and chlorophyll concentration (r=0.57, $p \leq 0.001$, n=32) (Ceccato et al., 2001). The intersection of features selected from the class ID scalogram with those of the chlorophyll (Fig. 2-6J) scalogram shows no concordance with the feature set observed for the June dataset (Fig. 2-6D). For the feature intersection of water and class ID (Fig. 2-6I), features observed in June (Fig. 2-6E) do not align with those of August but a number of features occur in the same spectral region.

Fig. 2-6K displays the class ID features common to the June and August 2007 datasets indicating that girdled and control samples can be distinguished with two feature regions observed between 1560-2150 nm at scales 3, 4 and 5. As indicated above a number of water features occur in these spectral regions for both datasets (Fig. 2-6E and I).

Table 2-4 summarizes the wavelength regions and scales of the features selected from the intersection of class ID features with those observed for correlation scalograms of water and chlorophyll. It is worth noting that features from scale 3 and 4 are common and features from scale 5 are consistently selected. Ferwerda & Jones (2006) also found that features at this scale were optimal for the prediction of leaf nitrogen concentration. These three scales appear to represent the optimal combination of scales of decomposition for the detection of changes in water and chlorophyll content in the girdled data. The August dataset produced more chlorophyll features for the class ID separation (Fig. 2-6J) than the June dataset ($total_{August}$=41, $total_{June}$=3), but less water features ($total_{August}$=40, $total_{June}$=128). The increased capability to detect chlorophyll deficit later in the growing season may be attributed to the presence of a chlorophyll stress following water stress.

2.4.3. Continuous wavelet analysis of the infested datasets

The correlation scalograms produced with the Jul13-2008 dataset are shown in Fig. 2-7L~O. Features strongly correlated to chlorophyll concentration

are not consistent in their wavelength location for both dates (Fig. 2-7L and R) and span the complete spectral region. A number of features observed for July have similar characteristics to those observed for June for the girdled dataset (Fig. 2-6A). For the Aug14-2008 dataset the chlorophyll features are primarily selected at high scales. The absence of intersection features between chlorophyll and class ID features for both infested datasets (Fig. 2-5) is consistent with the lack of statistical difference in chlorophyll between control and infested samples (Table 2-3). The results from the wavelet analysis and statistical test reveal the difficulty in separating control and infested samples based on chlorophyll abundance or spectral indicators of chlorophyll.

For the July and August 2008 data, features for the class ID (Fig. 2-7M and Q) and water (Fig. 2-7N and P) scalograms were found primarily in the NIR and SWIR regions. Both dates share a well defined feature region near 1310-1390nm (Fig. 2-7U) for class ID discrimination spanning multiple scales of which a narrower region (1318-1322 nm) of limited scale is attributed to water for both dates (Fig. 2-7T).

Table 2-5 summarizes the locations of features selected from the intersection of scalograms for both infested datasets. In contrast to the girdled datasets, more features are obtained from high scales with the infested datasets (e.g., scale 7 and 8). While the number of water features that might be used to distinguish control and infested samples declines from July to August ($total_{July}$=74, $total_{August}$=14), there are five features at scale 7 between 1318-1322 nm that are common to both datasets. Finally the class ID features common to both infested datasets (Fig. 2-7U) occur in a distinct region from the two key feature regions identified for the girdled datasets (Fig. 2-6K).

2.5. Discussion

2.5.1. Regression models for the infested datasets

The analysis of the scalograms has highlighted a narrow spectral region (1318-1322 nm) sensitive to needle water content that can be used to distinguish

needles of infested and control trees sampled in July and August. In this section the correlation and data distribution of water content with wavelet power at 1320 nm and scale 7 is examined (Fig. 2-8A). For August, a linear regression model shows a R^2 value of 0.49 and RMSE of 7.84% while for July the accuracy is lower (R^2=0.40; RMSE=9.77%). The slope and the intercept of the regression models for both dates are similar (Fig. 2-8A). These findings indicate that the feature at 1320 nm is consistently sensitive to needle water content for this part of the growing season. Fig. 2-8B and C provides a view of the distribution of the control and infested samples within each dataset. For both dates the infested samples span a wider range of water content and lower values than the control data as expected. Thus the regression for the infested samples is a closer match to that observed for the entire data (Fig. 2-8A). Infested samples for August provide the highest R^2 and lowest RMSE (6.93%). A paired *t*-test for control and infested samples showed that the mean wavelet power at 1320 nm for scale 7 was significantly different for both July and August (July: t = -2.8419, p = 0.0131; August: t = -3.1684, p = 0.0081).

2.5.2. Selection of scales for scalograms

Scale 7 is found to be promising for green-attack detection whereas recent studies have suggested that scales 5 and 6 are optimal for nitrogen and chlorophyll estimation (Blackburn & Ferwerda, 2008; Ferwerda & Jones, 2006). These differences are tied to the width of absorption features in spectra, the water absorption near 1400 nm being relatively broad and thus better captured at a large scale. In this study the CWT was conducted for 10 scales even though a greater number of scales were permitted for the 2151 spectral bands of the data. The wavelet signature at the highest scales can suffer from zero-padding during CWT calculation (Torrence & Compo, 1998) and do not always provide reliable information. For example, the features observed at scale 10 near 1550 nm for chlorophyll in Fig. 2-6R are not considered to be relevant to chlorophyll absorption (Curran, 1989). The lowest scale can capture high frequency components of the input signal and thus tend to capture noise. Therefore, a

filtering of scales may facilitate the selection of significant features. In this study few features in scale 1 were selected (12 of 496, Tables 2-5 & 2-6).

2.5.3. Wavelength regions of selected features

Previous studies by Ahern (1988) and Runesson (1991) examined visible and near infrared spectra of healthy and infested trees reporting that significant differences could be observed in the visible and red edge regions. In this study the most significant and consistent spectral features attributed to changes in water content were detected in the short wave infrared region. In the case of the infested data set, all the features selected (Table 2-5) can be related to known water absorptions in leaves located at varying distances from the nominal band centers at 980, 1200, 1440, and 1920 nm. The results for the girdled data are more difficult to interpret given the greater number and diversity of feature regions detected for both dates. In this case features are not only observed near known water absorptions but are also observed near 490nm, 660nm and 2300nm as seen in August. The first two of these regions also produced features that correlated well with total chlorophyll in August (Table 2-4). The considerably lower needle water content observed for the girdled trees as opposed to the infested trees (Table 2-7) may suggest significantly greater water stress for the girdled trees and explain the detection of features in the visible that correlate with water as well as chlorophyll. These observations are consistent with the significant correlations observed between leaf water and chlorophyll content for both dates of the girdling experiment (Table 2-2), correlations that are not observed for the infested datasets. The differing response of girdled and infested trees appears to indicate that the girdling process does not provide a perfect simulation of the effects caused by beetle infestation.

2.5.4. Implications for airborne detection of MPB infestation

In a study of hemlock abundance decline in the Catskills, USA, Pontius et al. (2005) used an index (R970/R900nm) applied to AVIRIS airborne imagery to

detect leaf water content. In this study the 970 nm feature was not found to be significantly correlated with water and a feature near 950nm correlated significantly with water only for July. However this study has revealed the presence of a narrow feature region (1318-1322 nm) for the detection of water stress occurring during green attack and observed in July and August. There are several implications of these findings for the potential airborne detection of green attack. It remains to be determined if the successful detection obtained at the leaf level study can be repeated at the canopy scale. The literature suggests that the detection of water content is enhanced from the leaf to the canopy level (Sims & Gamon, 2003). In this study needle stacks were measured as opposed to individual needles thus the measurements may already reasonably capture the spectral properties that would result from canopy scale observations particularly if the spatial resolution was commensurate with the dimensions of observed tree crowns (e.g. < 1.5 m).

The location of the key features on the edge of a strong atmospheric water absorption may negatively impact the use of these features for detection of green attack from airborne data but this remains to be evaluated. Negative effects would include reduced signal to noise quality of the data and the likely requirement for a rigorous atmospheric correction of the imagery (Asner et al., 2008; Clark et al., 2005; Kokaly et al., 2003). However the use of continuous wavelet analysis is well suited for the detection of key information because the noise component of the signal can be filtered by removal of low scale wavelets which in this study have not shown to incorporate key information for the detection of green attack.

Fig. 2-8B and C show that there is considerable overlap in the wavelet power data distribution of infested and control samples though the means of both groups are different. This observation would certainly preclude the separation of both groups with a high accuracy. It may be feasible to establish a threshold that would distinguish a substantial percentage of both populations, but a larger data set would be needed to facilitate this analysis.

2.5.5. Potential improvements

This study revealed the detection of infested trees for two sites investigated in July and August. The small number of sites provides a limited perspective for the potential detectability of green attack at the canopy scale. The results are certainly encouraging in that detection was possible and the lack of detection early in the season (e.g. June) could have been a function of the growing conditions such as moisture availability at the selected sites. A greater number of sites spanning a range of growing conditions are needed to assess any dependence of detection capability on specific growing conditions. The lack of detection in June may also indicate that trees have not had a chance to respond thus limiting the time span for detection.

The study established the correlation of features with class ID using wavelet analysis for the detection of infested trees. However, it has not provided an accuracy assessment of the class ID separation. The relatively small number of sites and samples meant that all measurements were used to develop the model.

2.6. Conclusions

A remote early detection of mountain pine beetle infestation would be of value to the monitoring and management of forests. Detailed spectral information provided by reflectance measurements of needles collected in July and August offer the potential for green-attack detection. Our work provides the following conclusions:

- The tree samples at the green-attack stage displayed measurable water stress as did the girdled trees. While a deficit in total chlorophyll content was documented for girdled trees, no chlorophyll deficit was observed for infested trees. The deficits in chlorophyll and water content were also detectable from the wavelet analysis of the reflectance data.
- A number of spectral features were defined to distinguish girdled and infested trees from healthy control trees. In general, the water features for the infested datasets occupied narrower spectral intervals. For the girdled trees, features attributed to changes in needle water content differed for June and August

(2007) and the majority were located in the SWIR region (1550-2370 nm) across scales 1 to 5. For the July and August (2008) datasets of infested trees, comparable water features were observed in the NIR and SWIR regions (950-1390 nm) from scales 1 to 8.

- Five features in the NIR (1318-1322 nm) spectral region at scale 7 were consistently found in the July and August datasets of infested trees and can be used to discriminate infested trees from healthy trees. These features are located on the edge of a strong water absorption centered at 1450 nm. Their spectral location and occurrence in the dataset of both dates imply they are the most promising features for green-attack detection. These features occur at longer wavelength than the range of wavelengths investigated in previous studies by Ahern (1988) and Runesson (1991).

Considering the effect of viewing geometry and canopy structural variability, it is unclear if the most persistent features could be enhanced or negatively impacted at the canopy level if measured with airborne hyperspectral systems.

2.7. References

Addison, P. S. (2005). Wavelet transforms and the ECG: A review. *Physiological Measurement, 26,* 155-199.

Ahern, F. J. (1988). The effects of bark beetle stress on the foliar spectral reflectance of lodgepole pine. *International Journal of Remote Sensing, 9,* 1451-1468.

Alberta Sustainable Resource Management. (2007). Mountain Pine Beetle Management Strategy. Edmonton, Alberta, Canada. http://srd.alberta.ca/forests/pdf/MPB_man_strategy.pdf

Amman, G. D. (1982). The mountain pine beetle—identification, biology, causes of outbreaks, and entomological research needs. *Proceedings of the joint Canada/USA workshop on mountain pine beetle related problems in western North America.* (pp 7-12). Victoria, British Columbia, Canada: Natural Resources Canada, Canadian Forest Services, Pacific Forest Center.

Asner, G. P., Jones, M. O., Martin, R. E., Knapp, D. E., & Hughes, R. F. (2008). Remote sensing of native and invasive species in Hawaiian forests. *Remote Sensing of Environment, 112,* 1912-1926.

Blackburn, G. A. (1998). Quantifying chlorophylls and carotenoids at leaf and canopy scales: An evaluation of some hyperspectral approaches. *Remote Sensing of Environment, 66,* 273-285.

Blackburn, G. A. (2007). Wavelet decomposition of hyperspectral data: A novel approach to quantifying pigment concentrations in vegetation. *International Journal of Remote Sensing, 28,* 2831-2855.

Blackburn, G. A., & Ferwerda, J. G. (2008). Retrieval of chlorophyll concentration from leaf reflectance spectra using wavelet analysis. *Remote Sensing of Environment, 112,* 1614-1632.

Brix, H., & Mitchell, A.K. (1985). Effects of disrupting stem sapwood water conduction on the water status in Douglas-fir crowns. *Canadian Journal of Forest Research, 15,* 982-985.

Bruce, L. M., & Li, J. (2001). Wavelets for computationally efficient hyperspectral derivative analysis. *IEEE Transactions on Geoscience and Remote Sensing, 39,* 1540-1546.

Bruce L.M., Li, J. & Huang, Y. (2002). Automated detection of subpixel hyperspectral targets with adaptive multichannel discrete wavelet transform, *IEEE Transactions on Geoscience and Remote Sensing, 40,* 977-979.

Bruce L. M., Mathur, A. & Byrd, J.D. (2006). Denoising and wavelet-based feature extraction of MODIS multi-temporal vegetation signatures, *GIScience & Remote Sensing, 43*, 170-180.

Bruce, L. M., Morgan, C., & Larsen, S. (2001). Automated detection of subpixel hyperspectral targets with continuous and discrete wavelet transforms. *IEEE Transactions on Geoscience and Remote Sensing, 39*, 2217-2226.

Ceccato, P., Flasse, S., Tarantola, S., Jacquemoud, S., & Grégoire, J. M. (2001). Detecting vegetation leaf water content using reflectance in the optical domain. *Remote Sensing of Environment, 77*, 22-33.

Clark, M. L., Roberts, D. A., & Clark, D. B. (2005). Hyperspectral discrimination of tropical rain forest tree species at leaf to crown scales. *Remote Sensing of Environment, 96*, 375-398.

Cocchi, M., Seeber, R., & Ulrici, A. (2003). Multivariate calibration of analytical signals by WILMA (wavelet interface to linear modelling analysis). *Journal of Chemometrics, 17*, 512-527.

Coops, N. C., Johnson, M., Wulder, M. A., & White, J. C. (2006a). Assessment of QuickBird high spatial resolution imagery to detect red attack damage due to mountain pine beetle infestation. *Remote Sensing of Environment, 103*, 67-80.

Coops, N. C., Wulder, M. A., & White, J. C. (2006b). Integrating remotely sensed and ancillary data sources to characterize a mountain pine beetle infestation. *Remote Sensing of Environment, 105*, 83-97.

Curran, P. J. (1989). Remote sensing of foliar chemistry. *Remote Sensing of Environment, 30*, 271-278.

Farge, M. (1992). Wavelet transforms and their applications to turbulence. *Annual Review of Fluid Mechanics, 24*, 395-458.

Ferwerda, J. G., & Jones, S. (2006). Continuous wavelet transformations for hyperspectral feature detection. *Proceedings of the 12th International Symposium on Spatial Data Handling*, 12-14 July, University of Vienna, Austria.

Foley, S., Rivard, B., Sánchez-Azofeifa, G. A., & Calvo, J. (2006). Foliar spectral properties following leaf clipping and implications for handling techniques. *Remote Sensing of Environment, 103*, 265-275.

Franklin, S. E., Wulder, M. A., Skakun, R. S., & Carroll, A. L. (2003). Mountain pine beetle red-attack forest damage classification using stratified Landsat

TM data in British Columbia, Canada. *Photogrammetric Engineering and Remote Sensing, 69*, 283-288.

Gamon, J. A., Peñuelas, J., & Field, C. B. (1992). A narrow-waveband spectral index that tracks diurnal changes in photosynthetic efficiency. *Remote Sensing of Environment, 41*, 35-44.

Gao, B. -C. (1996). NDWI - A normalized difference water index for remote sensing of vegetation liquid water from space. *Remote Sensing of Environment, 58*, 257-266.

Henigman, J., Ebata, T., Allen, E., Holt, J., & Pollard, A. (Eds.). (1999). *Field guide to forest damage in British Columbia.* Victoria, British Columbia, Canada: British Columbia Ministry of Forests.

Hunt Jr., E. R., & Rock, B. N. (1989). Detection of changes in leaf water content using near- and middle-infrared reflectances. *Remote Sensing of Environment, 30*, 43-54.

Kalacska, M., Sánchez-Azofeifa, G. A., Rivard, B., Caelli, T., White, H. P., & Calvo-Alvarado, J. C. (2007). Ecological fingerprinting of ecosystem succession: Estimating secondary tropical dry forest structure and diversity using imaging spectroscopy. *Remote Sensing of Environment, 108*, 82-96.

Kempeneers, P., De Backer, S., Debruyn, W., Coppin, P., & Scheunders, P. (2005). Generic wavelet-based hyperspectral classification applied to vegetation stress detection. *IEEE Transactions on Geoscience and Remote Sensing, 43*, 610-614.

Kent, D., Halcrow, D., Wyatt, T., & Shultz, S. (2004). Detecting stress in southern live oak (quercus virginiana) and sand live oak (Q. virginiana var. geminata). *Journal of Arboriculture, 30*, 146-153.

Koger, C. H., Bruce, L. M., Shaw, D. R., & Reddy, K. N. (2003). Wavelet analysis of hyperspectral reflectance data for detecting pitted morningglory (*Ipomoea lacunosa*) in soybean (*Glycine max*). *Remote Sensing of Environment, 86*, 108-119.

Kokaly, R. F., Despain, D. G., Clark, R. N., & Livo, K. E. (2003). Mapping vegetation in Yellowstone National Park using spectral feature analysis of AVIRIS data. *Remote Sensing of Environment, 84*, 437-456.

Kurz, W. A., Dymond, C. C., Stinson, G., Rampley, G. J., Neilson, E. T., Carroll, A. L., Ebata, T., & Safranyik, L. (2008). Mountain pine beetle and forest carbon feedback to climate change. *Nature, 452*, 987-990.

Li, J., & Bruce, L. M. (2004). Wavelet-based feature extraction for improved endmember abundance estimation in linear unmixing of hyperspectral signals, *IEEE Transactions on Geoscience and Remote Sensing, 42*, 644-649.

Mallat, S. (1999). *A Wavelet Tour of Signal Processing*, 2nd ed. San Diego, USA: Academic Press.

Milton, E. J., Schaepman, M. E., Anderson, K., Kneubühler, M., & Fox, N. (2007). Progress in field spectroscopy. *Remote Sensing of Environment.* doi: 10.1016/j.rse.2007.08.001.

Núñez, J., Otazu, X., Fors, O., Prades, A., Palà, V., & Arbiol, R. (1999). Multiresolution-based image fusion with additive wavelet decomposition. *IEEE Transactions on Geoscience and Remote Sensing, 37*, 1204-1211.

Peñuelas, J., Filella, I., Biel, C., Serrano, L., & Save, R. (1993). The reflectance at the 950-970 nm region as an indicator of plant water status. *International Journal of Remote Sensing, 14*, 1887-1905.

Peñuelas, J., Piñol, J., Ogaya, R., & Filella, I. (1997). Estimation of plant water concentration by the reflectance water index WI (R900/R970). *International Journal of Remote Sensing, 18*, 2869-2875.

Pontius, J., Hallett, R., & Martin, M. (2005). Using AVIRIS to assess hemlock abundance and early decline in the Catskills, New York. *Remote Sensing of Environment, 97*, 163-173.

Pu, R., & Gong, P. (2004). Wavelet transform applied to EO-1 hyperspectral data for forest LAI and crown closure mapping. *Remote Sensing of Environment, 91*, 212-224.

Reid, R.W. (1961). Moisture changes in lodgepole pine before and after attack by the mountain pine beetle. *Forest Chronicle*, 368–375.

Riggs, G.A., & Running, S.W. (1991). Detection of canopy water stress in conifers using the airborne imaging spectrometer. *Remote Sensing of Environment, 35*, 51-68.

Rivard, B., Feng, J., Gallie, A., & Sanchez-Azofeifa, A. (2008). Continuous wavelets for the improved use of spectral libraries and hyperspectral data. *Remote Sensing of Environment, 112*, 2850-2862.

Roberts, A., Northrup, J., & Reich, R. (2005). Mountain pine beetle detection and monitoring: Replication trials for early detection. *Proceedings of the Third International Workshop on the Analysis of Multi-Temporal Remote Sensing Images*, Biloxi, Mississippi, USA, 20-24.

Rock, B. N., Vogelmann, J. E., Williams, D. L., Vogelmann, A. F. & Hoshizaki, T. (1986). Remote detection of forest damage. *Bioscience*, *36*, 439-445.

Runesson, U. T. (1991). *Considerations for early remote detection of mountain pine beetle in green-foliaged lodgepole pine*. PhD Dissertation. University of British Columbia, Canada.

Running, S.W. (1980). Relating plant capacitance to the water relations of *Pinus contorta*. *Forest Ecology and Management, 2*, 237-252.

Safranyik, L. & Carroll, A. L. (2006). The biology and epidemiology of the mountain pine beetle in lodgepole pine forests. In Safranyik, L. & Wilson, W.R. (Ed.). *The Mountain Pine Beetle: a Synthesis of Biology, Management, and Impacts on Lodgepole Pine*. (pp. 3-66). Natural Resources Canada, Canadian Forest Service, Pacific Forestry Centre, Victoria, British Columbia.

Safranyik, L., Shrimpton, D., & Whitney, H. (1974). *Management of Lodgepole Pine to reduce losses from the mountain pine beetle.* Technical report 1. Environment Canada, Canadian Forestry Service, Victoria, British Columbia, Canada.

Schmidt, K. S., & Skidmore, A. K. (2004). Smoothing vegetation spectra with wavelets. *International Journal of Remote Sensing, 25*, 1167-1184.

Simhadri, K. K., Lyengar, S. S., Holyer, R. J., Lybanon, M., & Zachary Jr., J. M. (1998). Wavelet-based feature extraction from oceeanographic images. *IEEE Transactions on Geoscience and Remote Sensing, 36*, 767-778.

Sims, D. A., & Gamon, J. A. (2002). Relationships between leaf pigment content and spectral reflectance across a wide range of species, leaf structures and developmental stages. *Remote Sensing of Environment, 81*, 337-354.

Sims, D. A., & Gamon, J. A. (2003). Estimation of vegetation water content and photosynthetic tissue area from spectral reflectance: A comparison of indices based on liquid water and chlorophyll absorption features. *Remote Sensing of Environment, 84*, 526-537.

Skakun, R. S., Wulder, M. A., & Franklin, S. E. (2003). Sensitivity of the thematic mapper enhanced wetness difference index to detect mountain pine beetle red-attack damage. *Remote Sensing of Environment, 86*, 433-443.

Solheim, H. (1995). Early stages of blue-stain fungus invasion of lodgepole pine sapwood following mountain pine beetle attacks. *Canadian Journal of Botany, 73*, 70-74.

Taylor, S. W., Carroll, A. L., Alfaro, R. I. & Safranyik, L. (2006). Forest, climate and mountain pine beetle outbreak dynamics in western Canada. In Safranyik, L. & Wilson, W.R. (Ed.). *The Mountain Pine Beetle: a Synthesis of Biology, Management, and Impacts on Lodgepole Pine*. (pp. 67-94). Natural Resources Canada, Canadian Forest Service, Pacific Forestry Centre, Victoria, British Columbia.

Torrence, C., & Compo, G. P. (1998). A practical guide to wavelet analysis. *Bulletin of the American Meteorological Society, 79*, 61-78.

Wellburn, A.R. (1994). The spectral determination of chlorophylls a and b, as well as total carotenoids, using various solvents with spectrophotometers of different resolution. *Journal of Plant Physiology, 144*, 307-313.

Westfall, J. (2007). *2006 Summary of Forest Health Conditions in British Columbia*, British Columbia Ministry of Forests and Range, Victoria, British Columbia, Canada.

White, J. C., Coops, N. C., Hilker, T., Wulder, M. A., & Carroll, A. L. (2007). Detecting mountain pine beetle red attack damage with EO-1 Hyperion moisture indices. *International Journal of Remote Sensing, 28*, 2111-2121.

White, J. C., Wulder, M. A., Brooks, D., Reich, R., & Wheate, R. D. (2005). Detection of red attack stage mountain pine beetle infestation with high spatial resolution satellite imagery. *Remote Sensing of Environment, 96*, 340-351.

White, J. C., Wulder, M. A., & Grills, D. (2006). Detecting and mapping mountain pine beetle red-attack damage with SPOT-5 10-m multispectral imagery. *BC Journal of Ecosystem Management, 7*, 105-118.

Wulder, M. A., Dymond, C. C., White, J. C., Leckie, D. G., & Carroll, A. L. (2006). Surveying mountain pine beetle damage of forests: A review of remote sensing opportunities. *Forest Ecology and Management, 221*, 27-41.

Yamaoka, Y., Swanson, R. H., & Hiratsuka, Y. (1990). Inoculation of lodgepole pine with four blue-stain fungi associated with mountain pine beetle, monitored by a heat pulse velocity (HPV) instrument. *Canadian Journal of Forest Research, 20*, 31-36.

Zar, J. H. (1996). *Biostatistical Analysis*, Third Edition. New Jersey: Prentice Hall.

Zhang, J., Rivard, B., Sánchez-Azofeifa, A., & Castro-Esau, K. (2006). Intra- and inter-class spectral variability of tropical tree species at La Selva, Costa Rica:

Implications for species identification using HYDICE imagery. *Remote Sensing of Environment, 105*, 129-141.

Table 2-1. Description of sample size for each dataset

Treatment	Dataset	No. of pairs	No. of trees
Control & girdled	Jun18-2007	16	32
	Aug30-2007	16	32
Control & infested	Jun05-2008	15	30
	Jul13-2008	15	30
	Aug14-2008	13	26
	Sep20-2008	13	26
	Oct14-2008	12	24

If no green needles were available from a non-control tree, then the corresponding control tree was not sampled. The lower number of trees sampled for the infested datasets was caused by the inaccessibility of branches and the mortality of trees.

Table 2-2. Correlation coefficient (*r*) between chemical properties derived from the Lodgepole Pine needle samples

Treatment	Dataset	chl *vs* water	chl *vs* car
Control & girdled	Jun18-2007	0.41 *	0.94 ***
	Aug30-2007	0.57 **	0.96 ***
Control & infested	Jun05-2008	-0.13 ns	0.89 ***
	Jul13-2008	0.10 ns	0.95 ***
	Aug14-2008	-0.20 ns	0.94 ***
	Sep20-2008	-0.35 ns	0.86 ***
	Oct14-2008	N/A	N/A

Decimal values are correlation coefficients *r*. Significance is: ns = not significant ($p>0.05$), * $p\leq0.05$, ** $p\leq0.001$, *** $p\leq0.0001$. car = carotenoid; chl = total chlorophyll. The Oct14-2008 dataset only has measurements of water content.

Table 2-3. *p*-values of two-tailed paired student's *t*-test results for control and treatment samples for each dataset

Treatment	Dataset	Chl	Water
Control vs. Girdled	Jun18-2007	**0.0019**	**0.0004**
	Aug30-2007	**0.0001**	**0.0003**
Control vs. Infested	Jun05-2008	0.3985	0.3741
	Jul13-2008	0.3674	**0.0490**
	Aug14-2008	0.7968	**0.0320**
	Sep20-2008	0.3784	0.5222
	Oct14-2008	N/A	0.5610

p-values in bold indicate the significance at $p \leq 0.05$.

Table 2-4. Properties of features selected from the intersection of correlation scalograms for the girdled datasets

Dataset	Wavelengths (nm) and scales	R^2 [*min*, *max*]	
		1st variable	2nd variable
d. June: Class ID ∩ *chl*	S4: 1997-1998 (**2**) S5: 2004 (**1**) (total = 3)	[0.35, 0.55]	[0.37, 0.55]
e. June: Class ID ∩ water	S3: 1570-1593 (**24**) S4: 1572-1593, 1993-1998, 2097-2119 (**51**) S5: 1995-2006, 2102-2142 (**53**) (total = 128)	[0.35, 0.55]	[0.29, 0.47]
i. August: Class ID ∩ water	S1: 490, 2131 (**1**) S2: 660-661, 1559-1560, 1595-1599, 1704-1705 (**11**) S3: 570-571, 1561-1569, 1595-1598 (**15**) S5: 2351-2363 (**13**) (total = 40)	[0.33, 0.51]	[0.17, 0.40]
j. August: Class ID ∩ *chl*	S1: 489-490, 657-660, 2131 (**7**) S2: 657-661, 1596-1598 (**8**) S3: 1595-1599 (**5**) S5: 594-602 (**9**) S7: 717-728 (**12**) (total = 41)	[0.33, 0.51]	[0.20, 0.33]
k. Class ID: June ∩ August	S3: 1562-1574, 1582-1601 (**33**) S4: 1568-1597, 2102-2128 (**57**) S5: 2099-2142 (**44**) (total = 134)	[0.35, 0.55]	[0.33, 0.51]

S1, S2, …, S8 refers to the scale of the wavelet decomposition. Values in parentheses are the number of features selected at that scale. The total number of features summed for all scales are shown following the last scale. Chl = chlorophyll. R^2 [*min*, *max*] are the minimum and maximum values of R^2 for the selected features of individual variables (e.g., class ID, water, *chl*).

Table 2-5. Properties of features selected from the intersection of correlation scalograms for the infested datasets.

Dataset	Wavelengths (nm) and scales	R^2 [*min*, *max*]	
		1st variable	2nd variable
o. July: Class ID ∩ water	S1: 1142 (**1**) S3: 954-956 (**3**) S4: 953 (**1**) S7: 1316-1340 (**25**) S8: 1335-1378 (**44**) (total = **74**)	[0.19, 0.42]	[0.35, 0.54]
s. August: Class ID ∩ water	S1: 1743-1744 (**2**) S2: 1141, 1388-1390 (**4**) S3: 1388-1390 (**3**) S7: 1318-1322 (**5**) (total = **14**)	[0.17, 0.40]	[0.48, 0.71]
t. o ∩ ***s***	S7: 1318-1322 (**5**) (total = **5**)	See *o* and *s*	See *o* and *s*
u. Class ID: July ∩ August	S1: 1141 (**1**) S2: 1388-1390 (**3**) S3: 1388-1391 (**4**) S4: 1385-1390 (**6**) S5: 1376-1383 (**8**) S6: 1362-1370 (**9**) S7: 1315-1340 (**26**) (total = **57**)	[0.17, 0.40]	[0.19, 0.42]

Table 2-6. Summary of leaf water content (%) for four datasets with significant differences between control and treatment samples.

Dataset	Treatment	Min	Max	Mean ± S.D.
Jun18-2007	Control	79.70	102.51	92.52 ± 6.07
	Girdled	76.48	96.82	83.76 ± 5.86
Aug30-2007	Control	99.92	134.57	113.16 ± 8.32
	Girdled	92.06	109.66	100.91 ± 4.98
Jul13-2008	Control	107.70	142.94	129.81 ± 10.35
	Infested	101.18	146.12	120.10 ± 13.53
Aug14-2008	Control	114.34	143.27	128.91 ± 9.34
	Infested	96.51	138.72	120.10 ± 11.38

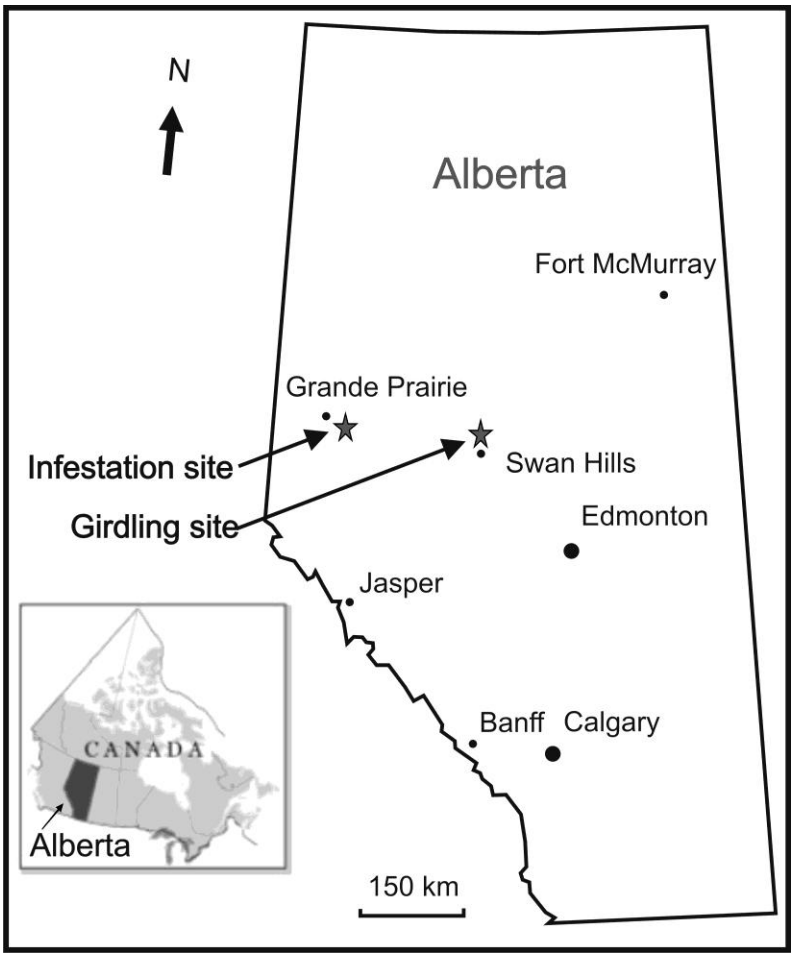

Fig. 2-1. Locations of the study sites in Alberta, Canada.

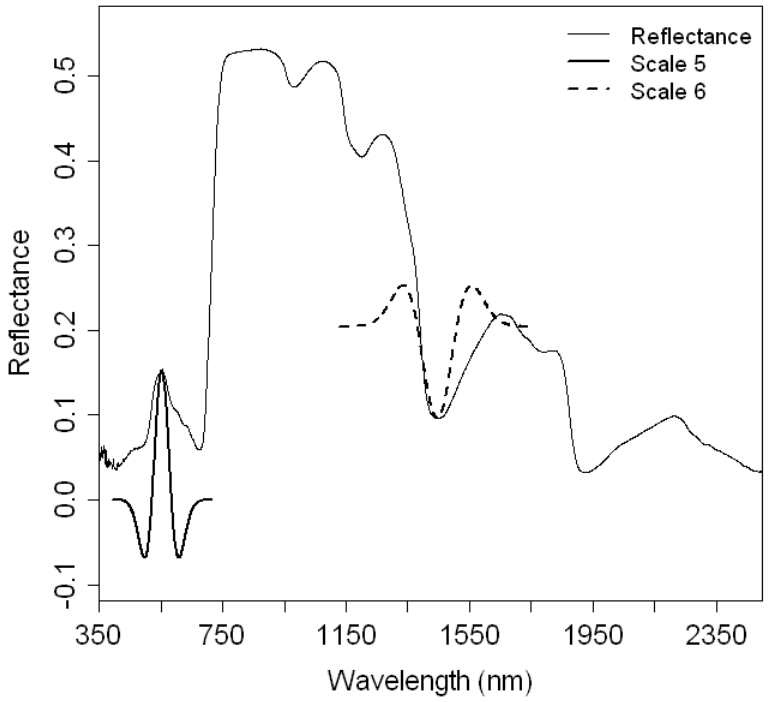

Fig. 2-2. Mexican Hat wavelets of scales 5 and 6 draped on a reflectance spectrum of healthy needles. The wavelet of scale 5 is an approximate match for the wavelength width of the green peak and the reversed wavelet of scale 6 is a reasonable match for the width of a major water absorption center. This feature and the green peak would be captured by wavelets of scale 6 and 5, respectively.

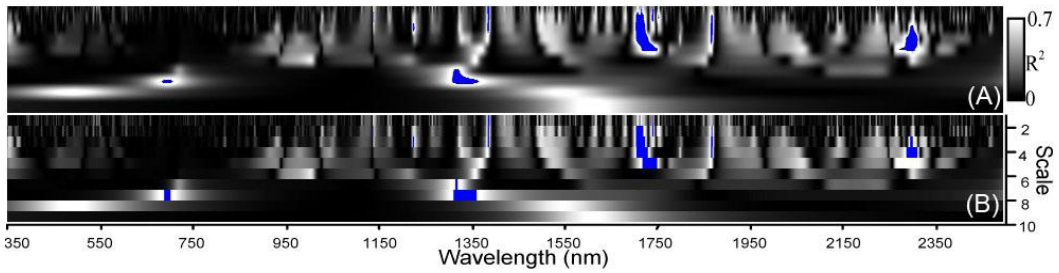

Fig. 2-3. Visualization of scalograms: (A) Scale interpolated; (B) Scale replicated. Scalograms were produced with the Aug14-2008 dataset (water features shown in blue). Wavelength is displayed along the horizontal direction and scale along the vertical axis. The R^2 value at each wavelength and scale is displayed as amplitude or brightness.

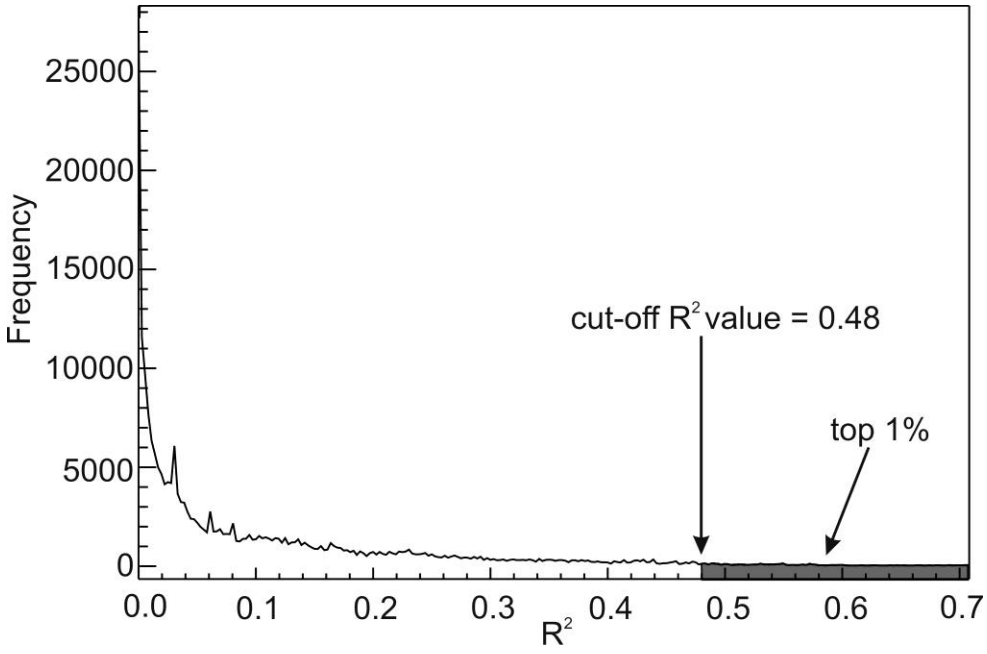

Fig. 2-4. Example of the frequency distribution of R^2 values observed for the scalogram in Fig. 2-3*B*. The cut-off R^2 value used to delineate features correlated to biochemical properties or class ID is defined by the highest R^2 values encompassing 1% of the data.

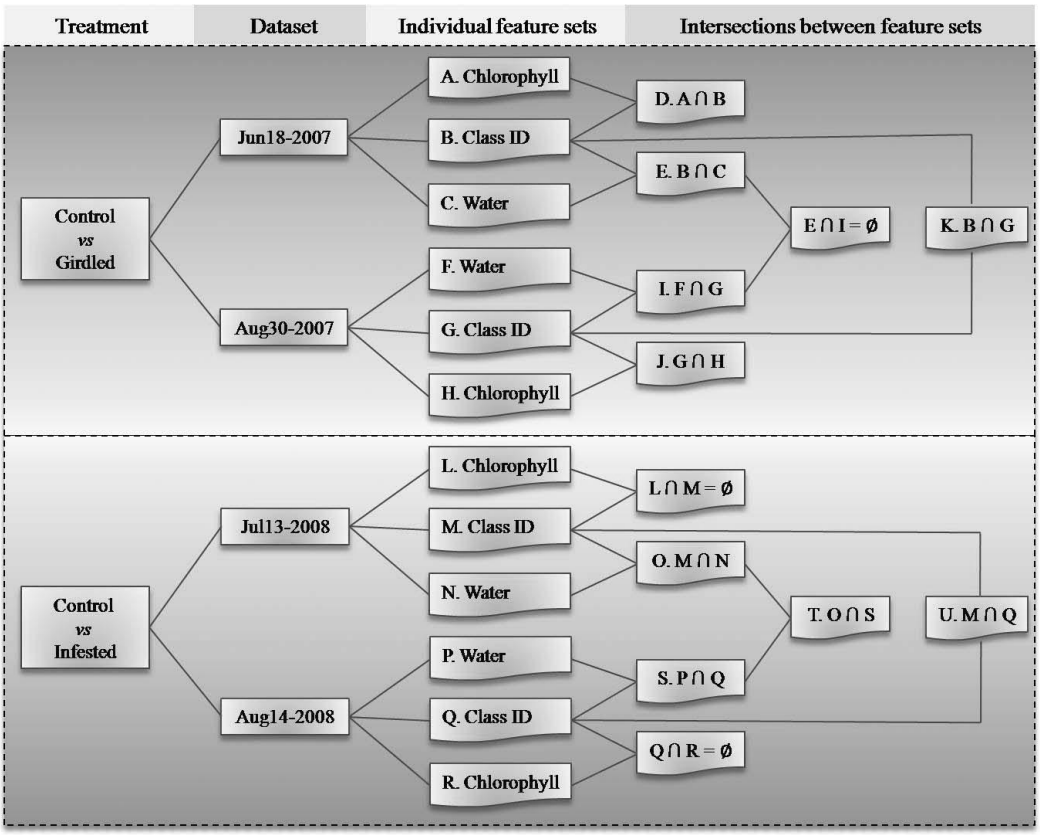

Fig. 2-5. Structure and labeling of feature sets derived from correlation scalograms indexed alphabetically from *A* to *U*. For example, the feature set *A* is derived from the correlation scalogram for the independent variable chlorophyll and the dataset Jun18-2007; *D*. $A \cap B$ refers to feature set *D* obtained by the intersection of feature set *A* and feature set *B*; $E \cap I = \varnothing$ indicates that the intersection of feature set *E* and feature set *I* is an empty set.

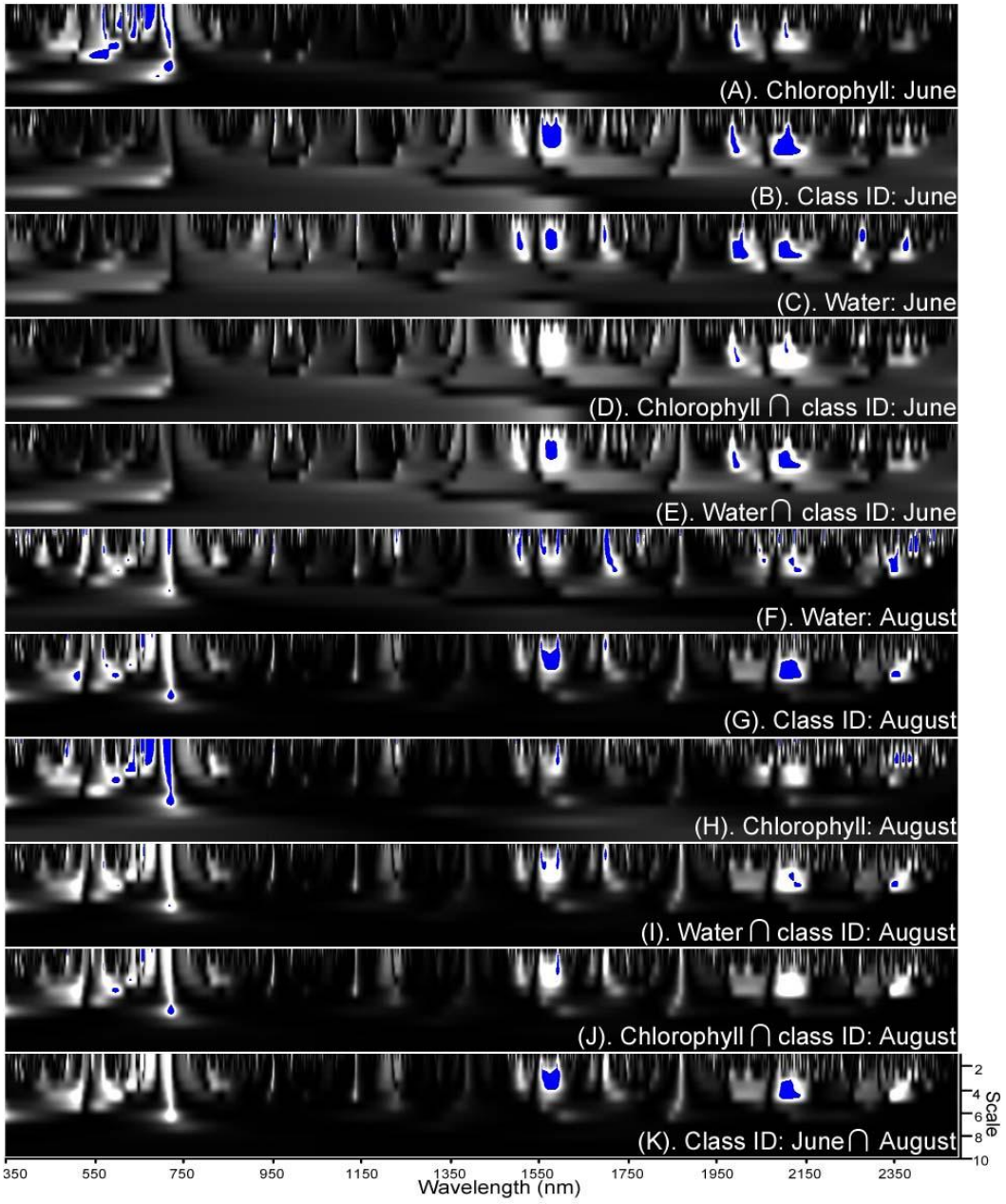

Fig. 2-6. Correlation scalograms *A*-*K* listed in Fig. 2-5 for the girdling datasets. The selected features are shown in blue on scalograms.

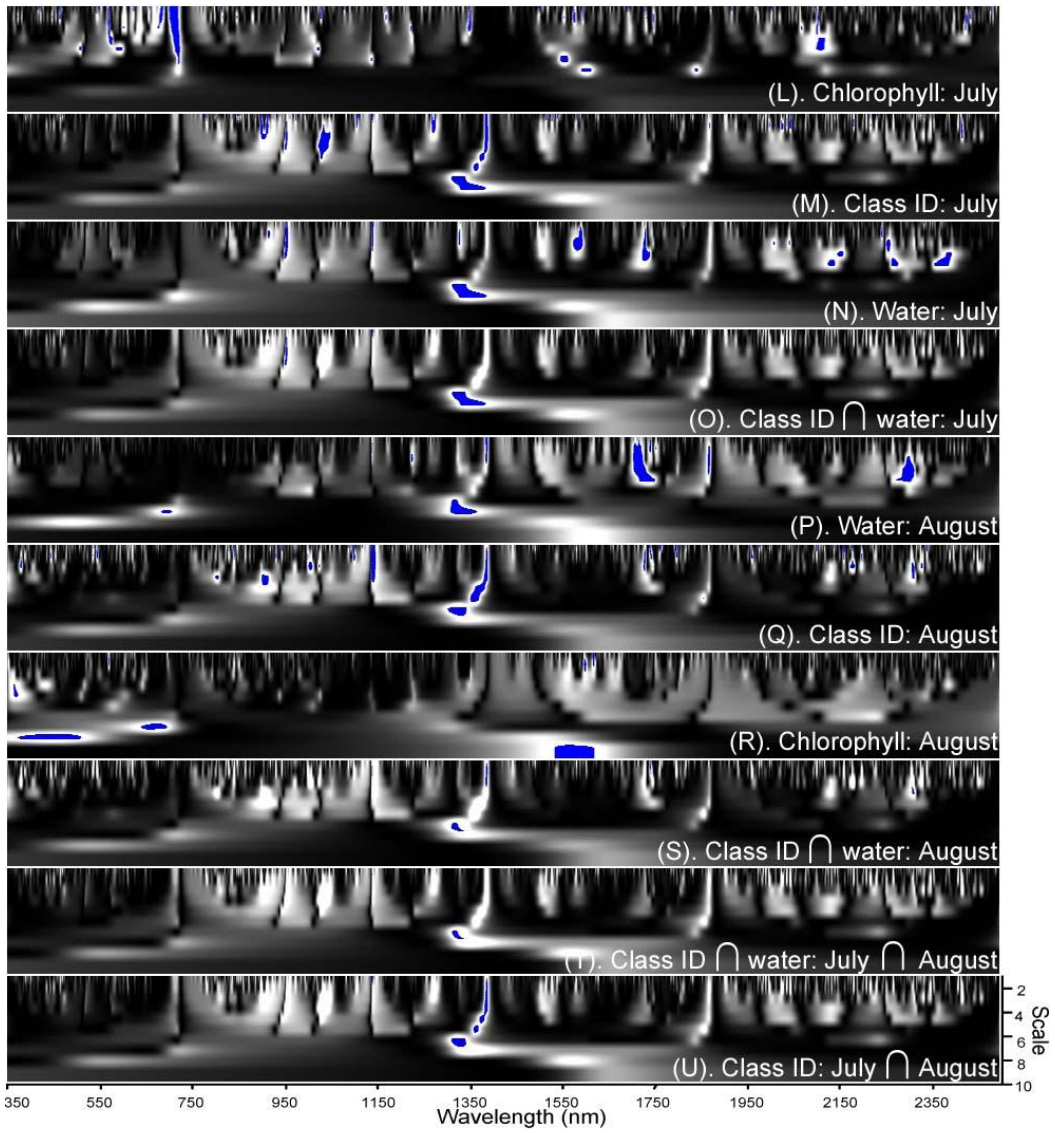

Fig. 2-7. Correlation scalograms *L*-*U* listed in Fig. 2-5 for the infested datasets.

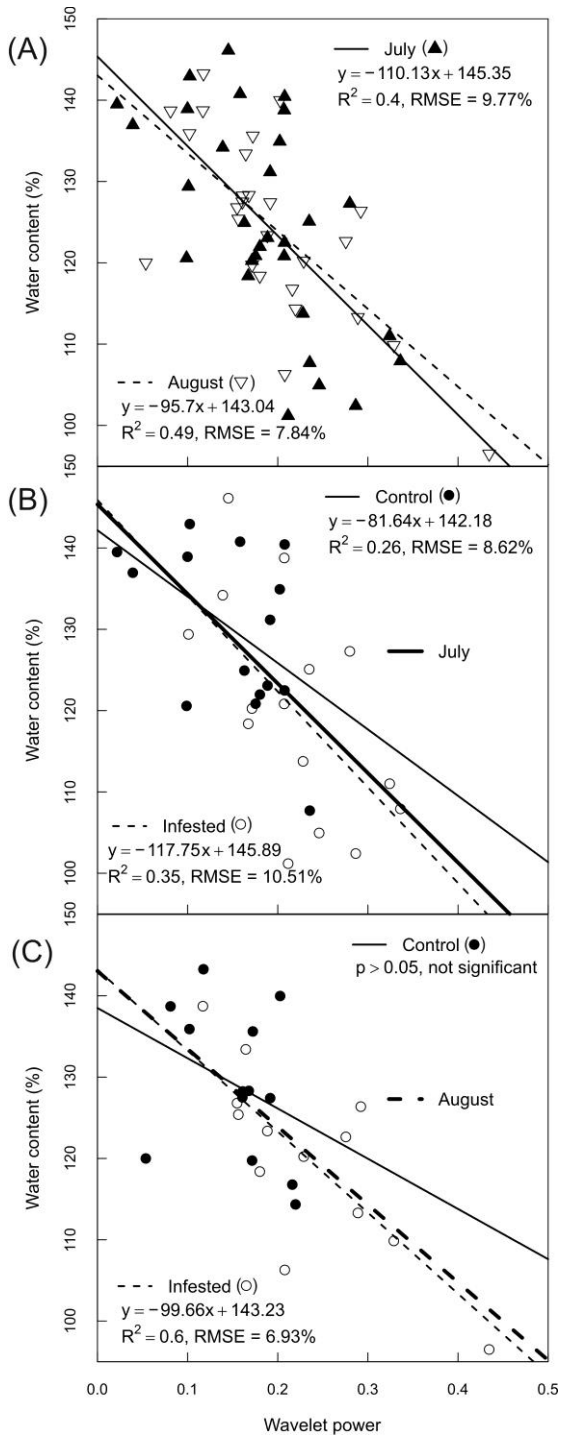

Fig. 2-8. Relationships between water content and the wavelet power at 1320 nm and scale 7 for the infested datasets: (A) combined control and infested data for July and August, (B) control and infested for July, (C) control and infested for August. The thicker solid and dashed lines in (B) and (C) are those seen in (A).

CHAPTER 3 – SPECTROSCOPIC DETERMINATION OF LEAF WATER CONTENT USING CONTINUOUS WAVELET ANALYSIS[2]

3.1. Introduction

Water is a fundamental chemical constituent of plants, and its abundance in leaves is closely tied to leaf vigor, phylogenic traits such as leaf structure and shape, and photosynthetic efficiency (Kramer & Boyer, 1995). Evaluation of plant water status plays an important role in assessing drought stress, predicting susceptibility to wildfire and monitoring the general physiological status of vegetation stands (Datt, 1999). Accurate retrieval of leaf water content via remotely sensed data is a long-sought goal of the biological remote sensing community (Hunt & Rock, 1989; Peñuelas et al., 1997).

Common methods for determining leaf water content include equivalent water thickness (EWT) and gravimetric water content (GWC) (Datt, 1999). The EWT expresses leaf water content in mass per unit leaf area (g/cm^2), whereas the GWC method employs a direct measurement that compares fresh leaf mass (with intrinsic water) to dry leaf mass (without intrinsic water). In general, the GWC is a preferred indicator of leaf water status when the measurement of leaf area is not easily achieved, as is the case for conifer needles. The GWC, which indicates the gravimetric proportions of water relative to other plant materials in leaves, can be expressed as leaf water content either by dry weight (LWC_D, %) or fresh weight (LWC_F, %). The LWC_D is extensively used in fire risk modeling and is referred to as the fuel moisture content (Chuvieco et al., 2002). The LWC_F serves as a key leaf trait in ecological studies (Garnier & Laurent, 1994).

---

[2] A version of this chapter has been submitted as: Cheng, T., Rivard, B., Sánchez-Azofeifa, G. A. Spectroscopic determination of leaf water content using continuous wavelet analysis.

Author contributions: Dr. Sánchez-Azofeifa provided the dataset. Dr. Rivard input critiques on the research. Dr. Rivard and Dr. Sánchez-Azofeifa discussed the results, and provided editing comments on the manuscript. I organized the data, wrote the codes for data processing, processed the data, interpreted the results, and composed the manuscript.

A number of studies have examined the empirical relationship of leaf reflectance in the near infrared (NIR) and shortwave infrared (SWIR) regions with leaf GWC or EWT (Ceccato et al., 2001; Danson et al., 1992; Danson & Bowyer, 2004; Sims & Gamon, 2003). Some studies have compared the estimation of GWC and EWT using leaf reflectance illustrating that GWC is considerably more difficult to estimate than EWT (Table 3-1) (Danson & Bowyer, 2004; Datt, 1999; Li et al., 2007; Maki et al., 2004; Riaño et al., 2005). Investigations estimating GWC from leaf reflectance report various strengths of correlation (Table 3-1). Some studies use spectral indices that employ a NIR or SWIR band to detect the leaf water content and a NIR band as a reference to normalize the effect of leaf structural variability (Colombo et al., 2008; Danson & Bowyer, 2004). Studies focusing on a single species (Dawson et al., 1998; Pu et al., 2004; Tian et al., 2001) are likely less influenced by variability in leaf structure and have achieved good predictions (Table 3-1, $R^2 \approx 0.86$) using neural networks or a combination of bands. However, the knowledge gained from studying either a limited number of plant species or a narrow range of GWC values is difficult to apply to more complex datasets encompassing a diversity of species or a wide range of GWC values. Riaño et al. (2005) investigated the inversion of the PROSPECT radiative transfer model to indirectly estimate LWC_D of 37 species and obtained a poor estimation of LWC_D due to the high uncertainty in estimating DMC (R^2 = 0.33). More recently, a combination of genetic algorithms with partial least squares (GA-PLS, Li et al, 2007) regression was proposed for the accurate estimations of LWC_D of 37 species (R^2 = 0.89). However, these methods are computationally intensive and complex, and thus of limited practical use.

Continuous wavelet analysis (CWA) is emerging as a promising tool in laboratory spectroscopy for deriving biochemical constituent concentrations from leaf reflectance spectra (Cheng et al. 2010; Blackburn, 2007; Blackburn & Ferwerda, 2008; Ferwerda & Jones, 2006). The continuous wavelet transform (CWT) provides a decomposition of leaf reflectance spectra into a number of scale components and each component is directly comparable to the reflectance

spectra. In this study, I aim to extract wavelet features (coefficients) that are sensitive to the change in GWC and insensitive to variations in leaf structural properties across a wide range of species. Inherent to the good estimation of GWC is the relationship of GWC to dry matter content (DMC), a topic that has received little attention in studies aiming to estimate GWC from leaf reflectance. Kokaly & Clark (1999) and Tian et al.(2001) noted that the spectral variation in the shortwave infrared induced by increasing leaf GWC included not only a decrease in the amplitude of reflectance but also changes in the depth and shape of absorption features centered near 1730 nm and 2100 nm and attributed to leaf dry matter. Continuous wavelet analysis is used in this study as a spectral feature analysis tool to examine the changes in leaf spectral response as a function of GWC and gain insights on the influence of water and DMC. Specifically, I seek to answer two questions: (i) Is CWT more effective than the commonly used spectral indices to estimate leaf GWC? (ii) What are the most informative wavelet features to estimate leaf GWC? Do they provide new insights into spectral variation due to changes in leaf water content?

3.2. Data set

3.2.1. Site description

Leaf samples were collected from two sites in the Republic of Panama. The first site is located in a tropical dry forest of Parque Natural Metropolitano (PNM) near the Pacific coast. This forest experiences a severe dry season from mid-December until the end of April and has an annual rainfall of about 1,740 mm. The second site is located in a tropical wet forest of Fort Sherman (FS) on the Caribbean coast. This ecosystem experiences a mild dry season from January to March and has an annual rainfall of about 3300 mm. Construction cranes owned by the Smithsonian Tropical Research Institute (STRI) were used at both sites to access the top of the canopy and collect leaf samples (Castro-Esau et al. 2004).

3.2.2. Data collection

At PNM, leaves were collected from 23 species of lianas and eight species of trees. At FS, eight species of lianas and eight species of trees were sampled. Collection of leaves took place in March 2007. All samples consisted of sun leaves.

Clipping of leaves and handling protocols were followed as described in Sánchez-Azofeifa et al. (2009). Reflectance measurements were recorded between 350 and 2500 nm with a FieldSpec® FR spectroradiometer (ASD Inc., Boulder, CO, USA). The instrument provides a resolution of 3 nm at 700 nm, 10 nm at 1500 nm, and 10 nm at 2100 nm. Five or ten leaf samples were collected per species and a total of 265 leaf samples were collected for the 47 species. Three reflectance spectra were taken per leaf using an ASD leaf clip covering a halogen bulb-illuminated area with a radius totaling 10mm. From these measurements, a mean reflectance spectrum was calculated for each leaf. The leaf water content was estimated by comparing the weight of the fresh leaf (the leaf's total mass less than one hour after clipping) and the mass of the same leaf after a three-day drying period at 60^{o}C.

3.3. Methods

3.3.1. Estimation of leaf gravimetric water content

Gravimetric water content in leaves was estimated using the following expressions:

$$LWC_D = \frac{FW-DW}{DW} \times 100\% \quad (3\text{-}1)$$

$$LWC_F = \frac{FW-DW}{FW} \times 100\% \quad (3\text{-}2)$$

where FW is the leaf fresh weight and DW is the dry weight. As the amount of water may exceed the leaf dry weight, some measurements of LWC_D were over 100% but all measurements of LWC_F were less than 100%. A summary of LWC_D

and LWC_F measurements is provided in Table 3-2. The two GWC expressions are convertible by:

$$LWC_F = \frac{LWC_D}{100\% + LWC_D} \times 100\% \quad (3\text{-}3)$$

$$LWC_D = \frac{LWC_F}{100\% - LWC_F} \times 100\% \quad (3\text{-}4)$$

This study's LWC_D or LWC_F value range exceeds the range reported in all similar studies, with the exception of studies investigating the LOPEX data (Table 3-1) (e.g. Danson & Bowyer, 2004). This sizeable range correlates to the wide range of species examined in this study, species that span both dry and wet tropical forest environments.

3.3.2. Wavelet analysis

Wavelet analysis is an effective signal-processing tool that functions by decomposing the original signal into multiple scales (Mallat, 1989). In the last two decades, wavelet analysis has been intensively explored for applications in medicine and biology (Addison, 2005; Unser & Aldroubi, 1996), chemistry (Leung et al., 1998) and geophysics (Farge, 1992; Torrence & Compo, 1998). In remote sensing, the wavelet analysis approach is widely applied to multispectral satellite imagery for image fusion (González-Audícana et al., 2004; Núñez et al., 1999; Shi et al., 2003; Zhang & Hong, 2005; Zhou et al., 1998) and texture classification (Arivazhagan & Ganesan, 2003; Laba et al., 2007; Myint et al., 2004; Ouma et al., 2008). Wavelet analysis is a promising method for processing hyperspectral signatures and has been successfully applied to hyperspectral data for dimensionality reduction (Bruce et al., 2002; Kaewpijit et al., 2003). Recent studies have compared the advantages of wavelet analysis to more conventional methods for identifying plant species (Kalácska et al., 2007; Koger et al., 2003; Zhang et al., 2006) and for estimating forest biophysical parameters (Pu & Gong, 2004) by means of hyperspectral imagery.

Wavelet transforms include two variations: the discrete wavelet transform (DWT) and the continuous wavelet transform (CWT) (Blackburn & Ferwerda, 2008; Bruce et al., 2001). The former method is mostly used for data compression and feature extraction/reduction, but the latter is preferred to generate a more readily interpretable multi-scale representation of signals (Bruce et al., 2001; Du et al., 2006). The DWT wavelet coefficients, after transformation, are difficult to interpret and require an inverse discrete wavelet transform for comparison with the original reflectance bands (Kalacska et al., 2007). In contrast, each CWT wavelet coefficient is directly comparable to a reflectance band and thus provides substantially more information on the shape and position of absorption features in leaf spectra (Blackburn & Ferwerda, 2008).

3.3.3. Continuous wavelet transform (CWT)

The CWT is a linear operation that uses a mother wavelet function to convert a hyperspectral reflectance spectrum $f(\lambda)$ (λ=1, 2,..., n, n is the number of wavebands and n=2151 herein) into sets of coefficients. Mathematically, the continuous wavelets $\psi_{a,b}(\lambda)$ are produced by scaling (dilating) and shifting (translating) the mother wavelet $\psi(\lambda)$ (Bruce et al., 2001):

$$\psi_{a,b}(\lambda) = \frac{1}{\sqrt{a}}\psi(\frac{\lambda - b}{a}) \quad (3\text{-}5)$$

where a and b are positive real numbers. a represents the scaling factor defining the width of the wavelet and b is the shifting factor determining the position. The output of CWT is given by (Mallat, 1991):

$$W_f(a,b) = \langle f, \psi_{a,b} \rangle = \int_{-\infty}^{+\infty} f(\lambda)\, \psi^*_{a,b}(\lambda) d\lambda \quad (3\text{-}6)$$

where $\psi^*_{a,b}(\lambda)$ is the *complex conjugate* of $\psi_{a,b}(\lambda)$[3].

[3] Note that *complex conjugation* changes the function only if a complex wavelet function such as Morlet function is used. The derivatives of Gaussian function are real functions.

For all scales of decomposition, the CWT coefficients ($W_f(a_i,b_j)$, $i=1, 2, ..., m$, $j=1,2,..., n$) constitute a 2-dimensional scalogram (i.e. a $m \times n$ matrix) of which one dimension is scale (1, 2, …, m) and the other is wavelength (or waveband, 1, 2, …, n). Each scale component of the scalogram is of the same length as the reflectance spectrum and this representation is readily interpretable. Low scale components are suitable to capture the characteristics of narrow absorption features and high scale components are well suited to define the overall spectral shape of leaf spectra (Blackburn & Ferwerda, 2008; Ferwerda & Jones, 2006; Rivard et al., 2008). The *wavelet power,* which refers to the magnitude of each wavelet coefficient, measures the correlation between the scaled and shifted mother wavelet and a segment of the reflectance spectrum and reflects the similarity of the local spectral shape to the mother wavelet (Rivard et al., 2008). It can be used to identify the change in shape and depth of absorption features across spectra and record the spectral variation introduced by changes in GWC.

A typical leaf reflectance spectrum in the 350-2500 nm range consists of a background continuum on which a number of absorption features attributable to pigments, water and dry matter are superimposed (Curran, 1989). Previous research suggests that the shape of the absorption features is similar to Gaussian or quasi-Gaussian function (Miller et al., 1990) or a combination of multiple Gaussian functions (le Maire et al., 2004). Therefore, the second derivative of Gaussian (DOG) also known as the Mexican Hat was used as the mother wavelet basis (Torrence & Compo, 1998). The effective support range of the Mexican Hat is [-5, 5] for the scale a=1 and [-5a_1, 5a_1] for $a=a_1$ (Du et al., 2006). The width of a scaled wavelet (10a_1) determines the number of wavebands that are to be convolved with the wavelet and attributed to the wavelet coefficient. Since the wavelet decomposition at a continuum of possible scales ($i=1, 2, ..., m.$) would be computationally expensive and lead to a large data volume, the dimensions of the scalogram were reduced by decomposing the reflectance spectra at dyadic scales 2^1, 2^2, 2^3, ..., and 2^{10}. For a simple representation of the scalograms, those scales are labeled as scales 1, 2, 3, …, and 10 in the following section and are comparable to the scales described in related studies by Blackburn & Ferwerda

(2008) and Rivard et al. (2008). For the leaf reflectance spectra from the ASD Fieldspec Pro spectrometer, there are 2151 bands available (350-2500 nm). Any scale greater than 2^{10}=1024 is discarded because the decomposed components at higher scales do not carry meaningful spectral information. All CWT operations were accomplished by means of the IDL 6.3 Wavelet Toolkit (ITT Visual Information Solutions, Boulder, CO, USA).

3.3.4. Feature selection from correlation scalograms

To deal with the redundancy of wavelet features caused by continuous decomposition, a feature-selection technique is required to identify the most important features used to derive the GWC. The method to select meaningful wavelet features comprises four main steps (Fig. 3-1). At Step 1, CWT was applied to all reflectance spectra to calculate the wavelet power as a function of wavelength and scale. Therefore, the wavelet data resulting from each spectrum were stored as a wavelet power scalogram with dimensions of power, wavelength, and scale. To identify features sensitive to variations in GWC, a correlation scalogram was constructed at Step 2 by establishing the Pearson's linear correlations between each element of wavelet power scalograms and GWC of all leaf samples. The correlation scalogram reports a squared correlation coefficient (R^2), ranging in magnitude from 0 to 1, at each wavelength and scale. Each element of the correlation scalogram represents a feature that could be selected. At Step 3, the features where R^2 is not statistically significant (p>=0.05) were masked. The remaining features were then sorted in descending order of R^2, and a threshold R^2 was applied to delineate the top 1% features that most strongly correlated with GWC. These features delineated by the threshold formed a number of scattered feature regions on the correlation scalogram (Fig. 3-2). Because features within each region were produced at consecutive wavelength positions and scales, they carried redundant spectral information. At step 4, the feature with the maximum R^2 within each region was determined to represent the spectral information captured by the feature region and expressed as (*wavelength*

in nm, *scale*). Eventually, a small number of sparsely distributed features were selected representing these regions and capturing the most important information related to changes in leaf water content.

3.3.5. Spectral indices

Three commonly used spectral indices (Table 3-3) designed to estimate vegetation water content were calculated to test their usefulness for estimating leaf GWC for the 47 tropical forest tree and liana species included in this study. The moisture stress index (MSI) was developed by Hunt et al. (1986) and further investigated by Hunt & Rock (1989) to relate leaf reflectance with leaf Relative Water Content (RWC). The normalized difference water index (NDWI) was originally proposed by Gao (1996) to remotely sense the EWT at the canopy level. The water index (WI) was originally designed by Peñuelas et al. (1997) to relate LWC_D with leaf reflectance spectra across species.

3.3.6. Calibration and validation of regression models

The entire dataset, consisting of reflectance spectra and leaf water content for 265 leaf samples, was split into two parts, with 60% of the data assigned to the calibration of regression models and 40% used for validating the models. The splitting led to 3 (or 6) samples per species in the calibration set and 2 (or 4) samples per species in the validation set. Suitable wavelet features were identified from the measurements in the calibration set using the method described in Section 3.4. Linear functions were applied to the calibration data to model the relationship between water content and wavelet features or spectral indices. For the wavelet approach, both individual and combinations of multiple spectral features were examined to calibrate the predictive models. Prior to combining features, a stepwise selection based on Akaike's Information Criterion (AIC) (Estes et al., 2008; Venables & Ripley, 2002; Zhou et al., 2006) was applied to determine the features that should be included in the model. Coefficients of

determination (R^2) and *p*-values were derived from analyses of data to assess how well the linear regressions corresponded to the calibration set. Calibrated models were then applied to the validation set and their predictive capabilities were assessed based on the predictive coefficient of determination (R^2) and the root mean square error (RMSE) between the measured and predicted water content.

3.4. Results

3.4.1. Response of leaf reflectance to variations in leaf water content

In Fig. 3-3, associations between five reflectance spectra and various LWC_D values are displayed. These associations illustrate the spectral variation in the 350-2500 nm range caused by changes in leaf water content. As LWC_D decreases from the highest (418.18%) to the lowest (32.31%) value, the strong water absorption features at 1445 nm and 1930 nm become weaker, and the amplitude of the reflectance spectrum in the SWIR region increases. In addition, the absorption features in the 1670-1830 nm and 2000-2200 nm regions, which have been found to correspond to leaf dry matter constituents (e.g., protein, lignin and cellulose) (Elvidge, 1990; Kokaly & Clark, 1999), become more apparent with decreasing LWC_D. In particular, the absorption centered in the 1670-1830 nm shifts towards shorter wavelength regions, and the spectral shape observed from 2000 to 2200 nm changes gradually from convex to concave as LWC_D decreases. Below, I illustrate that the wavelet analysis extracts information pertaining to water by capturing the aforementioned changes in overall amplitude and spectral shape.

3.4.2. Correlation of water indices with leaf water content for a wide range of species

Fig. 3-4 displays the linear regression models for spectral indices (Table 3-3) and water content expressed as LWC_D and LWC_F. MSI displays the weakest correlation (LWC_D: $R^2 = 0.05$; LWC_F: $R^2 = 0.08$). Low values of R^2 are observed

for the three indices (R^2 from 0.05 to 0.12) either for LWC_D or LWC_F. Most of the values of spectral indices were scattered vertically, indicating that these indices were not effective to capture the change in leaf water content for the wide range of plant species.

3.4.3. Most informative wavelet features to estimate leaf water content

Using continuous wavelet analysis of reflectance spectra, eight wavelet features (one per feature region) were extracted from the correlation scalogram for LWC_D. Similarly, eight wavelet features were extracted from the correlation scalogram for LWC_F. Regression models indicated that all extracted features significantly correlated to water content ($p<0.0001$). This represents an R^2 improvement of at least 0.3 over the values derived from linear regressions ($R^2>0.40$) obtained using spectral indices (Table 3-4). For LWC_D, the strongest correlation was produced by the wavelet power at 2165 nm at scale 4 ($R^2 = 0.62$) and the weakest by the wavelet power at 2227 nm at scale 3 ($R^2 = 0.43$). Wavelength locations of all extracted features for LWC_F were similar to those for LWC_D and the minimal differences were within the sampling uncertainty (10 nm) for the SWIR region of the spectrometer. The magnitude of R^2 values for LWC_F features (R^2 from 0.51 to 0.69) were higher than those for corresponding LWC_D features. The two groups of features differed in the ranking of R^2.

All wavelet features correlating with LWC_D and LWC_F are observed in the SWIR region (Fig. 3-5; LWC_F features are not shown because these are roughly equivalent to LWC_D features). Two high-scale features (1343nm, 7) and (1869nm, 6) (Table 3-5) occur on the left shoulder of two strong water absorption features (Fig. 3-5). The remaining features, primarily caused by leaf dry matter, occur at low scales and relate to absorption regions centered at approximately 1730, 2100 and 2300 nm. Feature (1734nm, 4) lies near a lignin-cellulose absorption center at 1730 nm, while features (2034nm, 3) and (2165nm, 4) are close to absorptions indicative of proteins, centered at 2054 nm and 2172 nm, respectively (Kokaly &

Clark, 1999; Kokaly, 2001). These three absorption bands become more prominent with decreasing water content in leaves.

The strongest relationship between leaf water content and wavelet power for an individual feature is observed for feature (2165nm, 4) as shown in Fig. 3-6. For LWC_D, the relationship was linear up to a water content of approximately 250% after which it became asymptotic and the wavelet power became insensitive to changes in leaf water content. This data pattern was observed for the eight features listed in Table 3-4. This data pattern was not observed for LWC_F (Fig. 3-6), though LWC_D with all other wavelet features showed similar relationships (data not shown). Excluding those observations of LWC_D above 250% led to a slight increase of R^2 by 0.02.

Models combining a number of features were then investigated. A stepwise selection of regression models based on AIC suggested that the combination of six features excluding (1579nm, 3) and (2227nm, 3) produced the best model for LWC_D with a R^2 of 0.69 (*I* in Table 3-4). For LWC_F, the best model was produced with six features excluding features (1870nm, 6) and (1576nm, 3). The reduced feature sets for LWC_D or LWC_F were then split into high-scale and low-scale feature subsets for modeling, and higher R^2 values were found for low-scale feature sets (e.g. *J* in Table 3-4).

3.4.4. Prediction of leaf water content using the wavelet features

The regression models calibrated using LWC_D and LWC_F wavelet features were applied to the validation set to determine the accuracy with which water content could be estimated. Feature (2165 nm, 4) produced the most accurate predictions of LWC_D and LWC_F, with RMSE values of 28.33% and 4.86%, respectively (Table 3-6). LWC_D and LWC_F were best predicted using a linear combination of six individual features resulting in a RMSE of 26.04% (R^2 = 0.71) and 4.34% (R^2 = 0.75) respectively. The latter compares to the accuracy of LWC_F estimation reported by Asner & Martin (2008; Fig. 2).

The results obtained from applying the most accurate single feature and multiple feature models (*A* & *I* in Table 3-6) to the validation set are shown on Fig. 3-7. The data points for both models are scattered near the 1:1 line except for LWC_D values exceeding 250%. This poor sensitivity at high levels of water content was also observed in the results of Danson & Bowyer (2004) where the WI underestimated most of the LWC_D observations ranging from 250% to 1400% and the accuracy was much lower. Interestingly, this phenomenon was not seen for the estimations and predictions of LWC_F (Figs. 3-6, 3-7).

3.5. Discussion

I investigated the relationship between spectral properties and leaf water content expressed as LWC_D and LWC_F for a diverse tropical species dataset (Sánchez-Azofeifa et al. 2009). To the best of our knowledge, this investigation is the first successful study linking the two measures of leaf water content to reflectance spectroscopy.

3.5.1. Wavelet features for the estimation of leaf water content

The wavelet features used to estimate LWC_D and LWC_F were not significantly different. Two high-scale LWC_D features (1343nm, 7) and (1869nm, 6) were found on the leading edge of the two strongest water absorption bands, and they captured the variations in amplitude of leaf reflectance over a broad spectral interval. The remaining significant features (1734nm, 4), (2034nm, 3), (2165nm, 4), and (2375nm, 4) that were found at low scales appeared away from strong water absorptions and accounted for changes in the depth and shape of dry matter absorption features. More information on LWC_D was captured by the variation in depth and shape of dry matter absorptions than by changes in water absorptions. The use of CWT has facilitated the detection of dry matter absorption features that are obscured by the presence of leaf water. Past studies by Danson & Bowyer (2004) and Riaño et al. (2005) concluded that the presence of spectral

features due to dry matter similarly complicated the estimation of LWC_D from leaf reflectance spectra. However, the results of this study suggest that the variable strength of dry matter absorptions in response to changes in leaf water content in our data contributes significantly to the estimation of LWC_D. Indeed, the correlation of leaf water content with the dry matter wavelet feature (2165nm, 4) is the strongest among those observed for an individual feature in this study. However, a combination of low-scale and high-scale features results in the best leaf water content predictive capability.

3.5.2. Why do spectral indices not work?

The results confirm the difficulty in relating LWC_D or LWC_F to commonly used spectral indices (Maki et al. 2004). One reason spectral indices relate poorly to leaf water content could be the large spectral variability that arises from the richness of species composition (Sims & Gamon, 2002). This has been documented in a number of studies of tropical ecosystems (Castro-Esau et al., 2006; Sánchez-Azofeifa et al., 2009). The poor sensitivity of MSI, WI and NDWI to the changes in LWC_D and LWC_F may indicate that ratios and normalized differential ratios are not effective in addressing the confounding effects of variable leaf structural properties across a wide selection of tropical species. This is not surprising given that MSI and NDWI were designed for the analysis of multispectral data, and thus have limitations in terms of the optimization of the location of bands that could be selected. WI may perform poorly because it was fashioned from an investigation including only thirteen species. However, it is likely that the spectral range (390-1100 nm) selected for the WI is the most likely cause of the inconsistent results as our findings suggest that the key features related to leaf water content are observed beyond 1100nm.

3.5.3. Advantages of the continuous wavelet analysis

This study presented CWA as an effective method for both analyzing the spectra and selecting features for the estimation of leaf water content. Unlike spectral indices that use ratios to normalize variations in the magnitude of reflectance, CWA provides a multiscale representation of a reflectance spectrum isolating absorption features at various scales from within the continuum. The correlation scalogram resulting from the analysis of multiple leaf samples then enables the optimal selection of spectral features most indicative of leaf water (Fig. 3-2). Therefore, no ratios of wavelet power are necessary for normalization. For example, the wavelet feature at (1579nm, 3) is a close match to the index wavelength (1600 nm) of the MSI but it yields a stronger correlation to water content (LWC_D: $R^2_{wp.(1579,\ 3)} = 0.44$, $R^2_{MSI} = 0.05$). The continuum removal technique is also capable of isolating specific absorption features from the continuum. CWA however, provides more robust information by using scaled wavelets to separate narrow and broad absorptions into different scales. The continuous displacement of the wavelet along the spectrum ensures that no absorption features are omitted and that all absorption features are detected at one time. The partial least squares (PLS) regression is comparable to CWA in predictive performance, but it is a more difficult operation with complex calibration requirements.

A small number of wavelet features are selected from the correlation scalogram based on thousands of input reflectance bands. The number of features extracted is dependent on the number of feature regions that are delineated on the correlation scalogram (Fig. 3-2) by the adjustable percentage threshold. In this study, a 1% threshold was utilized, since a smaller percentage threshold would have reduced the number of feature regions. The feature selection process ensures an optimization of wavelet features that correlate with leaf water content. The multi-scale analysis of absorption features offers an opportunity to capture water and dry matter absorptions that are manifested at different scales.

In a study aiming to determine the leaf water content (EWT) for a variety of species, Danson et al., (1992) attempted to suppress the variations in leaf internal structure by relating EWT to the first derivative of reflectance spectra. Our results suggest that the decomposition of reflectance spectra with CWT also effectively decreases the influence of leaf structural variation for the spectroscopic estimation of LWC_D and LWC_F.

3.5.4. Improvements of leaf water content by dry mass (LWC_D)

The data set of this study displays values of LWC_D ranging from 32.3% to 418.2%. For values of LWC_D exceeding 250%, our wavelet-based predictive models display poor sensitivity to changes in LWC_D (Fig. 3-6). This poor sensitivity was also observed, but not discussed in the study of Danson & Bowyer (2004; Fig. 5a) where LWC_D values ranged from 9% to 1258% and underestimation occurred for most observations above 250%. However, LWC_F with high levels of water content corresponded well to the predictions generated by wavelet-based models (Fig. 3-7). I demonstrated that LWC_F was more strongly correlated to wavelet power than LWC_D based on a linear fit. According to Eq. (3-4), if LWC_F is linearly related to wavelet power, then LWC_D, which is a non-linear function of LWC_F, would have a non-linear relation to wavelet power (Fig. 3-8). Thus, non-linear functions (e.g., power, exponential) might be explicitly employed to more completely describe the relationship between wavelet power and LWC_D over a wide range of values. However, the relatively low number of samples in this study with a high water content (ten data points with LWC_D>250%) precludes a thorough investigation of non-linear functions. In addition, ideally the water content would be more uniformly distributed across the data set to explore such functions.

As an attempt to improve the estimation of LWC_D, Eq. (3-4) was used to transform the LWC_F values predicted from the wavelet models shown in Fig. 3-7, C and D. The corresponding LWC_D estimates are shown in Fig. 3-9, A and B, respectively. The indirect estimates of LWC_D resulted in higher accuracies than

the direct estimates (Table 3-6) and the sensitivity at high water content levels was slightly enhanced (Fig. 3-9). Using the best feature combination (*I* in Table 3-6), the RMSE value of the indirect LWC_D estimation decreased by 3% (from 26.04% to 23.04%) and the R^2 value increased by 0.07 (from 0.71 to 0.78). The transformation of LWC_F to LWC_D offers an opportunity to bridge the studies estimating LWC_F and LWC_D from leaf reflectance.

3.6. Conclusion

This study has demonstrated the use of CWA applied to leaf reflectance spectra for the accurate prediction of leaf water content expressed as percent of dry mass (LWC_D) and fresh mass (LWC_F). A small number of wavelet features were strongly correlated to LWC_D and LWC_F, whereas established spectral indices were more poorly correlated. By decomposing the reflectance spectra into various scales, CWA was shown to be effective in identifying meaningful spectral information that relates to the estimation of leaf water content. The eight wavelet features used to predict LWC_D and LWC_F were not significantly different, but the predictive models were different. The method more accurately estimated LWC_F than it did LWC_D, and LWC_D values exceeding 250% tended to be underestimated.

The wavelength positions of the eight wavelet features occur in the SWIR region (1300–2500 nm). The high-scale features captured amplitude variations in the broad shape of the reflectance spectra. The low-scale features captured variations in the shape and depth of dry matter absorptions centered near 1730 nm and 2100 nm. Our results provide new insights into the role of dry matter absorption features in the SWIR region for the accurate spectral estimation of LWC_D and LWC_F. The advantages of wavelet analysis over existing spectral indices for the estimation of leaf water content should appeal to communities interested in the accurate estimation of LWC_D or LWC_F particularly for investigations of diverse ecosystems. The method developed for estimating leaf water content is promising for determining leaf biochemistry from spectra and

may be extended to the estimation of chlorophyll, lignin, cellulose, and nitrogen concentrations in ecosystem studies.

3.7. References

Addison, P. S. (2005). Wavelet transforms and the ECG: A review. *Physiological Measurement, 26,* 155-199.

Arivazhagan, S., & Ganesan, L. (2003). Texture classification using wavelet transform. *Pattern Recognition Letters, 24,* 1513-1521.

Asner, G. P., & Martin, R. E. (2008). Spectral and chemical analysis of tropical forests: Scaling from leaf to canopy levels. *Remote Sensing of Environment, 112,* 3958-3970.

Blackburn, G. A. (2007). Wavelet decomposition of hyperspectral data: A novel approach to quantifying pigment concentrations in vegetation. *International Journal of Remote Sensing, 28,* 2831-2855.

Blackburn, G. A., & Ferwerda, J. G. (2008). Retrieval of chlorophyll concentration from leaf reflectance spectra using wavelet analysis. *Remote Sensing of Environment, 112,* 1614-1632.

Bowyer, P., & Danson, F. M. (2004). Sensitivity of spectral reflectance to variation in live fuel moisture content at leaf and canopy level. *Remote Sensing of Environment, 92,* 297-308.

Bruce L.M., Li, J. & Huang, Y. (2002). Automated detection of subpixel hyperspectral targets with adaptive multichannel discrete wavelet transform, *IEEE Transactions on Geoscience and Remote Sensing, 40,* 977-979.

Bruce, L. M., Morgan, C., & Larsen, S. (2001). Automated detection of subpixel hyperspectral targets with continuous and discrete wavelet transforms. *IEEE Transactions on Geoscience and Remote Sensing, 39,* 2217-2226.

Carter, G. A. (1991). Primary and secondary effects on water content on the spectral reflectance of leaves. *American Journal of Botany, 78,* 916-924.

Castro-Esau, K. L., Sánchez-Azofeifa, G. A., & Caelli, T. (2004). Discrimination of lianas and trees with leaf-level hyperspectral data. *Remote Sensing of Environment, 90,* 353-372.

Castro-Esau, K. L., Sánchez-Azofeifa, G. A., Rivard, B., Wright, S. J., & Quesada, M. (2006). Variability in leaf optical properties of mesoamerican trees and the potential for species classification. *American Journal of Botany, 93,* 517-530.

Ceccato, P., Flasse, S., Tarantola, S., Jacquemoud, S., & Grégoire, J. M. (2001). Detecting vegetation leaf water content using reflectance in the optical domain. *Remote Sensing of Environment, 77*, 22-33.

Ceccato, P., Gobron, N., Flasse, S., Pinty, B. & Tarantola, S. (2002). Designing a spectral index to estimate vegetation water content from remote sensing data: Part 1: Theoretical approach. *Remote Sensing of Environment, 82*, 188-197.

Cheng, T., Rivard, B., Sánchez-Azofeifa, G. A., Feng, J. & Calvo-Polanco, M. (2010). Continuous wavelet analysis for the detection of green attack due to mountain pine beetle infestation. *Remote Sensing of Environment, 114*, 899-910.

Chuvieco, E., Riaño, D., Aguado, I., & Cocero, D. (2002). Estimation of fuel moisture content from multitemporal analysis of Landsat Thematic Mapper reflectance data: Applications in fire danger assessment. *International Journal of Remote Sensing, 23*, 2145-2162.

Colombo, R., Meroni, M., Marchesi, A., Busetto, L., Rossini, M., Giardino, C., & Panigada, C. (2008). Estimation of leaf and canopy water content in poplar plantations by means of hyperspectral indices and inverse modeling. *Remote Sensing of Environment, 112*, 1820-1834.

Curran, P. J. (1989). Remote sensing of foliar chemistry. *Remote Sensing of Environment, 30*, 271-278.

Danson, F. M., & Bowyer, P. (2004). Estimating live fuel moisture content from remotely sensed reflectance. *Remote Sensing of Environment, 92*, 309-321.

Danson, F. M., Steven, M. D., Malthus, T. J., & Clark, J. A. (1992). High-spectral resolution data for determining leaf water content. *International Journal of Remote Sensing, 13*, 461-470.

Datt, B. (1999). Remote sensing of water content in *Eucalyptus* leaves. *Australian Journal of Botany, 47*, 909-923.

Dawson, T. P., Curran, P. J., North, P. R. J., & Plummer, S. E. (1999). The propagation of foliar biochemical absorption features in forest canopy reflectance: A theoretical analysis. *Remote Sensing of Environment, 67*, 147-159.

Du, P., Kibbe, W. A., & Lin, S. M. (2006). Improved peak detection in mass spectrum by incorporating continuous wavelet transform-based pattern matching. *Bioinformatics, 22*, 2059-2065.

Elvidge, C. D. (1990). Visible and near infrared reflectance characteristics of dry plant materials. *International Journal of Remote Sensing, 11*, 1775-1795.

Estes, L. D., Okin, G. S., Mwangi, A. G., & Shugart, H. H. (2008). Habitat selection by a rare forest antelope: A multi-scale approach combining field data and imagery from three sensors. *Remote Sensing of Environment, 112*, 2033-2050.

Farge, M. (1992). Wavelet transforms and their applications to turbulence. *Annual Review of Fluid Mechanics, 24*, 395-458.

Ferwerda, J. G., & Jones, S. (2006). Continuous wavelet transformations for hyperspectral feature detection. *Proceedings of the 12th International Symposium on Spatial Data Handling*, 12-14 July, University of Vienna, Austria.

Gao, B. -C. (1996). NDWI - A normalized difference water index for remote sensing of vegetation liquid water from space. *Remote Sensing of Environment, 58*, 257-266.

Garnier, E., & Laurent, G. (1994). Leaf anatomy, specific mass and water content in congeneric annual and perennial grass species. *New Phytologist, 128*, 725-736

Gausman, H. W. (1985). Plant leaf optical properties in visible and near-infrared light. *Graduate studies No. 29.* Lubbock, Texas: Texas Tech Press.

González-Audícana, M., Saleta, J. L., Catalán, R. G., & García, R. (2004). Fusion of multispectral and panchromatic images using improved IHS and PCA mergers based on wavelet decomposition. *IEEE Transactions on Geoscience and Remote Sensing, 42*, 1291-1299.

Horler, D. N. H., Dockray, M., & Barber, J. (1983). The red edge of plant leaf reflectance. *International Journal of Remote Sensing, 4*, 273-288.

Hunt Jr., E. R., & Rock, B. N. (1989). Detection of changes in leaf water content using near- and middle-infrared reflectances. *Remote Sensing of Environment, 30*, 43-54.

Kaewpijit, S., Moigne, J. L., & El-Ghazawi, T. (2003). Automatic reduction of hyperspectral imagery using wavelet spectral analysis. *IEEE Transactions on Geoscience and Remote Sensing, 41*, 863-871.

Kalácska, M., *Sánchez-Azofeifa,* G. A., Rivard, B., Caelli, T., White, H. P., & Calvo-Alvarado, J. C. (2007). Ecological fingerprinting of ecosystem

succession: Estimating secondary tropical dry forest structure and diversity using imaging spectroscopy. *Remote Sensing of Environment, 108*, 82-96.

Koger, C. H., Bruce, L. M., Shaw, D. R., & Reddy, K. N. (2003). Wavelet analysis of hyperspectral reflectance data for detecting pitted morningglory (*Ipomoea lacunosa*) in soybean (*Glycine max*). *Remote Sensing of Environment, 86*, 108-119.

Kokaly, R. F. (2001). Investigating a physical basis for spectroscopic estimates of leaf nitrogen concentration. *Remote Sensing of Environment, 75*, 153-161.

Kokaly, R. F., & Clark, R. N. (1999). Spectroscopic determination of leaf biochemistry using band-depth analysis of absorption features and stepwise multiple linear regression. *Remote Sensing of Environment, 67*, 267-287.

Kramer, P. J. & Boyer, J. S. (1995). *Water relations in plants and soils*. San Diego, CA: Academic Press.

Laba, M., Smith, S., Sullivan, P., Philpot, W., & Baveye, P. (2007). Influence of wavelet type on the classification of marsh vegetation from satellite imagery using a combination of wavelet texture and statistical component analyses. *Canadian Journal of Remote Sensing, 33*, 260-265.

le Maire, G., François, C., & Dufrêne, E. (2004). Towards universal broad leaf chlorophyll indices using PROSPECT simulated database and hyperspectral reflectance measurements. *Remote Sensing of Environment, 89*, 1-28.

Leung, A. K., Chau, F., & Gao, J. (1998). A review on applications of wavelet transform techniques in chemical analysis: 1989-1997. *Chemometrics and Intelligent Laboratory Systems, 43*, 165-184.

Li, L., Ustin, S. L., & Riaño, D. (2007). Retrieval of fresh leaf fuel moisture content using genetic algorithm partial least squares (GA-PLS) modeling. *IEEE Geoscience and Remote Sensing Letters, 4*, 216-220.

Maki, M., Ishiahra, M., & Tamura, M.. (2004). Estimation of leaf water status to monitor the risk of forest fires by using remotely sensed data. *Remote Sensing of Environment, 90*, 441-450.

Mallat, S. G. (1989). A theory for multiresolution signal decomposition: The wavelet representation. *IEEE Transactions on Pattern Analysis and Machine Intelligence, 11*, 674-693.

Mallat, S. (1991). Zero-crossings of a wavelet transform. *IEEE Transactions on Information Theory, 37*, 1019-1033.

Miller, J. R., Hare, E. W., & Wu, J. (1990). Quantitative characterization of the vegetation red edge reflectance 1. An inverted-Gaussian reflectance model. *International Journal of Remote Sensing, 11*, 1755-1773.

Myint, S. W., Lam, N. S. -N., & Tyler, J. M. (2004). Wavelets for urban spatial feature discrimination: Comparisons with fractal, spatial autocorrelation, and spatial co-occurrence approaches. *Photogrammetric Engineering and Remote Sensing, 70*, 803-812.

Núñez, J., Otazu, X., Fors, O., Prades, A., Palà, V., & Arbiol, R. (1999). Multiresolution-based image fusion with additive wavelet decomposition. *IEEE Transactions on Geoscience and Remote Sensing, 37*, 1204-1211.

Ouma, Y. O., Tetuko, J., & Tateishi, R. (2008). Analysis of co-occurrence and discrete wavelet transform textures for differentiation of forest and non-forest vegetation in very-high-resolution optical-sensor imagery. *International Journal of Remote Sensing, 29*, 3417-3456.

Peñuelas, J., Filella, I., Biel, C., Serrano, L., & Save, R. (1993). The reflectance at the 950-970 nm region as an indicator of plant water status. *International Journal of Remote Sensing, 14*, 1887-1905.

Peñuelas, J., Piñol, J., Ogaya, R., & Filella, I. (1997). Estimation of plant water concentration by the reflectance water index WI (R900/R970). *International Journal of Remote Sensing, 18*, 2869-2875.

Pu, R., Foschi, L., & Gong, P. (2004). Spectral feature analysis for assessment of water status and health level in coast live oak (*Quercus agrifolia*) leaves. *International Journal of Remote Sensing, 25*, 4267-4286.

Pu, R., & Gong, P. (2004). Wavelet transform applied to EO-1 hyperspectral data for forest LAI and crown closure mapping. *Remote Sensing of Environment, 91*, 212-224.

Riaño, D., Ustin, S. L., Usero, L., & Patricio, M. A. (2005a). Estimation of fuel moisture content using neural networks. *Lecture Notes in Computer Science*, 3562, 489-498.

Riaño, D., Vaughan, P., Chuvieco, E., Zarco-Tejada, P. J., & Ustin, S. L. (2005b). Estimation of fuel moisture content by inversion of radiative transfer models to simulate equivalent water thickness and dry matter content: Analysis at leaf and canopy level. *IEEE Transactions on Geoscience and Remote Sensing, 43*, 819-826.

Rivard, B., Feng, J., Gallie, A., & Sánchez-Azofeifa, A. (2008). Continuous wavelets for the improved use of spectral libraries and hyperspectral data. *Remote Sensing of Environment, 112*, 2850-2862.

Rock, B.N., Vogelmann, J.E., Williams, D.L., Vogelmann, A.F. & Hoshizaki, T. (1986). Remote detection of forest damage. *Bioscience, 36*, 439-445.

Sánchez-Azofeifa, G. A., Castro, K., Wright, S. J., Gamon, J., Kalacska, M., Rivard, B., Schnitzer, S. A. & Feng, J. L. (2009). Differences in leaf traits, leaf internal structure, and spectral reflectance between two communities of lianas and trees: Implications for remote sensing in tropical environments. *Remote Sensing of Environment, 113*, 2076-2088.

Shi, W., Zhu, C., Zhu, C., & Yang, X. (2003). Multi-band wavelet for fusing SPOT panchromatic and multispectral images. *Photogrammetric Engineering and Remote Sensing, 69*, 513-520.

Sims, D. A., & Gamon, J. A. (2002). Relationships between leaf pigment content and spectral reflectance across a wide range of species, leaf structures and developmental stages. *Remote Sensing of Environment, 81*, 337-354.

Sims, D. A., & Gamon, J. A. (2003). Estimation of vegetation water content and photosynthetic tissue area from spectral reflectance: A comparison of indices based on liquid water and chlorophyll absorption features. *Remote Sensing of Environment, 84*, 526-537.

Tian, Q., Tong, Q., Pu, R., Guo, X., & Zhao, C. (2001). Spectroscopic determination of wheat water status using 1650-1850 nm spectral absorption features. *International Journal of Remote Sensing, 22*, 2329-2338.

Torrence, C., & Compo, G. P. (1998). A practical guide to wavelet analysis. *Bulletin of the American Meteorological Society, 79*, 61-78.

Tucker, C. J. (1980). Remote sensing of leaf water content in the near infrared. *Remote Sensing of Environment, 10*, 23-32.

Unser, M., & Aldroubi, A. (1996). A review of wavelets in biomedical applications. *Proceedings of the IEEE, 84*, 626-638.

Venables, W. N. and Ripley, B. D. (2002) Modern Applied Statistics with S. Fourth edition. Springer.

Zhang, J., Rivard, B., Sánchez-Azofeifa, A., & Castro-Esau, K. (2006). Intra- and inter-class spectral variability of tropical tree species at La Selva, Costa Rica: Implications for species identification using HYDICE imagery. *Remote Sensing of Environment, 105*, 129-141.

Zhang, Y., & Hong, G. (2005). An IHS and wavelet integrated approach to improve pan-sharpening visual quality of natural colour IKONOS and QuickBird images. *Information Fusion, 6,* 225-234.

Zhou, J., Civco, D. L., & Silander, J. A. (1998). A wavelet transform method to merge Landsat TM and SPOT panchromatic data. *International Journal of Remote Sensing, 19,* 743-757.

Zhou, W., Wang, S., Zhou, Y., & Troy, A. (2006). Mapping the concentrations of total suspended matter in Lake Taihu, China, using Landsat-5 TM data. *International Journal of Remote Sensing, 27,* 1177-1191.

Table 3-1. Summary of studies on the spectroscopic determination of leaf water content with a focus on LWC_D and LWC_F. The references are indexed by the year of publication and summarized with the species examined, the spectral range of the reflectance data, the analytical method, the expression of leaf water content, and the best result within each study. Note that the studies not related to LWC_D and LWC_F but only related to EWT are beyond the scope of this research and not listed.

Reference	Species	Spectral range (nm)	Method	Related to	Best accuracy
Curran et al., 1992	*Amaranthus tricolor*	400-2400	First derivative spectra	LWC_D (22.31-91.43 %)	R^2 = 0.45, RMSE = 15.9%
Peñuelas et al., 1997	5 species (from field) 8 species (potted seedlings)	390-1100	Spectral index WI	LWC_D LWC_D	R^2 = 0.31 R^2 = 0.49
Dawson et al., 1998	*Pinus elliottii*	400-2500	Artificial Netural Network	LWC_D (52-63 %)	R^2 = 0.86, RMSE = 1.3%
Datt, B., 1999	21 *Eucalyptus* species	400-2500	Spectral indices MSI, WI, $(R_{850} - R_{2218})/(R_{850} - R_{1928})$; $(R_{850} - R_{1788})/(R_{850} - R_{1928})$; NDWI and TM5/TM7	EWT (0.009-0.025 g/cm^2) LWC_F (40.8-71.7 %) LWC_D (70.4-221.5 %)	R^2 = 0.61 Not significant Not significant
Tian et al., 2001	winter wheat	350-2500	CR over 1650-1850 nm	LWC_F (39.62-80.12 %)	R^2 = 0.87
Pu et al., 2003	*Quercus agrifolia*	350-2500	CR centered at 975 nm, 1200 nm and 1750 nm; three-band ratio indices derived at 975 nm and 1200 nm	LWC_F (0.45-57.94 %)	R^2 = 0.86
Maki et al., 2004	*Nerium oleander var. indicum, Liriodendron tulipifera, Betula platyphylla*	400-2400	Spectral index: NDWI	EWT (0.002-0.138 g/cm^2) LWC_D (33.33-285.71 %)	R^2 = 0.62 R^2 = 0.08

Continued to Table 3-1

Reference	Species	Spectral range (nm)	Method	Related to	Best accuracy
Danson & Bowyer, 2004	subset of LOPEX Simulations with PROSPECT model	400-2500 400-2500	Spectral indices MSI, WI, NDWI, TM5/TM7 and GVMI	EWT (0.0003-0.0655 g/cm^2) LWC_D (9-1258 %) EWT (0.0425 $\pm$ 0.0142 g/cm^2) LWC_D (184 $\pm$ 101%)	R^2 = 0.88, N.L. R^2 = 0.54, N.L. R^2 = 0.88, N.L. R^2 = 0.78, N.L.
Riaño et al., 2005	37 species from LOPEX	400-2500	PROSPECT model inversion	EWT LWC_D	R^2 = 0.94 R^2 = 0.33
Stimson et al., 2005	*Pinus edulis* *Juniperus monosperma*	350-2300	CR based absorption indices at 970 nm and 1200 nm; red edge; spectral indices NDWI and NDVI	LWC_D (approx. 30-60 %) LWC_D (approx. 35-45 %)	R^2 = 0.71 R^2 = 0.50
Li et al., 2007	37 species from LOPEX	400-2500	Genetic Algorithm Partial Least Squares (GA-PLS)	EWT LWC_D	R^2 = 0.94, RMSE = 0.0017 g/cm^2 R^2 = 0.89, RMSE = 68.5%
Colombo et al., 2008	poplar trees	350-1800	Spectral indices WI, NDWI, SRWI, NDII, MSI, SR, $(R_{895} - R_{675})/(R_{895} + R_{675})$ PROSPECT model inversion	EWT (0.0091-0.0154 g/cm^2) LWC_D (110.65-217.64 %) EWT (0.0091-0.0154 g/cm^2) LWC_D (110.65-217.64 %)	R^2 = 0.52 R^2 = 0.25 R^2 = 0.65 R^2 = 0.00
Asner & Martin, 2008	162 tropical forest species	400-2500	PLS regression	LWC_F (43-79 %)	R^2 = 0.69, RMSE = 4%

CR: continuum removal; REIP: red edge inflection point

WI = R_{900}/R_{970}; MSI = R_{1600}/R_{820}; NDWI = $(R_{860} - R_{1240})/(R_{860} + R_{1240})$; GVMI = ((NIR + 0.1) – (SWIR + 0.02))/((NIR + 0.1) + (SWIR + 0.02))

NDVI = $(R_{860} - R_{690})/(R_{860} + R_{690})$; MDWI = $(R\max_{1500\text{-}1750} - R\min_{1500\text{-}1750})/(R\max_{1500\text{-}1750} + R\min_{1500\text{-}1750})$, SR = R_{895}/R_{675}, SRWI = R_{860}/R_{1240}

Table 3-2. Summary of water content measurements for 265 leaf samples collected from tropical forests in Panama.

Leaf water content	Mean	S.D.	Minimum	Maximum
LWC_D (%)	143.60	52.44	32.31	418.20
LWC_F (%)	57.23	8.62	24.42	80.70

Table 3-3. Spectral indices for predicting vegetation water content

Spectral index	Acronym	Formula	Reference
Water index	WI	$WI = \frac{R_{900}}{R_{970}}$	Peñuelas et al. (1993, 1997)
Normalized difference water index	NDWI	$NDWI = \frac{(R_{860} - R_{1240})}{(R_{860} + R_{1240})}$	Gao (1996)
Moisture stress index	MSI	$MSI = \frac{R_{1600}}{R_{820}}$	Hunt et al. (1987), Hunt & Rock (1989)

Table 3-4. Coefficients of determination (R^2) for correlations between water content and spectral metrics (wavelet features and spectral indices) derived from the calibration set (n = 159)

	LWC_D			LWC_F		
	Feature location			Feature location		
Feature code	Wavelength (nm)	Scale	R^2	Wavelength (nm)	Scale	R^2
A	2165	4	0.62***	2165	4	0.69***
B	1343	7	0.57***	1344	7	0.62***
C	1869	6	0.51***	1870	6	0.62***
D	1736	4	0.47***	1736	4	0.51***
E	2375	4	0.44***	2378	4	0.51***
F	2034	3	0.44***	2029	3	0.54***
G	1579	3	0.44***	1576	3	0.52***
H	2227	3	0.43***	2226	3	0.54***
I	combo = *A, B, C, D, E, F, (G, H)*	high & low	0.69***	combo = *A, B, D, E, F, H, (C, G)*	high & low	0.77***
J	combo = *A, D, F, (E)*	low	0.67***	combo = *A, D, E, H, (F)*	low	0.76***
K	combo = *B, C*	high	0.60***	combo = *B*	high	0.62***
L	MSI		0.05*	MSI		0.08**
M	NDWI		0.09***	NDWI		0.12***
N	WI		0.09***	WI		0.10***

LWC_D: leaf water content by dry mass; LWC_F: leaf water content by fresh mass. Scales were divided into two groups: high (6 and 7) and low (3 and 4). The features in brackets (e.g. *G* & *H* in *I*) were not included in the feature combination models because they were rejected during the stepwise regression procedure. Significance is: *p<0.005, **p<0.0005, ***p<0.0001.

Table 3-5. Wavelet features related to major absorptions of particular leaf biochemical constituents and obtained for LWC_D using the calibration set

Feature	Related to
(2165, 4)	Protein @2172 nm
(1343, 7)	Water @ 1400 nm
(1869, 6)	Water @ 1940 nm
(1736, 4)	Lignin, cellulose @ 1730 nm
(2375, 4)	Cellulose, protein @ 2350 nm
(2034, 3)	Protein @ 2054 nm
(1579, 3)	Not attributable
(2227, 3)	Not attributable

* Information on wavelengths of absorption features is from Curran (1989), Kokaly (2001) and Kokaly & Clark (1999).

Table 3-6. Coefficient of determination (R^2) and RMSE values comparing the measured water content with that estimated from the predictive models applied to the validation set (*n* = 106).

	LWC_D				LWC_F				LWC_D inverted from LWC_F	
Feature code	Feature location		Accuracy		Feature location		Accuracy		Accuracy	
	WL (nm)	Scale	R^2	RMSE (%)	WL (nm)	Scale	R^2	RMSE (%)	R^2	RMSE (%)
A	2165	4	0.66	28.34	2165	4	0.68	4.86	0.70	26.53
B	1343	7	0.60	30.69	1344	7	0.62	5.28	0.64	29.26
C	1869	6	0.55	32.62	1870	6	0.64	5.20	0.60	30.79
D	1736	4	0.48	35.22	1736	4	0.50	6.07	0.52	33.60
E	2375	4	0.44	36.51	2378	4	0.47	6.27	0.43	36.88
F	2034	3	0.45	36.06	2029	3	0.50	6.09	0.47	35.56
G	1579	3	0.46	35.91	1576	3	0.51	6.02	0.45	36.02
H	2227	3	0.44	36.45	2226	3	0.51	6.05	0.43	36.74
I	combo = *A, B, C, D, E, F*	high & low	0.71	26.04	combo = *A, B, D, E, F, H*	high & low	0.75	4.34	0.78	23.04
J	combo = *A, D, F*	low	0.69	26.91	combo = *A, D, E, H*	low	0.73	4.47	0.76	23.91
K	combo = *B, C*	high	0.64	29.30	combo = *B*	high	0.62	5.28	0.64	29.26

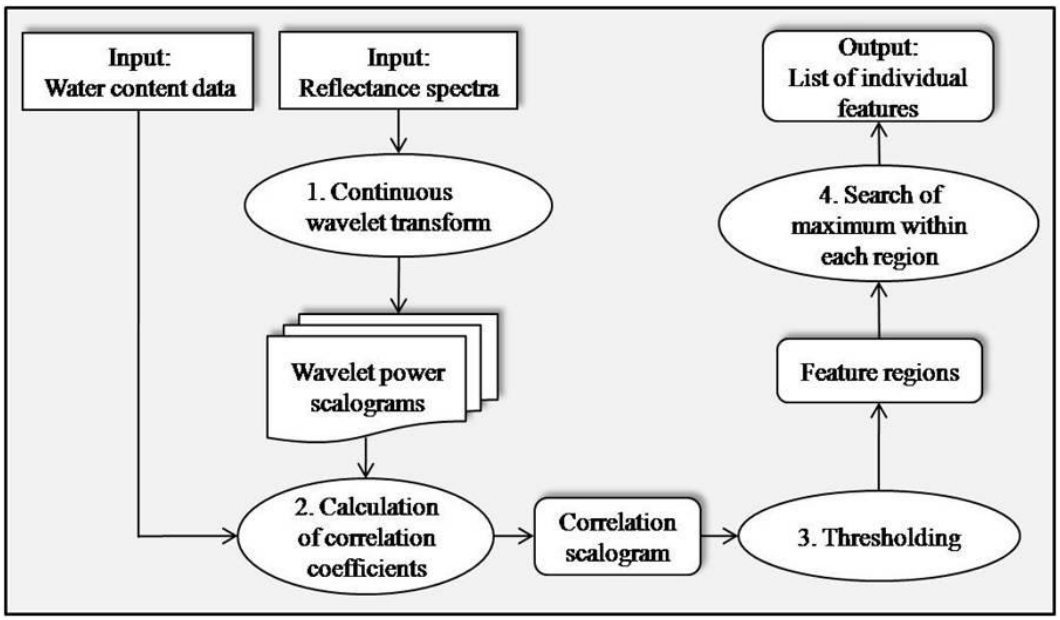

Fig. 3-1. Schematic representation of the feature extraction method using continuous wavelet analysis. Input data sets include the water content and reflectance measurements of leaf samples. Output is a list of wavelet features extracted for the estimation of leaf water content.

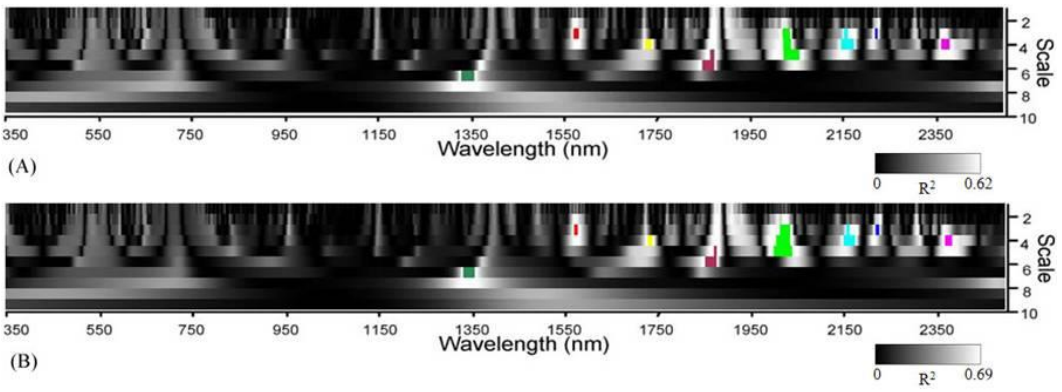

Fig. 3-2. Feature regions extracted from the correlation scalograms relating wavelet power with water content expressed on the basis of (A) dry mass (LWC_D) and (B) fresh mass (LWC_F) in the calibration dataset (n = 159).

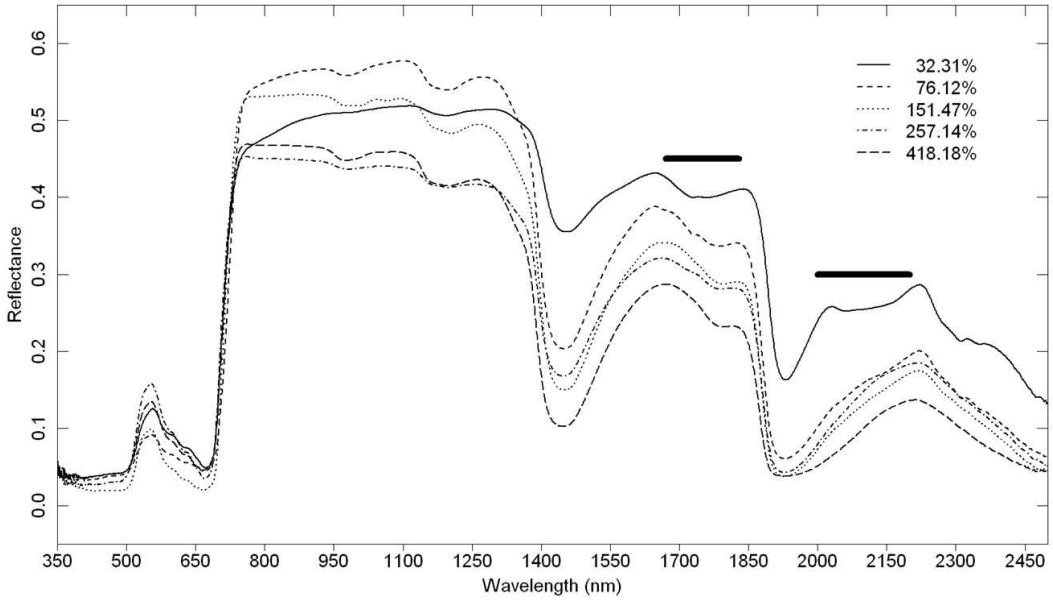

Fig. 3-3. Example spectra illustrating the effect of different amounts of LWC_D on the reflectance response. Note the change in the amplitude of reflectance in the 1300–2500 nm region and the variations in depth and shape of the absorption features in the wavelength regions 1670–1830 nm and 2000–2200 nm (denoted by the horizontal bars) as LWC_D changes from the minimum (32.31%) to the maximum (418.18%) value.

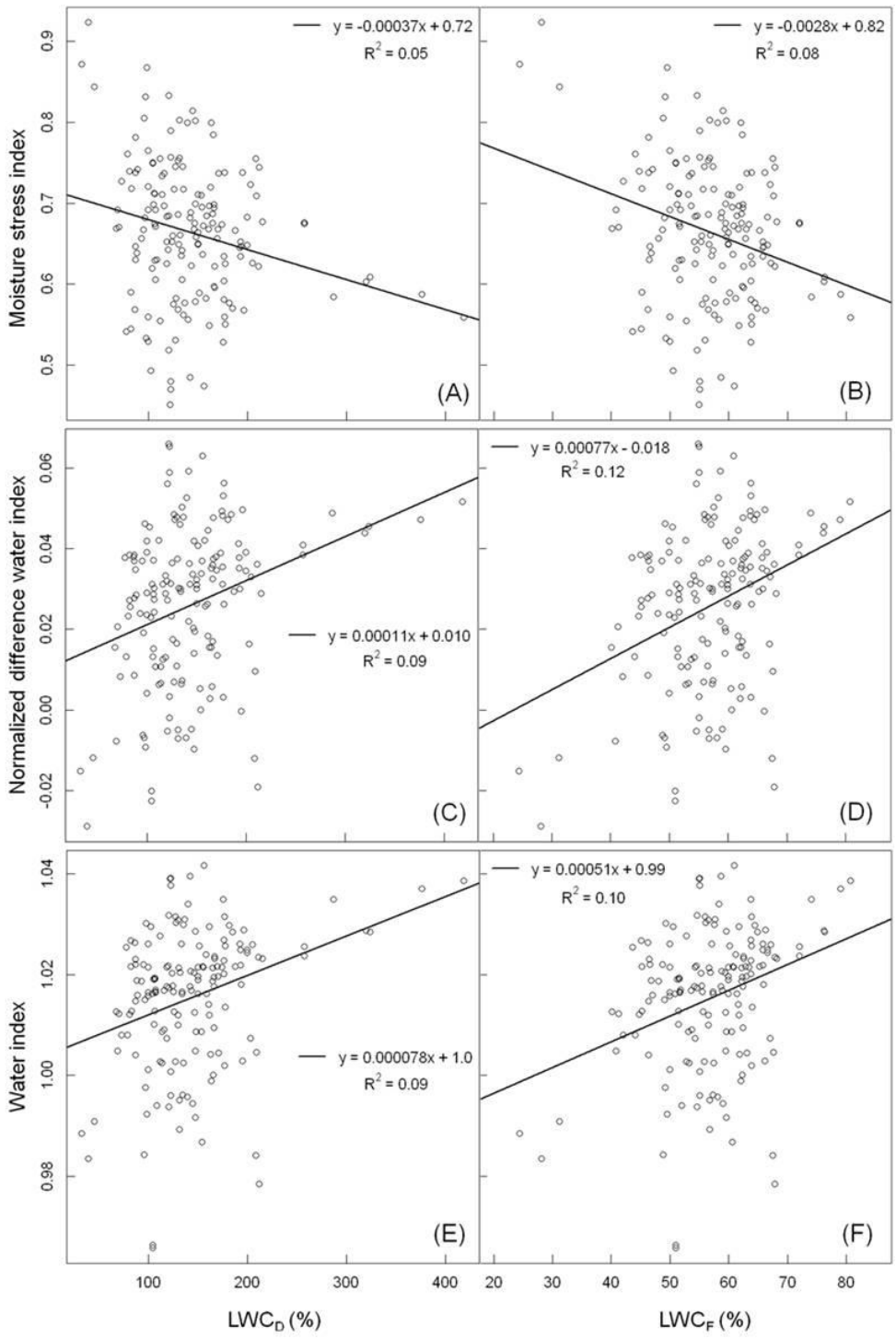

Fig. 3-4. Relationships between water content and spectral indices calculated from the calibration set. Rows represent the same spectral indices. The left column is for LWC_D and the right column for LWC_F. All relationships are statistically significant (p<0.005).

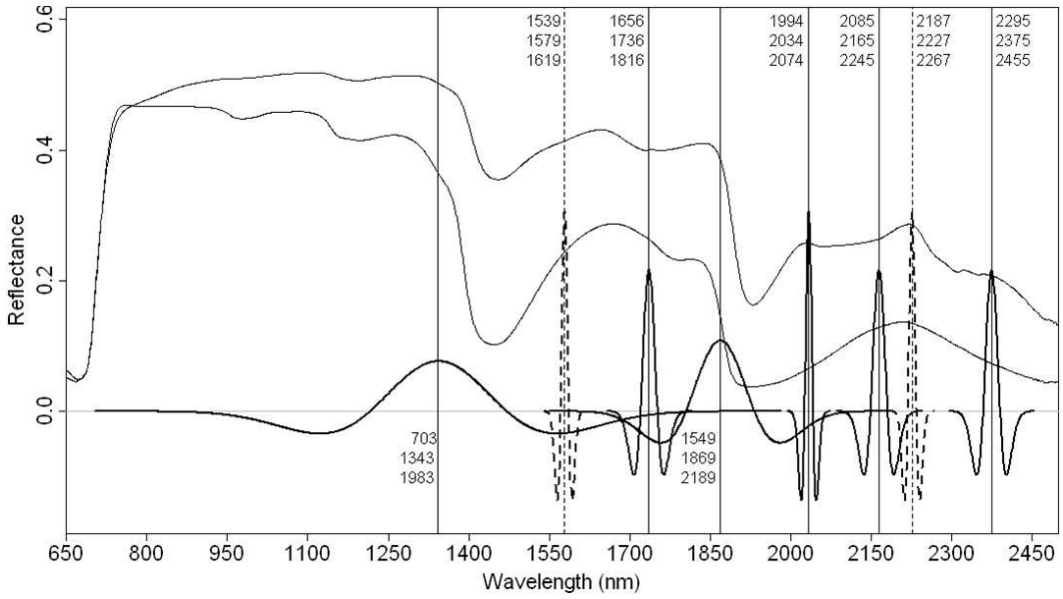

Fig. 3-5. Wavelength location of wavelet features indicated by vertical lines and the corresponding wavelets. The two reflectance spectra are associated with highest (top) and lowest (bottom) LWC_D. Each wavelet feature is positioned on the spectra with the scaled and shifted continuous wavelet used to compute the wavelet power. The three numbers beside each vertical line are wavelengths of start, center and end points of the wavelet. The two dashed vertical lines denote two features which are removed during the stepwise multiple regression procedure.

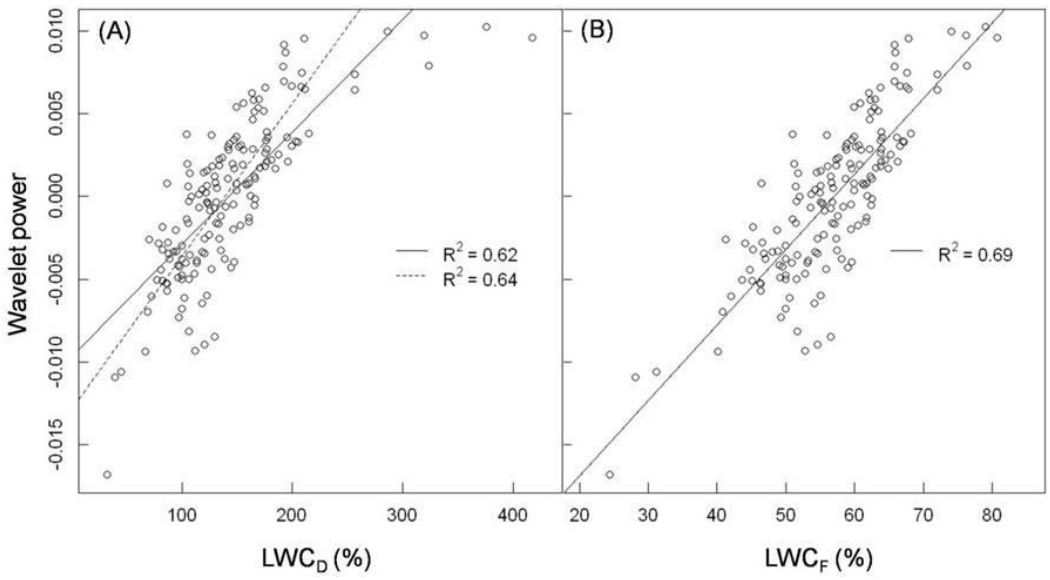

Fig. 3-6. Relationships between the wavelet power at (2165 nm, 4) and water content (A) LWC_D and (B) LWC_F established with the calibration data set (p<0.0001). The solid lines are for the entire data set and the dashed line in (A) is for a subset excluding observations of LWC_D above 250%.

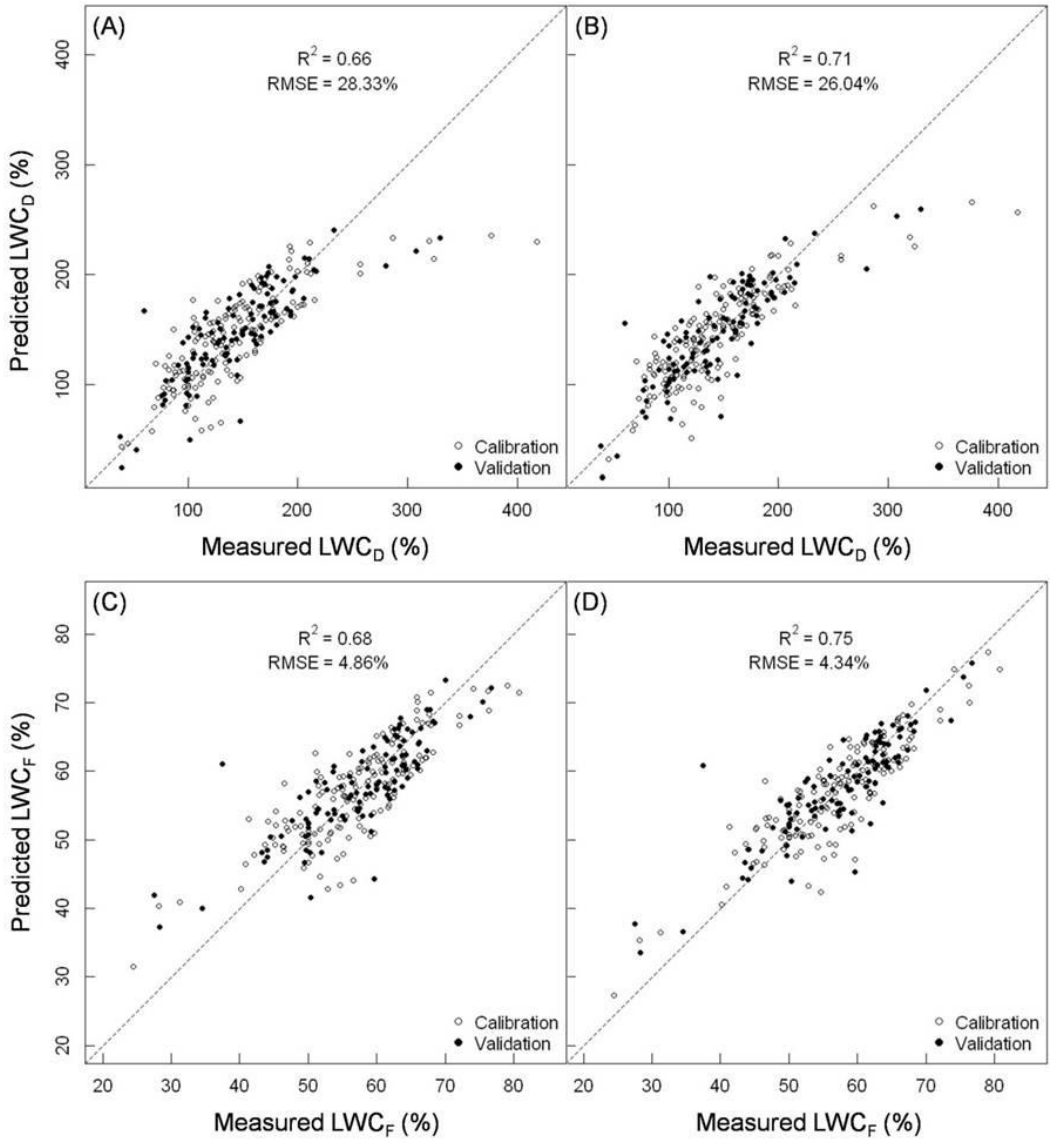

Fig. 3-7. (A) and (B) are plots of measured versus predicted water contents LWC_D using wavelet feature (2165, 4) and a combination of six features (I, Table 3-6), respectively. (C) and (D) are plots of measured versus predicted LWC_F using wavelet feature (2165 nm, 4) and a combination of six features, respectively. The predictive R^2 and RMSE values shown are obtained for the validation set. Dashed lines are 1:1 lines.

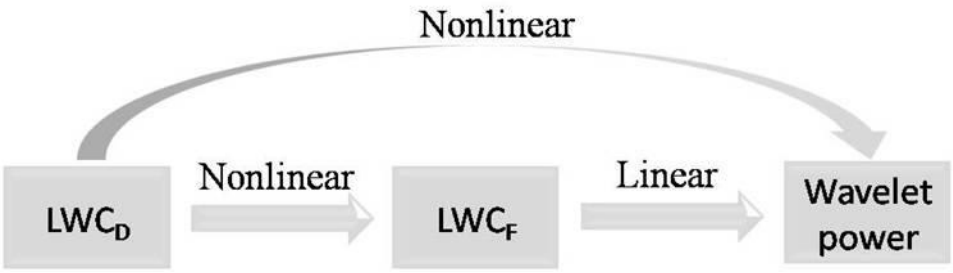

Fig. 3-8. Inter-relationships between wavelet power, LWC_D, and LWC_F.

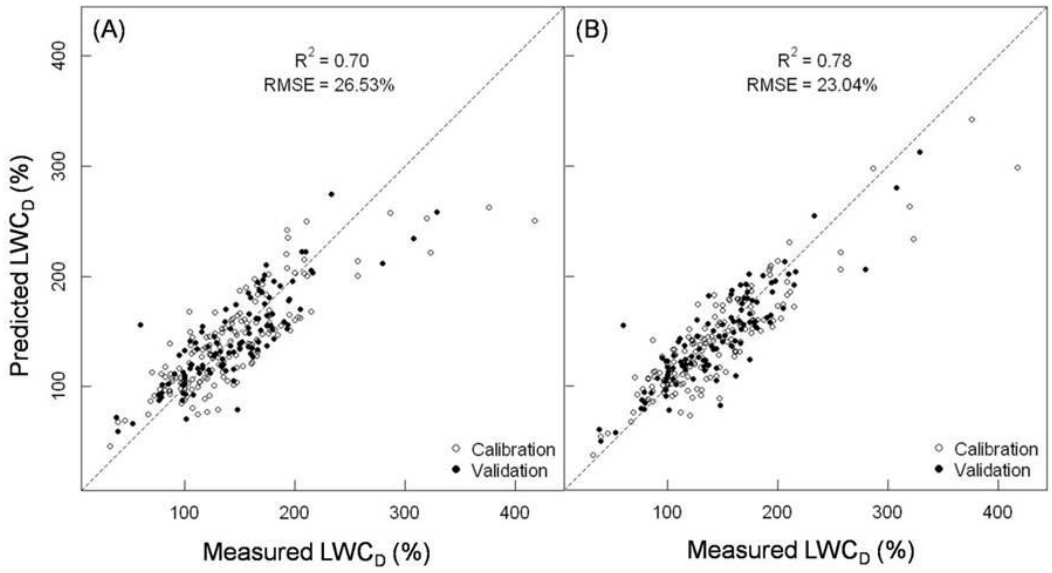

Fig. 3-9. Measured versus predicted LWC_D transformed from LWC_F estimates presented in Fig. 3-7 C and D. Note the differences as compared to the upper plots in Fig. 3-7.

CHAPTER 4 – EVALUATION OF THE PROSPECT MODEL AND CONTINUOUS WAVELET ANALYSIS FOR EFFICIENT ESTIMATION OF LEAF WATER CONTENT[4]

4.1. Introduction

Over the last two decades, laboratory and imaging spectroscopy data have been extensively used to estimate chemical constituents (e.g., chlorophyll, water, nitrogen) in vegetation in response to the need for information on vegetation chemistry (Asner & Vitousek, 2005; Curran et al., 2001; Kokaly & Clark, 1999; Peterson et al., 1988; Smith et al., 2002). In particular, the accurate retrieval of vegetation water content is crucial to the assessment of plant physiological status (Peñuelas et al., 1997; Pu et al., 2004; Stimson et al., 2005), to the determination of wildfire risk (Chuvieco et al., 2002; Dennision & Moritz, 2009; Dennison et al., 2008; Maki et al., 2004; Yebra et al., 2008) and as a critical leaf trait in ecological applications (Asner & Martin, 2008; Garnier & Laurent, 1994; Sánchez-Azofeifa et al., 2009).

A common measure of water content in leaves is the leaf gravimetric water content (GWC) which is defined as the amount of water as a percentage of dry mass or fresh mass (Datt, 1999). The detection of leaf GWC in the optical domain has been estimated based on the relationship between the reflectance at the 700-2500 nm and the abundance of water (Carter, 1991; Tucker, 1980). Many studies suggest that it is difficult to derive accurate estimates of GWC from leaf reflectance, particularly for a variety of species (Colombo et al., 2008; Danson & Bowyer, 2004; Datt, 1999; Li et al., 2007; Maki et al., 2004; Riaño et al., 2005).

Some studies have established strong relationships between leaf GWC and spectral indices that are designed to capture the spectral variation in water absorption features centered near 970 nm, 1200 nm, and 1450 nm (Danson &

[4] Thanks to Stéphane Jacquemoud, Jean-Baptiste Feret, and Christophe Francois for making the version 4 of the PROSPECT model available online (http://teledetection.ipgp.jussieu.fr/prosail/).

Bowyer, 2004; Peñuelas et al., 1997). Changes in leaf GWC may also be related to variations in reflectance associated with dry matter absorption features that are clearly discernable in the reflectance spectra of dry plants but obscured due to the presence of leaf water. Ceccato et al. (2001) have shown that leaves with different values of GWC are likely to have different amounts of dry mass (i.e., dry matter content) that directly affects the spectral reflectance in the shortwave infrared (SWIR) region. Tian et al. (2001) provided the only study that paid particular attention to the absorption features of dry matter in the 1650-1850 nm range in relation to leaf GWC. However, there has been no assessment of the relative merits of dry matter and water absorption features over the entire SWIR region for the purpose of leaf GWC estimation.

Continuous wavelet analysis (CWA) is an emerging spectral analysis tool for decomposing leaf reflectance spectra into a number of scale components. CWA provides an effective way to examine all absorption features in leaf reflectance at various scales (Blackburn & Ferwerda, 2008). The use of CWA also makes it possible to extract wavelet features (coefficients) that capture useful spectral information pertinent to leaf water (Cheng et al., 2010). In Chapter three, CWA was applied to measured leaf reflectance spectra from a collection of tropical forest species and models for the prediction of leaf GWC were presented. Using this methodology, a number of wavelet features were extracted from leaf reflectance spectra and used to derive accurate estimates of leaf GWC. In this study, I conduct a comparative assessment of the CWA method when applied to a leaf spectral database simulated with the PROSPECT leaf radiative transfer model.

The radiative transfer model PROSPECT has been successfully used to design or evaluate vegetation indices (Ceccato et al., 2002; Haboudane et al., 2002) and develop inversion approaches (Demarez et al., 1999; Jacquemoud et al., 1996; Zarco-Tejada et al., 2003), to retrieve vegetation properties from remotely sensed reflectance. The principal aim of this study is to evaluate the performance of the wavelet-based methodology for the estimation of leaf GWC using spectra simulated with PROSPECT and to determine whether the wavelet

features derived from the simulated spectra are consistent with those obtained in Chapter three from the measured spectra. A secondary objective of this study is to assess the ability of the PROSPECT model to simulate leaf reflectance for a range of Mesoamerican tropical forest species. Few studies have evaluated the performance of PROSPECT against experimental data (Feret et al., 2008; Jacquemoud et al., 1996; Jacquemoud et al., 2000; le Maire et al., 2004).

4.2. Materials and methods

4.2.1. Description of leaf reflectance and mass measurements

Leaf samples were collected from two tropical forest sites in the Republic of Panama. The first site is located in the dry forest of Parque Natural Metropolitano (PNM) near the Pacific coast and the second site in the wet forest of Fort Sherman (FS) on the Caribbean coast. The PNM forest experiences a severe dry season from mid-December to the end of April and has an annual rainfall of about 1,740 mm. The FS forest experiences a mild dry season from January to March and has an annual rainfall of about 3300 mm. Construction cranes owned by the Smithsonian Tropical Research Institute (STRI) at both sites allow flexible access to the top of the canopy and convenient collection of leaf samples (Castro-Esau et al. 2004).

In March 2007, 265 leaf samples were collected from twenty-three species of lianas and eight species of trees at PNM and from eight species of lianas and eight species of trees at FS. All samples consisted of sun leaves. Protocols for leaf clipping and handling presented in Sánchez-Azofeifa et al. (2009) were followed to prepare for reflectance and leaf mass measurements. The reflectance of leaves was recorded from 350 to 2500 nm with a FieldSpec® FR spectroradiometer (ASD Inc., Boulder, CO, USA) that provides a spectral resolution of 3 nm at 700 nm, 10 nm at 1500 nm and 10 nm at 2100 nm. Three reflectance measurements were taken per leaf with an ASD leaf clip covering a halogen bulb illuminated area with a radius totaling 10 mm. The mean of the three reflectance measurements provided a representative reflectance spectrum for each leaf. Five

or ten leaf samples were measured per species. For each leaf, the wet weight was determined within one hour after clipping and the dry weight was obtained from the sample after a three-day drying process at 60^{o}C. Leaf water content was then estimated using the wet weight and the dry weight.

4.2.2. Simulation of leaf reflectance with the PROSPECT model

4.2.2.1. Principle of the PROSPECT model

PROSPECT is a radiative transfer model that describes the leaf optical properties from 400 nm to 2500 nm (Jacquemoud & Baret, 1990). With a new version of the model (PROSPECT-4, Feret et al., 2008), leaf reflectance spectra can be simulated at 1nm steps with four input parameters: leaf structure *N*, leaf chlorophyll *a+b* concentration (C_{a+b}), equivalent water thickness (C_w), and dry matter content (C_m). All parameters can be measured from leaves except *N*. The model considers a leaf to consist of *N* stacked elementary homogeneous layers that account for leaf internal scattering and absorption by specific biochemical constituents. Therefore, *N* affects the reflectance in the entire spectral range with a dominant influence in the near-infrared (NIR) region. C_{a+b} mainly controls spectral variation in the visible and NIR regions, while C_w coupled with C_m affects the reflectance in the NIR and SWIR regions. As described below, chlorophyll concentration was kept constant for the simulations of this study. As a physically based model, PROSPECT is commonly used to represent leaf optical properties for specific ecosystems based on a range of parameter values that are site specific (Danson & Bowyer, 2004; Yebra et al., 2008; Yebra & Chuvieco, 2009).

4.2.2.2. Parameterization for the simulations

Simulations of leaf reflectance spectra were conducted as part of two experiments. In the first experiment, the simulation of reflectance for each leaf sample was optimized to match the measured reflectance spectrum. Measurements of C_w and C_m for each leaf were used to optimize *N* during simulations. From this experiment, I estimated the range of *N* values necessary to

simulate all spectral measurements and assessed the performance of PROSPECT to simulate the reflectance measurements from tropical leaves. In the second experiment, leaf reflectance spectra were simulated for a range of input parameters and used to test the wavelet-based method for the estimation of leaf GWC.

- ***Experiment I:*** *simulation of the measured leaf reflectance*

The first experiment aimed to simulate the measured reflectance from 800 to 2500 nm (n=265). To constrain the simulation, C_w and C_m were obtained from the measured leaves and C_{a+b} was kept at a constant value of 33 μg/cm^2 (Ceccato et al., 2001). For each observation, a number of simulations were conducted by varying N from a value of 1 to 4 at increments of 0.1. The optimal N value for each leaf was taken as the value that minimized the Euclidean distance between the measured spectrum and the simulated spectrum. The N values determined in this experiment were then used to constrain the range of N values utilized in the second experiment. The overall ability of PROSPECT to model the observed leaf reflectance was evaluated using the root mean square error (RMSE) per wavelength defined as follows:

$$RMSE(\lambda) = \sqrt{\frac{\sum_{i=1}^{n}(\rho_i(\lambda)_{measured} - \rho_i(\lambda)_{simulated})^2}{n}} \quad (4\text{-}1)$$

where $\rho_i(\lambda)_{measured}$ and $\rho_i(\lambda)_{simulated}$ are the measured and simulated reflectance values at wavelength λ for sample i, respectively.

- ***Experiment II:*** *simulation of leaf spectra for the estimation of leaf GWC*

In the second experiment, a total of 530 simulations were conducted using a combination of input values for each of the four PROSPECT parameters. The outcome was a spectral database twice as large as that of the measured spectra (n=265). The simulated spectral database was divided into two portions, with 60% of the data being used to develop predictive models for the estimation of leaf GWC and 40% to validate the predictive models. For each simulation C_{a+b} was kept at a constant value of 33 μg/cm^2 and N, C_w and C_m were randomly selected

from uniform distributions within specific data ranges. The measured ranges of C_w and C_m values were used and the range of N value was set to that obtained in Experiment *I*. A summary of all parameters is provided in Table 4-1. For each simulation, GWC was computed as follows on the basis of dry weight (LWC_D) and fresh weight (LWC_F):

$$LWC_D = \frac{C_w}{C_m} \times 100\% \quad (4\text{-}2)$$

$$LWC_F = \frac{LWC_D}{100\% + LWC_D} \times 100\% \quad (4\text{-}3)$$

In Chapter three I was able to obtain more accurate estimates of LWC_F than LWC_D. Estimates of LWC_D can be determined from estimates of LWC_F using the following equation:

$$LWC_D = \frac{LWC_F}{100\% - LWC_F} \times 100\% \quad (4\text{-}4)$$

A summary of the LWC_F values measured for the 265 leaf samples and calculated for the 530 simulated leaf reflectance spectra is shown in Fig. 4-1.

4.2.3. Feature extraction from wavelet analysis to estimate leaf GWC

4.2.3.1. Wavelet analysis

Wavelet analysis is a useful mathematical tool that provides a way to analyze spectral signatures at various scales by decomposing the original data into multiple scale components (Bruce et al., 2001; Kaewpijit et al., 2003; Mallat, 1989; Rivard et al., 2008). In particular, wavelet analysis of hyperspectral data has proven to be effective for a variety of vegetation studies such as forest species identification (Kalácska et al., 2007; Zhang et al., 2006), biochemical/biophysical parameter estimation (Blackburn, 2007; Blackburn & Ferwerda, 2008; Ferwerda & Jones, 2006; Pu & Gong, 2004) and stress detection (Cheng et al., 2010).

Wavelet transforms include the discrete wavelet transform (DWT) and the continuous wavelet transform (CWT) (Blackburn & Ferwerda, 2008; Bruce et al., 2001). The latter is adopted in this study because each scale component is directly comparable to the input reflectance spectrum (Bruce et al., 2001; Du et al., 2006). In addition, CWT is able to provide valuable information pertinent to the shape

and position of spectral features in leaf reflectance spectra (Blackburn & Ferwerda, 2008).

4.2.3.2. Continuous wavelet transform (CWT)

The CWT is a linear operation that uses a mother wavelet function $\psi_{a,b}(\lambda)$ to convert a reflectance spectrum $f(\lambda)$ into sets of coefficients based on the following equation (Mallat, 1991):

$$W_f(a,b) = \langle f, \psi_{a,b} \rangle = \int_{-\infty}^{+\infty} f(\lambda)\, \psi_{a,b}^*(\lambda) d\lambda \qquad (4\text{-}5)$$

where $\psi_{a,b}^*(\lambda)$ is the *complex conjugate* of $\psi_{a,b}(\lambda)$[5]. a and b are positive real numbers with the scaling factor a defining the width of a continuous wavelet and the shifting factor b defining the position. The magnitude of a wavelet coefficient, also referred to as *wavelet power*, denotes the correlation between a scaled and shifted version of the mother wavelet and a spectral segment of the input spectrum. The scale components are of the same length and are suited to characterize absorption features of various widths.

In order to detect the absorption features attributable to leaf water and dry matter, the second derivative of Gaussian (DOG), also known as the Mexican Hat, was used as the mother wavelet basis (Torrence & Compo, 1998; Cheng et al., 2010). The effective support range of the Mexican Hat is [-5, 5] for the scale a=1 and [-5a_1, 5a_1] for a=a_1 (Du et al., 2006). The width of a scaled wavelet (10a_1) determines the number of input wavebands that are to be convolved with the wavelet and attributed to the wavelet coefficient. To reduce the data volume, the CWT was performed at dyadic scales 2^1, 2^2, 2^3, ..., and 2^8. Those scales were labeled as scales 1, 2, 3, …, and 8 and were comparable to the scales described in relevant studies by Blackburn & Ferwerda (2008) and Rivard et al. (2008). For the PROSPECT-simulated reflectance spectra, 1701 wavebands were available (800-2500 nm). Any scale greater than 2^8=256 was discarded as they were not observed to carry meaningful spectral information (Cheng et al., 2010). All CWT

[5] Note that *complex conjugation* changes the function only if a complex wavelet function such as Morlet function is used. The derivatives of Gaussian function are real functions.

operations were conducted using the IDL 6.3 Wavelet Toolkit (ITT Visual Information Solutions, Boulder, CO, USA).

4.2.3.3. Feature selection from correlation scalograms

Four procedural steps were involved to define spectral features that significantly correlated with LWC_F. A brief description of the procedure is provided in this section and readers are referred to Chapter three for further detail. Firstly, CWT was applied to each of the reflectance spectra simulated in Experiment *II* to generate a wavelet power scalogram representing the wavelet power as a function of wavelength and scale. Secondly, a correlation scalogram was constructed by establishing the Pearson's correlation for each element of the wavelet power scalograms and LWC_F across all simulations. The correlation scalogram formed a feature set from which wavelet features most sensitive to LWC_F could be selected. Thirdly, features with the least statistically significant R^2 (p>=0.05) values were discounted. The remaining features were sorted in descending order of R^2 and a R^2 cut-off value was applied to retain the 1% features that most strongly correlated to LWC_F. This process delineated a number of feature regions on the correlation scalogram. As a last step, the feature with the maximum R^2 within each feature region was selected and expressed as (*wavelength* in nm, *scale*). This feature selection approach resulted in a small number of wavelet features that were sparsely distributed on the correlation scalogram and capable of capturing the most important information with respect to changes in LWC_F.

4.2.4. Calculation of spectral indices

The wavelet-based method was compared to three spectral indices reported in the literature and designed to estimate vegetation water content from remotely sensed reflectance were calculated. The water index (WI), originally developed to relate LWC_D with leaf reflectance in narrow wavebands, is formulated as follows (Peñuelas et al., 1993, 1997):

$$WI = \frac{R_{900}}{R_{970}} \quad (4\text{-}6)$$

The moisture stress index (MSI) was developed using Landsat TM bands TM4 and TM5 (Hunt et al., 1987) and tested with high spectral resolution data. MSI was calculated using the following equation (Hunt & Rock, 1989):

$$MSI = \frac{R_{1600}}{R_{820}} \quad (4\text{-}7)$$

The normalized difference water index (NDWI) was designed by Gao (1996) to remotely sense the EWT from space and was originally formulated using two narrow wavebands from MODIS imagery as follows:

$$NDWI = \frac{(R_{860} - R_{1240})}{(R_{860} + R_{1240})} \quad (4\text{-}8).$$

4.3. Results

4.3.1. Experiment I: simulation of the measured leaf reflectance

Fig. 4-2A shows a summary of leaf reflectance for measured and simulated spectra. The shape of the mean reflectance spectra and deviations to the mean for the two data sets is similar in the entire spectral range with exception for the 800-900 nm region. For the 900 to 2500 nm region, of interest for estimating leaf water content, the spectral RMSE was less than 0.03, indicating a very good agreement between the simulated and measured leaf reflectance spectra (Feret et al., 2008; Jacquemoud et al., 1996; Jacquemoud et al., 2000) (Fig. 4-2B).

Specifically, the globally lowest RMSE of 0.006 was observed at 1370 nm on the leading edge (1310-1386 nm) of a broad water absorption region where PROSPECT performed best. Two other spectral regions at 1660-1780 nm and 2130-2230 nm displayed locally low values in RMSE ($RMSE_{1702}$ = 0.009, $RMSE_{2159}$ = 0.020). These two regions denote absorption by dry matter. The following section shows that the three spectral regions carry considerable spectral information sensitive to changes in LWC_F.

4.3.2. Experiment II: simulation of leaf spectra for the estimation of leaf GWC

4.3.2.1. Feature regions determined from the correlation scalogram

Six feature regions that correlate with leaf water content were determined from the correlation scalogram (Fig. 4-3). All feature regions were located in the SWIR region (1300-2500 nm) and the largest extended from 1692 nm to 1748 nm across scale 3 to 5. The spatial pattern of the feature regions was highly uneven, with the largest region encompassing 81.36% of the features (96 of 118 features) and the remaining five regions encompassing 18.64%.

4.3.2.2. Wavelet features most strongly correlated to LWC_F

Six wavelet features (one per feature region) were identified and shown to be strongly sensitive to LWC_F (Table 4-2). The R^2 value of the linear regression for each feature was high (R^2 from 0.989 to 0.975). The difference in R^2 between the strongest (feature *A*) and weakest feature (feature *F*) was only 0.014. All features except feature *F* (scale 7) are observed in low scales (scales 3 and 4). Feature *D* (1802 nm) is spectrally redundant with feature *C* (1800 nm) given the spectral uncertainties of the spectrometer used in the SWIR region.

Fig. 4-4A displays the wavelength and scale of the five distinct wavelet features. These are shown with reflectance spectra for the lowest (16.80%) and highest LWC_F (85.57%). The low-scale features occurred in two spectral regions where leaf dry matter (e.g., protein, lignin, cellulose) constituents produce broad and overlapping absorption features (Curran, 1989). In response to changes in LWC_F, four of the low-scale features captured spectral variation in the 1660-1820 nm range that is primarily influenced by the presence of lignin and cellulose in plants (Table 4-2). Feature *E* captured the spectral variation in the 2140-2220 nm range attributed to the presence of protein, lignin, and cellulose (Curran, 1989; Kokaly, 2001). Feature *F* (1337 nm, 7) occurred on the edge of a broad water absorption and was attributed to broader changes in the shape of reflectance spectra affected by changes in LWC_F.

4.3.2.3. Relative performance of wavelet features and spectral indices

Fig. 4-5 shows the regression model for the best performing wavelet feature (1740nm, 4) and the comparison between measured and predicted LWC_F values derived from the model. The relationship between measured LWC_F and wavelet power at this feature is strongly linear. Similarly strong linear relationships were observed for all features in Table 4-2.

When the regression model for each feature is applied to the validation set for the prediction of LWC_F, the ranking of R^2 for the six feature (Table 4-3) is almost the same as that obtained for the calibration set (Table 4-2). The accuracy for the estimation of LWC_F based on the six wavelet features ranged from RMSE values of 1.58% (R^2 = 0.988) to 2.37% (R^2 = 0.974) (Table 4-3). A model based on the combination of the five low-scale features predicted LWC_F with the same accuracy as the combination of all features (R^2 = 0.990, RMSE = 1.46%), whereas the model based on the high-scale feature resulted in a lower accuracy (R^2 = 0.974, RMSE = 2.37%). These accuracy values are higher than those reported in the literature (Asner & Martin, 2008). Fig. 4-6 compares the actual LWC_F for simulated spectra with LWC_F predicted using the combination of all features and the data were distributed more uniformly around the 1:1 line than that observed using the best performing individual feature (Fig. 4-5).

All three spectral indices yielded significantly less accurate estimates of LWC_F than wavelet features with the WI being the best performing index (Table 4-3). The calibration model obtained for WI displays a weaker correlation (R^2 = 0.575) (Fig. 4-7A) compared to that obtained for the best wavelet feature (Fig. 4-5A**)**. Using WI, LWC_F values of less than 35% appeared to be substantially overestimated (Fig. 4-7B) and the RMSE of the prediction was 7.65% higher than that for feature (1740 nm, 4) (RMSE=1.58%).

4.3.2.4. Transformation of LWC_F to LWC_D

To facilitate comparison with previous studies on LWC_D, LWC_F estimates were transformed to LWC_D using Eq. (4-4). For this purpose I used LWC_F predicted with the best performing wavelet feature (1740nm, 4) and the

combination of six wavelet features (Table 4-3). The accuracy of LWC_D estimated using feature (1740nm, 4) (Fig. 4-8A, R^2 = 0.933, RMSE = 25.07%) and the combination of the six features (Fig. 4-8B, R^2 = 0.950, RMSE = 21.70%) were higher than that reported for PROSPECT simulated spectra (Danson & Bowyer, 2004) and LOPEX data (Danson & Bowyer, 2004; Li et al., 2007; Riaño et al., 2005). The LWC_D estimates compare well with the actual values at low values but the comparison degrades with increasing values of LWC_D (Fig. 4-8). Such a pattern was not observed for predicted LWC_F (Figs. 4-5, 4-6).

4.4. Discussion

This study introduces a wavelet-based methodology applied to simulated reflectance spectra to achieve accurate estimates of both measures of leaf GWC (LWC_F or LWC_D). This method is effective to extract spectral information indicative of changes in leaf GWC and differs from that reported in related studies (Asner & Martin, 2008; Danson & Bowyer, 2004; Tian et al., 2001).

4.4.1. Advantages of the continuous wavelet analysis

As a response to changes in a leaf chemical, significant spectral variation tends to occur over particular absorption regions rather than at scattered individual wavelengths. The use of CWA provides a multiscale representation of input reflectance information and facilitates the analysis of all absorption features of various widths. The wavelet features are especially important for capturing variations in the shape of relevant spectral regions. Furthermore, the selection of optimal features from the entire correlation scalogram ensures that the significant spectral variation is captured regardless of its width and wavelength locations. In contrast, spectral indices simply use a small number of wavebands to characterize the leaf water-induced spectral variation over a broad range, which explains their poorer performance.

Empirical relationships between leaf GWC and the reflectance at water absorption bands have been employed to estimate leaf GWC (Danson & Bowyer,

2004; Peñuelas et al., 1997). For this purpose, little attention has been paid to date to the use of spectral regions recording light absorption by dry matter. Tian et al., (2001) examined the 1650-1850 nm dry matter absorption feature and found a strong relationship between continuum-removed reflectance spectra and GWC. The wavelet-based method of this study exploited a number of absorption features of dry matter in the SWIR region, thereby emphasizing the important role of dry matter features in estimating GWC.

4.4.2. Comparison of wavelet features derived from the simulated spectra and the measured spectra

To compare the performance of the wavelet-based methodology across data sets, the procedures presented in Section 4.2.3 were also applied to the measured reflectance data set. The wavelet features derived are displayed in Fig. 4-4B and their predictive capabilities are summarized in Table 4-4. The PROSPECT-simulated spectra resulted in a smaller number of informative wavelet features that showed stronger capabilities to predict leaf GWC (Tables 4-3 & 4-4). Six significant features were extracted from the simulated spectra and eight were extracted from the measured spectra. The smaller number of features for the simulated spectra might be explained by a large feature region (Fig. 4-3) that accounted for a large portion of the top 1% features in the correlation scalogram.

Three features ((1740nm, 4), (2180nm, 3), (1337nm, 7)) determined from the simulated spectra were closely matched by features from the measured spectra ((1736nm, 4), (2165nm, 4), (1344nm, 7)). Interestingly, these similar wavelet features occurred in spectral regions where the simulated leaf reflectance was in good agreement with the measured reflectance (Fig. 4-2). Differences in the location of the remaining features between the two data sets cannot be explained at this time but may be related to the relatively lower accuracy of simulation in the remaining spectral regions.

4.4.3. Distribution of spectral information across scales

The most apparent spectral change for dehydrating leaves is the increase in reflectance throughout the 400-2500 nm range, with the most prominent increase occurring in the SWIR region (1300-2500 nm) (Aldakheel & Danson, 1997; Carter, 1991, Lee et al., 2007). Thus one might expect that changes in leaf GWC might be best captured by high-scale wavelet features in response to changes over broad spectral regions. However, the relative importance of high-scale features among all features for each data set was significantly different. Among the eight features derived from the measured spectra, two high-scale features ((1344nm, 7) & (1870nm, 6)) showed relatively strong correlations with leaf GWC, ranking immediately below the feature with the strongest correlation. This feature distribution across scales for the measured spectra is not unexpected. For the simulated spectra, the high-scale feature (1337nm, 7) provided the weakest correlation amongst the six features, which is unexpected.

The unexpectedly least important high-scale feature for the simulated data set might be explained by the difficulty in parameterizing the PROSPECT model in an appropriate way. The PROSPECT model provides a user with control of four input variables but random selections of each variable value can lead to unrealistic input combinations (Yebra & Chuvieco, 2009). N affects the spectral variation throughout the 800-2500 nm range, and it impacts variations in reflectance amplitude as GWC does (i.e., C_w and C_m) (Fig. 4-9). Usually, a leaf with low GWC would be accompanied by a high value of structural parameter N giving a reasonably high reflectance. Through random combinations of input variables, a low GWC value (derived from C_w and C_m) can be assigned to any N in the defined range, resulting in an unrealistic combination. Fig. 4-10 illustrates some problematic spectra generated by unrealistic combinations of input variables. As LWC_F decreased from 83.65% to 67.47% (top to bottom in Fig. 4-10), the leaf reflectance should have increased in the infrared region but decreased due to the considerable influence of N. In our simulation I did not fix N as doing so would have failed to represent leaf structural variations present in measured spectra. A large number of such problematic spectra resulting from unrealistic

parameter combinations might confound the link between GWC and spectral reflectance. At the very least, they may prevent high-scale wavelet features from capturing significant information on amplitude variation over a broad spectral region.

To reduce the risk of generating a large number of problematic spectra, further efforts could eliminate the simulations resulting from unrealistic combinations of N, C_w and C_m by applying a filter criterion based on the empirical relationships between input variables (Yebra et al., 2008). Alternatively, some conditions could be applied to constrain the combination of input parameters prior to simulation. Previous studies have kept all variables independent because no accurate information on the relationship between variables was available for a specific geographic site. To avoid the presence of site-specific information in the model, future versions of PROSPECT may need to incorporate more input variables to account for the interacting effect between the current variables.

This study suggests that the wavelet features derived for the estimation of leaf GWC are not sensitive to variability in N that represents the leaf structural variation for a wide range of tropical forest species. With the use of the wavelet-based methodology, the influence of variation in leaf structure was implicitly suppressed but never explicitly removed. This suppression is beneficial in tropical ecosystem studies for reducing the spectral variability that often changes significantly with species diversity (Castro-Esau et al., 2006).

4.5. Conclusions

The PROSPECT model was able to well represent the reflectance of leaves collected from Mesoamerican tropical forest environments and performed best while reconstructing the reflectance in three local regions (1310-1386 nm, 1660-1780 nm, and 2130-2230 nm). Using the wavelet-based method, six significant wavelet features were determined from the PROSPECT-simulated spectra and all were able to produce accurate estimates of leaf GWC. Three of

these features closely matched those obtained in Chapter three for the measured spectra. These recurrent features occurred in spectral regions where the leaf reflectance was best modeled by PROSPECT. It appears that these features may serve as robust and efficient predictors of leaf GWC for a broad variety of tropical forest species. Results from both the simulated spectra and measured spectra showed that low-scale features were reliable for the estimation of leaf water content but observations regarding the importance of high-scale features remain inconclusive.

This research provided a valuable opportunity to assess the ability of PROSPECT to simulate the spectral reflectance of Mesoamerican tropical forest species with particular considerations paid to their link to leaf water content. It also demonstrated the robustness of the wavelet-based methodology to extract meaningful spectral features in the wavelet domain through a modeling approach. The three wavelet features consistently determined from the simulated spectra and the measured spectra are thereby recommended to the reflectance spectroscopy community for efficient estimation of GWC at least as a supplement to spectral indices. If one is to design any GWC metric for a specific application without relation to wavelets, attention to the spectral regions covered by the wavelet features of this study is recommended.

4.6. References

Aldakheel, Y. Y., & Danson, F. M. (1997). Spectral reflectance of dehydrating leaves: Measurements and modelling. *International Journal of Remote Sensing*, 18, 3683-3690.

Asner, G. P., & Martin, R. E. (2008). Spectral and chemical analysis of tropical forests: Scaling from leaf to canopy levels. *Remote Sensing of Environment, 112*, 3958-3970.

Asner, G. P., & Vitousek, P. M. (2005). Remote analysis of biological invasion and biogeochemical change. *Proceedings of the National Academy of Sciences of the United States of America, 102*, 4383-4386.

Blackburn, G. A. (2007). Wavelet decomposition of hyperspectral data: A novel approach to quantifying pigment concentrations in vegetation. *International Journal of Remote Sensing, 28*, 2831-2855.

Blackburn, G. A., & Ferwerda, J. G. (2008). Retrieval of chlorophyll concentration from leaf reflectance spectra using wavelet analysis. *Remote Sensing of Environment, 112*, 1614-1632.

Bruce, L. M., Morgan, C., & Larsen, S. (2001). Automated detection of subpixel hyperspectral targets with continuous and discrete wavelet transforms. *IEEE Transactions on Geoscience and Remote Sensing, 39*, 2217-2226.

Carter, G. A. (1991). Primary and secondary effects on water content on the spectral reflectance of leaves. *American Journal of Botany, 78*, 916-924.

Castro-Esau, K. L., Sánchez-Azofeifa, G. A., Caelli, T. (2004). Discrimination of lianas and trees with leaf-level hyperspectral data. *Remote Sensing of Environment, 90*, 353-372.

Castro-Esau, K. L., Sánchez-Azofeifa, G. A., Rivard, B., Wright, S. J., & Quesada, M. (2006). Variability in leaf optical properties of mesoamerican trees and the potential for species classification. *American Journal of Botany, 93*, 517-530.

Ceccato, P., Flasse, S., & Grégoire, J. -M. (2002). Designing a spectral index to estimate vegetation water content from remote sensing data: Part 1: Theoretical approach. *Remote Sensing of Environment, 82*, 188-197.

Ceccato, P., Flasse, S., Tarantola, S., Jacquemoud, S., & Grégoire, J. -M. (2001). Detecting vegetation leaf water content using reflectance in the optical domain. *Remote Sensing of Environment, 77*, 22-33.

Cheng, T., Rivard, B., Sánchez-Azofeifa, G. A., Feng, J. & Calvo-Polanco, M. (2010). Continuous wavelet analysis for the detection of green attack due to mountain pine beetle infestation. *Remote Sensing of Environment, 114*, 899-910.

Chuvieco, E., Riaño, D., Aguado, I., & Cocero, D. (2002). Estimation of fuel moisture content from multitemporal analysis of Landsat Thematic Mapper reflectance data: Applications in fire danger assessment. *International Journal of Remote Sensing, 23*, 2145-2162.

Colombo, R., Meroni, M., Marchesi, A., Busetto, L., Rossini, M., Giardino, C., & Panigada, C. (2008). Estimation of leaf and canopy water content in poplar plantations by means of hyperspectral indices and inverse modeling. *Remote Sensing of Environment, 112*, 1820-1834.

Curran, P. J., Dungan, J. L., & Peterson, D. L. (2001). Estimating the foliar biochemical concentration of leaves with reflectance spectrometry: Testing the Kokaly and Clark methodologies. *Remote Sensing of Environment, 76*, 349-359.

Danson, F. M., & Bowyer, P. (2004). Estimating live fuel moisture content from remotely sensed reflectance. *Remote Sensing of Environment, 92*, 309-321.

Datt, B. (1999). Remote sensing of water content in *Eucalyptus* leaves. *Australian Journal of Botany, 47*, 909-923.

Demarez, V., Gastellu-Etchegorry, J. P., Mougin, E., Marty, G., Proisy, C., Dufrêne, E., et al. (1999). Seasonal variation of leaf chlorophyll content of a temperate forest. inversion of the PROSPECT model. *International Journal of Remote Sensing, 20*, 879-894.

Dennison, P. E., & Moritz, M. A. (2009). Critical live fuel moisture in chaparral ecosystems: A threshold for fire activity and its relationship to antecedent precipitation. *International Journal of Wildland Fire, 18*, 1021-1027.

Dennison, P. E., Moritz, M. A., & Taylor, R. S. (2008). Evaluating predictive models of critical live fuel moisture in the Santa Monica Mountains, California. *International Journal of Wildland Fire, 17*, 18-27.

Ferwerda, J. G., & Jones, S. (2006). Continuous wavelet transformations for hyperspectral feature detection. *Proceedings of the 12th International Symposium on Spatial Data Handling*, 12-14 July, University of Vienna, Austria.

Feret, J. -B., François, C., Asner, G. P., Gitelson, A. A., Martin, R. E., Bidel, L. P. R., Ustin, S. L., le Maire, G., & Jacquemoud, S. (2008). PROSPECT-4 and 5:

Advances in the leaf optical properties model separating photosynthetic pigments. *Remote Sensing of Environment, 112*, 3030-3043.

Gao, B. -C. (1996). NDWI - A normalized difference water index for remote sensing of vegetation liquid water from space. *Remote Sensing of Environment, 58*, 257-266.

Garnier, E., & Laurent, G. (1994). Leaf anatomy, specific mass and water content in congeneric annual and perennial grass species. *New Phytologist, 128*, 725-736.

Haboudane, D., Miller, J. R., Tremblay, N., Zarco-Tejada, P. J., & Dextraze, L. (2002). Integrated narrow-band vegetation indices for prediction of crop chlorophyll content for application to precision agriculture. *Remote Sensing of Environment, 81*, 416-426.

Hosgood, B., Jacquemoud, S., Andreoli, G., Verdebout, J., Pedrini, G., & Schmuck, G. (1995). *Leaf Optical Properties EXperiment 93 (LOPEX93)*, European Commission, Joint Research Centre, Institute for Remote Sensing Applications, Report EUR 16095 EN.

Hunt Jr., E. R., & Rock, B. N. (1989). Detection of changes in leaf water content using near- and middle-infrared reflectances. *Remote Sensing of Environment, 30*, 43-54.

Hunt Jr., E. R., Rock, B. N., & Nobel, P. S. (1987). Measurement of leaf relative water content by infrared reflectance. *Remote Sensing of Environment, 22*, 429-435.

Jacquemoud, S., & Baret, F. (1990). PROSPECT: A model of leaf optical properties spectra. *Remote Sensing of Environment, 34*, 75-91.

Jacquemoud, S., Ustin, S. L., Verdebout, J., Schmuck, G., Andreoli, G., & Hosgood, B. (1996). Estimating leaf biochemistry using the PROSPECT leaf optical properties model. *Remote Sensing of Environment, 56*, 194-202.

Kaewpijit, S., Moigne, J. L., & El-Ghazawi, T. (2003). Automatic reduction of hyperspectral imagery using wavelet spectral analysis. *IEEE Transactions on Geoscience and Remote Sensing, 41*, 863-871.

Kalácska, M., Sánchez-Azofeifa, G. A., Rivard, B., Caelli, T., White, H. P., & Calvo-Alvarado, J. C. (2007). Ecological fingerprinting of ecosystem succession: Estimating secondary tropical dry forest structure and diversity using imaging spectroscopy. *Remote Sensing of Environment, 108*, 82-96.

Kokaly, R. F., & Clark, R. N. (1999). Spectroscopic determination of leaf biochemistry using band-depth analysis of absorption features and stepwise multiple linear regression. *Remote Sensing of Environment, 67*, 267-287.

le Maire, G., François, C., & Dufrêne, E. (2004). Towards universal broad leaf chlorophyll indices using PROSPECT simulated database and hyperspectral reflectance measurements. *Remote Sensing of Environment, 89*, 1-28.

Lee, K. -S., Kook, M. -J., Shin, J. -I., Kim, S. -H., & Kim, T. -G. (2007). Spectral characteristics of forest vegetation in moderate drought condition observed by laboratory measurements and spaceborne hyperspectral data. *Photogrammetric Engineering and Remote Sensing, 73*, 1121-1127.

Maki, M., Ishiahra, M., & Tamura, M.. (2004). Estimation of leaf water status to monitor the risk of forest fires by using remotely sensed data. *Remote Sensing of Environment, 90*, 441-450.

Peñuelas, J., Filella, I., Biel, C., Serrano, L., & Save, R. (1993). The reflectance at the 950-970 nm region as an indicator of plant water status. *International Journal of Remote Sensing, 14*, 1887-1905.

Peñuelas, J., Piñol, J., Ogaya, R., & Filella, I. (1997). Estimation of plant water concentration by the reflectance water index WI (R900/R970). *International Journal of Remote Sensing, 18*, 2869-2875.

Peterson, D. L., Aber, J. D., Matson, P. A., Card, D. H., Swanberg, N., Wessman, C., Spanner, M. (1988). Remote sensing of forest canopy and leaf biochemical contents. *Remote Sensing of Environment, 24*, 85-108.

Pu, R., Foschi, L., & Gong, P. (2004). Spectral feature analysis for assessment of water status and health level in coast live oak (*Quercus agrifolia*) leaves. *International Journal of Remote Sensing, 25*, 4267-4286.

Pu, R., & Gong, P. (2004). Wavelet transform applied to EO-1 hyperspectral data for forest LAI and crown closure mapping. *Remote Sensing of Environment, 91*, 212-224.

Riaño, D., Vaughan, P., Chuvieco, E., Zarco-Tejada, P. J., & Ustin, S. L. (2005). Estimation of fuel moisture content by inversion of radiative transfer models to simulate equivalent water thickness and dry matter content: Analysis at leaf and canopy level. *IEEE Transactions on Geoscience and Remote Sensing, 43*, 819-826.

Sánchez-Azofeifa, G. A., Castro, K., Wright, S. J., Gamon, J., Kalacska, M., Rivard, B., Schnitzer, S. A. & Feng, J. L. (2009). Differences in leaf traits, leaf internal structure, and spectral reflectance between two communities of

lianas and trees: Implications for remote sensing in tropical environments. *Remote Sensing of Environment, 113*, 2076-2088.

Smith, M. L., Ollinger, S. V., Martin, M. E., Aber, J. D., Hallett, R. A., & Goodale, C. L. (2002). Direct estimation of aboveground forest productivity through hyperspectral remote sensing of canopy nitrogen. *Ecological Applications, 12*, 1286-1302.

Stimson, H. C., Breshears, D. D., Ustin, S. L., & Kefauver, S. C. (2005). Spectral sensing of foliar water conditions in two co-occurring conifer species: *Pinus edulis* and *Juniperus monosperma*. *Remote Sensing of Environment, 96*, 108-118.

Torrence, C., & Compo, G. P. (1998). A practical guide to wavelet analysis. *Bulletin of the American Meteorological Society, 79*, 61-78.

Tucker, C. J. (1980). Remote sensing of leaf water content in the near infrared. *Remote Sensing of Environment, 10*, 23-32.

Yebra, M., & Chuvieco, E. (2009). Linking ecological information and radiative transfer models to estimate fuel moisture content in the Mediterranean region of Spain: Solving the ill-posed inverse problem. *Remote Sensing of Environment, 113*, 2403-2411.

Yebra, M., Chuvieco, E., & Riaño, D. (2008). Estimation of live fuel moisture content from MODIS images for fire risk assessment. *Agricultural and Forest Meteorology, 148*, 523-536.

Zarco-Tejada, P. J., Rueda, C. A., & Ustin, S. L. (2003). Water content estimation in vegetation with MODIS reflectance data and model inversion methods. *Remote Sensing of Environment, 85*, 109-124.

Zhang, J., Rivard, B., Sánchez-Azofeifa, A., & Castro-Esau, K. (2006). Intra- and inter-class spectral variability of tropical tree species at La Selva, Costa Rica: Implications for species identification using HYDICE imagery. *Remote Sensing of Environment, 105*, 129-141.

Table 4-1. Ranges of input variables used for the PROSPECT simulations in Experiment *II*

Input parameter	Unit	Range
Chlorophyll	$\mu g/cm^2$	33
Equivalent water content (EWT)	cm or g/cm^2	0.0037-0.0255
Dry matter content (DMC)	g/cm^2	0.0041-0.0189
Structural parameter *N*	-	1.1-2.9

Table 4-2. List of wavelet features ranked by R^2 using the calibration set and relating wavelet power to measured leaf water content

Feature	Wavelength (nm)	Scale	R^2	Attributed to
A	1740	4	0.989	Cellulose, lignin @ 1730 nm
B	1780	3	0.987	Cellulose, sugar @ 1780 nm
C	1800	4	0.984	Not attributable
D	1802	3	0.982	Not attributable
E	2180	3	0.976	Protein, nitrogen @ 2180 nm
F	1337	7	0.975	Water @ 1400 nm

Note: Wavelet features were associated with broad absorptions tabled in Curran (1989) and Kokaly & Clark (1999).

Table 4-3. Accuracies for the estimation of LWC_F in the validation set using spectral indices, individual wavelet features or a combination of wavelet features derived from the simulated spectra.

Feature code	Feature location		Accuracy	
	Wavelength (nm)	Scale	R^2	RMSE (%)
A	1740	4	0.988	1.58
B	1780	3	0.982	1.94
C	1800	4	0.982	1.96
D	1802	3	0.982	1.95
E	2180	3	0.978	2.18
F	1337	7	0.974	2.37
G	Combo = *A, B, C, D, E, F*	High & Low	0.990	1.46
H	Combo = *A, B, C, D, E*	Low	0.990	1.46
I	Combo = *F*	High	0.974	2.37
J	MSI		0.308	12.1
K	NDWI		0.495	10.3
L	WI		0.599	9.23

Table 4-4. Accuracies for the estimation of LWC_F in the validation set using individual wavelet features derived from the measured spectra.

Feature code	Feature location		Accuracy	
	Wavelength (nm)	Scale	R^2	RMSE (%)
A	2165	4	0.68	4.86
B	1344	7	0.62	5.28
C	1870	6	0.64	5.20
D	1736	4	0.50	6.07
E	2378	4	0.47	6.27
F	2029	3	0.50	6.09
G	1576	3	0.51	6.02
H	2226	3	0.51	6.05

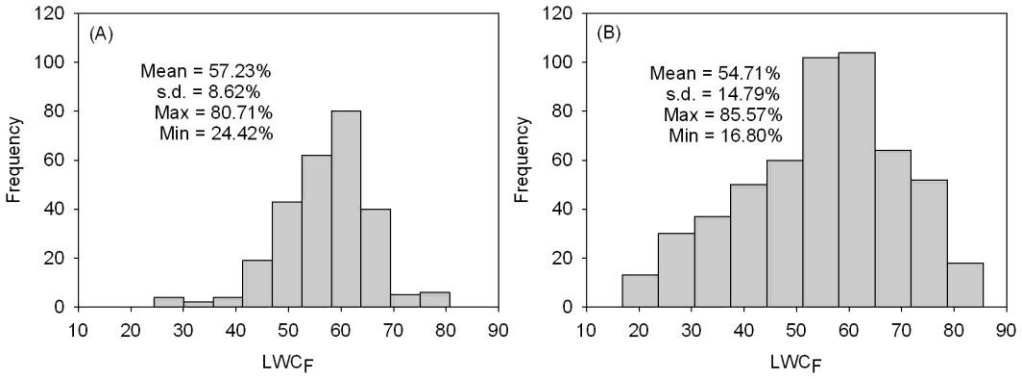

Fig. 4-1. Histograms of leaf water content by fresh weight (LWC_F) derived from (A) the laboratory measurements on each leaf and (B) values of C_w and C_m for the PROSPECT simulations.

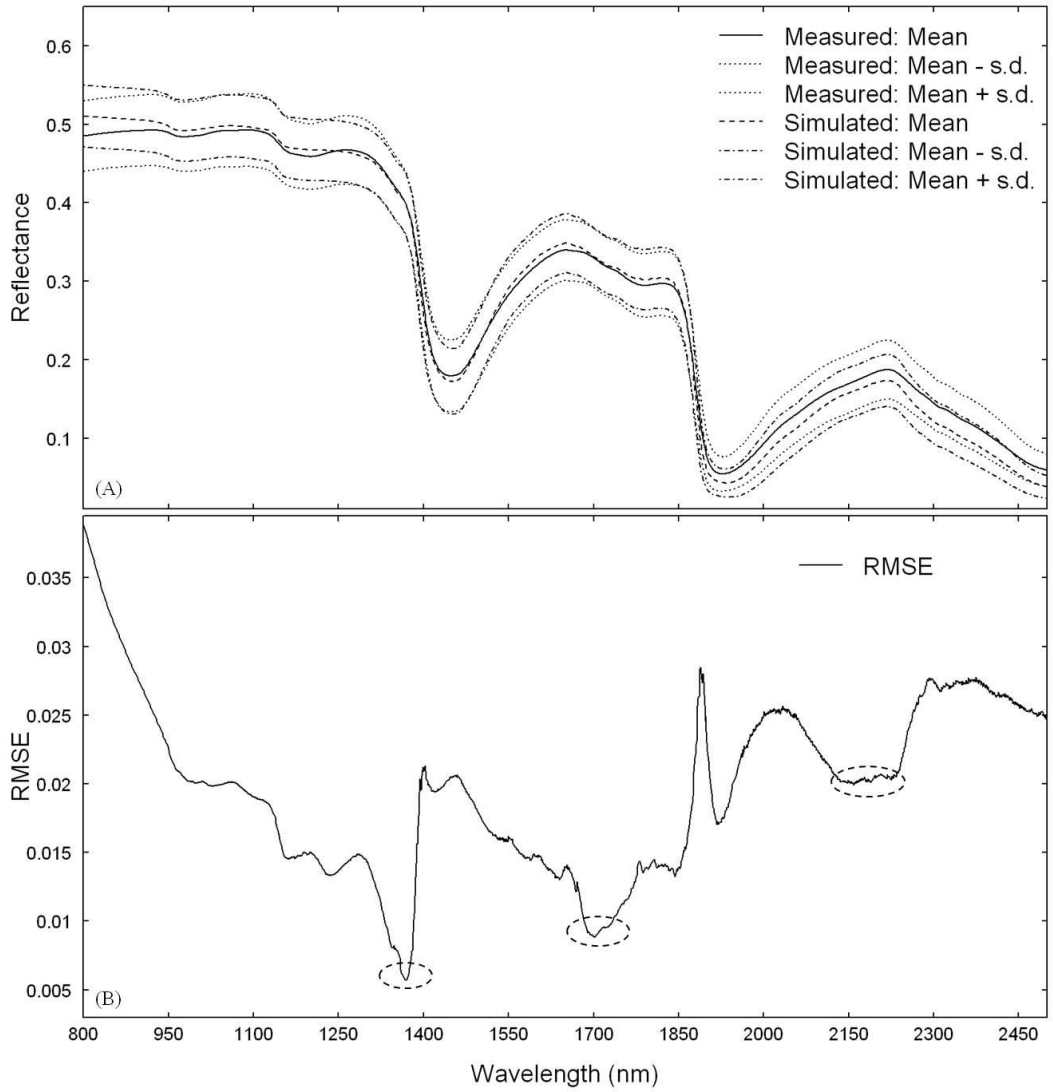

Fig. 4-2. (A) Plot of mean and mean ± s.d. of reflectance spectra for the measured leaf reflectance dataset and the PROSPECT simulated dataset. (B) The root mean square error (RMSE) per wavelength as described in Eq. (4-1). The dashed circles highlight spectral regions displaying local minimum in RMSE.

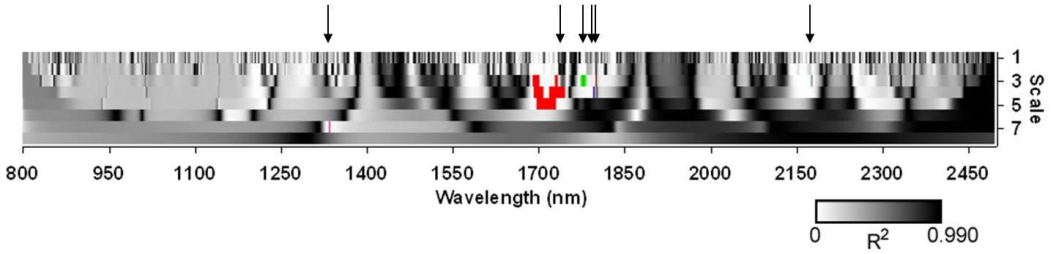

Fig. 4-3. Features regions extracted from the correlation scalogram relating wavelet power and leaf water content (LWC_F). The feature with strongest correlation (1740 nm, 4) originates from the largest feature region. Arrows mark the wavelength position of wavelet features representative of each feature region.

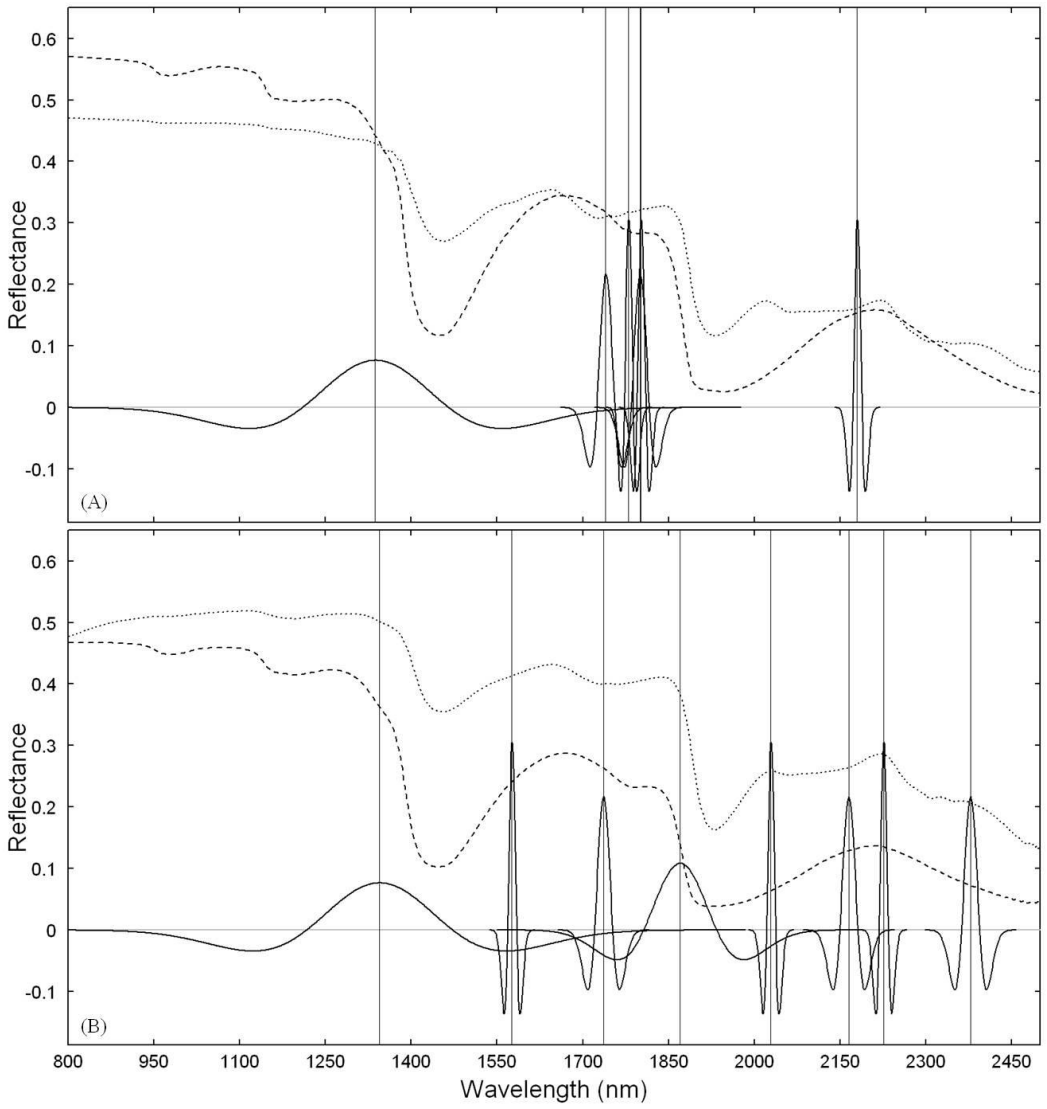

Fig. 4-4. Wavelet features used for the estimation of LWC_F. The wavelength position and scale of those features are indicated by vertical lines and the corresponding wavelets. Also shown are reflectance spectra for highest LWC_F (dashed line) and lowest LWC_F (dotted line). Each wavelet feature is positioned on the spectra with the scaled and shifted continuous wavelet used to compute its wavelet power. (A) Wavelet features derived from the PROSPECT simulated reflectance spectra. (B) Wavelet features derived from the measured reflectance spectra.

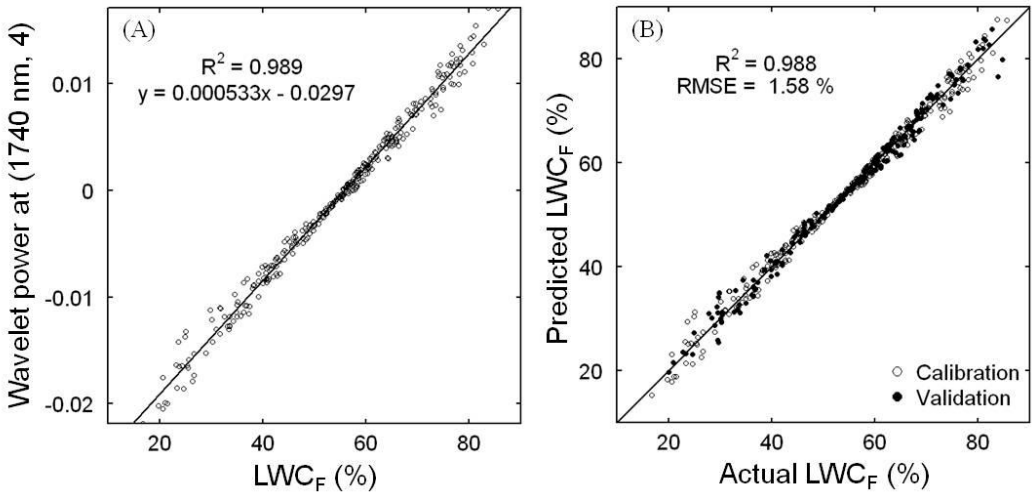

Fig. 4-5. (A) Correlation between the best performing wavelet feature (1740 nm, 4) and leaf water content (LWC_F) for the calibration set. (B) Estimates of LWC_F derived from the regression model in (A).

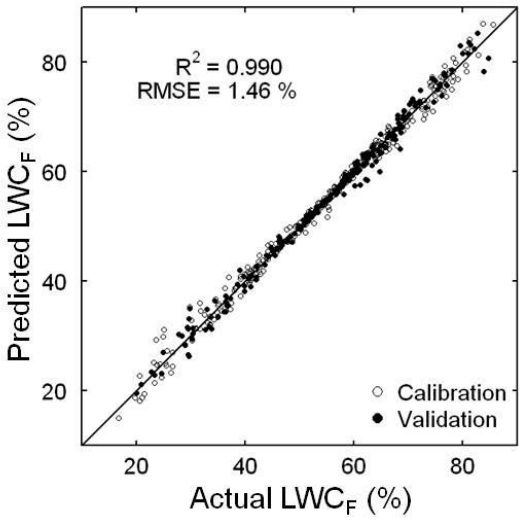

Fig. 4-6. Plot of actual versus predicted LWC_F derived using a combination of the six wavelet features for the simulated spectra.

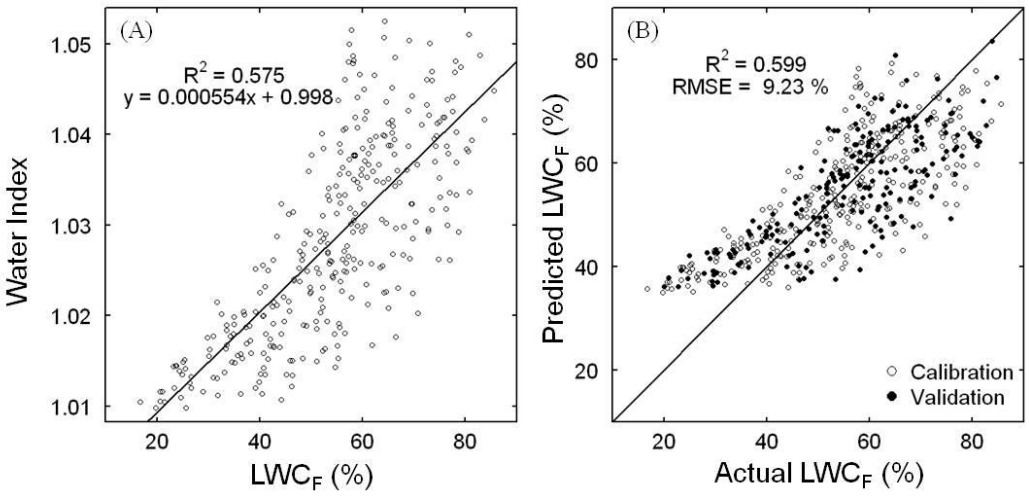

Fig. 4-7. (A) Relationship between the water index (WI) and leaf water content (LWC_F) for the calibration set. (B) Estimates of LWC_F derived with the regression model in (A).

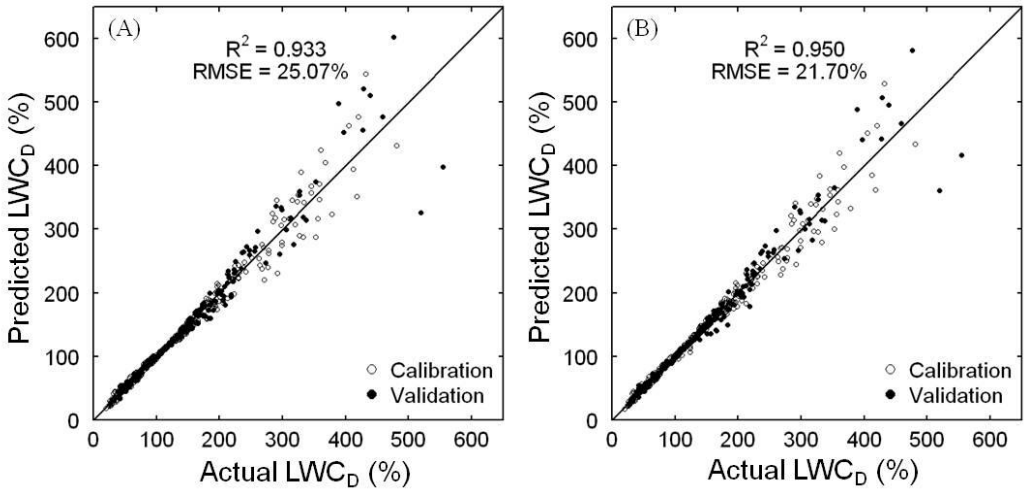

Fig. 4-8. Actual LWC_D plotted against predicted LWC_D inverted from LWC_F estimates. The LWC_F were obtained from wavelet feature (1740 nm, 4) for (A) and from the combination of all features for (B).

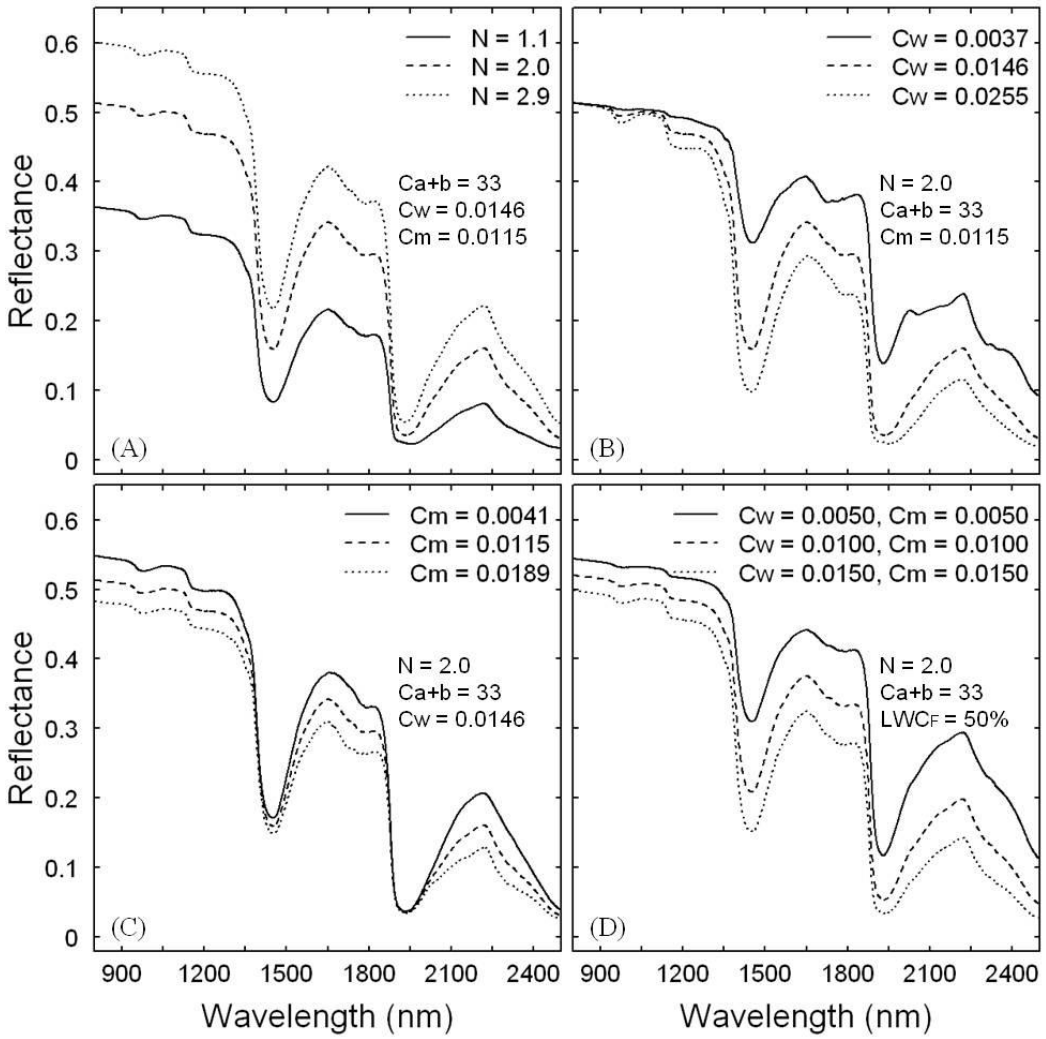

Fig. 4-9. Effects of leaf properties on the reflectance simulated by the PROSPECT model: (A) leaf structure, (B) equivalent water thickness, and (C) dry matter content. Also shown in (D) is the coupled effect of equivalent water thickness and dry matter content.

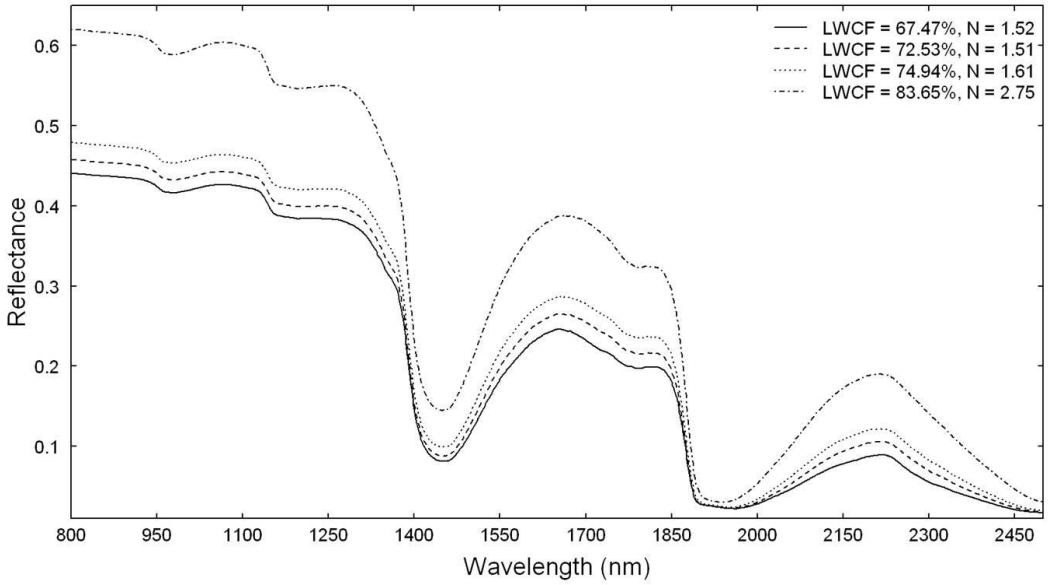

Fig. 4-10. Example PROSPECT-simulated reflectance spectra with randomly generated combinations of LWC_F and *N*. Note that reflectance spectra simulated with higher LWC_F values should display lower reflectance in the infrared region but do not as a result of unrealistic combinations of input variables.

CHAPTER 5 - CONCLUSIONS

5.1. Summary

This research has focused on the development of methodologies to extract useful spectral information from leaf reflectance spectra using continuous wavelet analysis (CWA). One methodology has been used for detecting the effect of mountain pine beetle infestation at the early stage on lodgepole pine trees, and the other for deriving robust predictors of leaf water content from measured and simulated reflectance spectra. As presented in the preceding chapters, CWA provides a novel approach to optimize the selection of wavelet features as a function of wavelength and scale.

Three research issues were addressed in this thesis. The first issue dealt with the development of an effective method to detect the green attack stage on lodegepine trees affected by mountain pine beetles. Through the use of CWA, a small number of wavelet features were determined to distinguish healthy trees from infested trees at the green attack stage. Water was found to be a physiological indicator of the beetle infestation at the early stage, therefore the second issue focused on the development of a methodology to determine the universal spectral information that relates to the leaf gravimetric water content (GWC) for a variety of forest species. In an effort to derive accurate estimates of leaf GWC, eight meaningful wavelet features were extracted to account for the spectral variations linked to changes in leaf GWC. To further determine the robust wavelet features pertinent to leaf water, the third issue addressed a simulation study to test the newly developed methodology for the estimation of leaf GWC from the reflectance spectra simulated by the radiative transfer model PROSPECT.

5.2. Synthesis of contributions

In the context of vegetation studies, previous research involved with wavelet analysis of hyperspectral data has focused on the exploration of discrete wavelet transform (DWT) as a means to reduce the dimensionality of

hyperspectral signatures (Bruce et al., 2001; Koger et al., 2003; Pu & Gong, 2004). I chose continuous wavelet transform (CWT) instead of DWT to decompose the leaf reflectance spectra because it is easier to interpret the outputs of CWT and to compare them with the input spectra (Blackburn & Ferwerda, 2008; Rivard et al., 2008). To date, there are very few studies that apply CWA to hyperspectral signatures of vegetation (Blackburn & Ferwerda, 2008; Ferwerda & Jones, 2006). This is likely due to the research gap in the development of effective feature extraction/selection techniques that serve to derive a small number of useful features from a large volume of CWT outputs. A methodological highlight of this work lies in the development of a new way to select in the wavelet domain the most significant features for detecting the green attack damage and for predicting leaf GWC.

Chapter 2 reports the most promising findings to date on the remote detection of green attack damage due to mountain pine beetle infestation. The two relevant studies (Ahern, 1988; Runesson, 1991) focused on the examination of spectral variations in the visible and near infrared regions (350-1100 nm) and thus precluded the potential contribution of spectral signatures from water. However, the reflectance measurements from 350 to 2500 nm are readily available now with the advancement of the state of the art of reflectance spectrometry. The primary findings of this study are: 1) The infested trees at the green attack stage suffer from water deficit. This study presents the first explicit examination of tree-level water availability related to mountain pine beetle green attack damage, although White et al. (2007) indicated the water deficiency at the stand level as a consequence of beetle attack at a later stage (red attack). The finding increases our understanding of the physiological mechanism of the pre-visual stress from mountain pine beetle attack. 2) The water deficit occurring in infested trees could be detected with hyperspectral reflectance measurements of pine needles. Despite the reported challenge in detecting green attack damage via remote sensing (Wulder et al., 2006), the use of CWA allows us to capture the spectral response to the water deficit triggered by the beetle attack on pine trees. It is shown that the spectral detection of green attack damage should focus on spectral regions where

the variation in reflectance is strongly associated with changes in foliage water. In recognition of the importance of water content as an indicator of green attack damage, the following two chapters focus on examining the spectral contributions of water and strive to achieve accurate estimates of leaf GWC.

Chapter 3, unlike previous investigations conducted on a limited number of species or a narrow range of water content levels, is based on a data set encompassing 47 species from two tropical forest environments (dry forest and rainforest) in Panama. CWA was shown to be effective to capture the spectral variations in response to changes in GWC despite the diverse composition of species. The most interesting finding of this chapter stems from the outcome of the selection of optimal wavelet features through the use of CWA. Two groups of features were determined at various scales to be sensitive to changes in leaf GWC. The first group, found at high scales, captures the amplitude variation across a broad spectral range that is primarily attributed to changes in the amount of leaf water. The second group, found at low scales, captures the variations in the shape and depth of absorption features by dry matter that comprises the dry mass of leaves such as protein, lignin, and cellulose. Although GWC is dependent on the absolute amount of leaf water and the dry matter content (Danson & Bowyer, 2004), the results suggest that spectral information pertinent to both leaf water and dry matter is useful for the spectroscopic estimation of leaf GWC. In addition, it adds a new dimension to the understanding of the spectral variations induced by changes in leaf GWC. This study is the first to use a species-rich data set collected from the Mesoamerican tropical ecosystem to address the estimation of leaf chemistry. The most similar published study was conducted by Asner & Martin (2008) who used a Partial Least Squares (PLS) method to investigate the estimation of leaf chemistry for 162 Australian tropical forest species. Compared with CWA, PLS requires more effort to calibrate models and does not provide determinant information to interpret the relative importance of wavelengths involved in the regression equations (Martin et al., 2008; Smith et al., 2002; Smith et al., 2003). The methodology developed in this chapter to estimate leaf chemistry would be beneficial to ecologists, in particular those who are involved

with spectral and chemical analysis of tropical forests because it is less affected by variations in species composition.

Chapter 4 employs a simulated spectral database to provide an evaluation of the methodology developed in Chapter 3 to determine effective predictors of leaf GWC. The PROSPECT radiative transfer model is able to accurately represent the measured reflectance in the 800-2500 nm range, with RMSE's less than 0.03. Three of the six wavelet features derived from the simulated spectra are in accordance with those derived from the measured spectra. The predictive capability of these consistent wavelet features demonstrates that more spectral information associated with leaf GWC could be extracted from the absorption features of dry matter than from those of water. It is the decline in the strength of water absorptions that makes the dry matter absorption more detectable in leaf reflectance spectra (Kokaly & Clark; Tian et al., 2001). The wavelet-based methodology, developed using measured spectra and tested using simulated spectra, proves to be effective in predicting leaf GWC from reflectance spectra even in the presence of a diverse set of tree species.

5.3. Avenues of future research

This thesis has investigated the detection of beetle attack stress and the quantification of leaf water content using spectroscopic measurements at the leaf level. Future research seeks to extend these studies to canopy level using airborne or spaceborne hyperspectral imagery. Further research should either apply the leaf-level wavelet features to hyperspectral imagery or revisit the problem using canopy-level data. The methodologies presented in the thesis would first have to be adapted to process imagery negatively impacted by atmospheric absorption. For the spectral detection of green attack damage, a narrow feature region (1318-1322 nm) was located on the edge of a strong atmospheric absorption region and may still be of use dependent on the quality of the atmospheric correction for hyperspectral imagery. High-frequency noise in imagery data is not a concern since it could be readily removed with low-scale wavelets. As to the estimation of

water content in vegetation canopies, there are also possibilities for implementation on airborne data because multiple wavelet features have been determined from across the shortwave infrared region (1300-2500 nm). However, a question that arises is whether spectral properties at the leaf level could be transferred to the canopy level due to the confounding effect of canopy architecture and background materials within (Ahern, 1988; Daughtry et al., 2000; Sánchez-Azofeifa & Castro-Esau, 2006). Fortunately, the reflectance signals from water could be enhanced at the canopy level due to the more intensive multiple scattering process within canopies (Asner, 1998; Sims & Gamon, 2003) and background materials such as soil typically have little high frequency spectral information.

Research opportunities also exist to apply the developed methodologies to other data sets collected under different scenarios. The approach to detect green attack damage could be evaluated using samples collected from other areas that are also affected by the current outbreak of mountain pine beetle (e.g., British Columbia). As to the estimation of leaf water content, the wavelet features consistently derived in Chapter 3 and Chapter 4 are particularly useful for ecosystems with considerable diversity in species composition, such as tropical forests in Australia (Asner & Martin, 2008) and in Americas (Castro-Esau et al., 2006; Sánchez-Azofeifa et al., 2009). Experience gained utilizing other data sets will help to improve the procedure of feature selection on the correlation scalogram. The number of features selected was dependent on the percentage threshold that was set to an empirical value of 1% for all analyses. Further exploration of the relationship between the threshold and the size and spatial pattern of feature regions might suggest a better strategy to determine the threshold. The distribution of a feature region as a function of wavelength and scale also has implications for potential detection of representative features as constrained by the resolution of airborne and spaceborne sensors. The pattern of feature regions is also useful for refining feature selection in the future. As a result of the feature selection procedure, the feature set may also be useful for refining feature selection in the future.

While constructing correlation scalograms, linear models were used to fit the relationships between wavelet power and all dependent variables and these models worked well as shown in Chapter 2. It was not appropriate to apply linear fitting to LWC_D in Chapter 3 but non-linear fitting could be avoided by converting linearly modeled LWC_F to LWC_D. As this conversion is not generally applicable, future work should investigate non-linear models such as polynomial functions for the wavelet-based methodology to fit the relationship between wavelet power and other leaf chemical constituents.

Although the wavelet features derived for the estimation of leaf GWC were insensitive to species, the question of how to explicitly suppress the effect of leaf structural variability on spectral reflectance using CWA remains. The variation in leaf structural characteristics represented by the wide range of species in the tropical data set could be quantified by a number of structural parameters (Castro-Esau et al., 2006; Sánchez-Azofeifa et al., 2009). Future research could focus on how to relate structural properties to spectral features in the wavelet domain and then reducing the influences of those wavelet features on spectral estimation of leaf water content. In addition, it is worth investigating whether it is feasible to separate the spectral variability caused by structural properties and chemical properties by means of multiscale representation of CWA. This is important for hyperspectral applications where the effect of leaf structural variability on spectral reflectance is to be minimized (Danson et al., 1992; Sims & Gamon, 2002).

Other than foliar water, the methodology developed using the tropical leaf data set could also be applied to quantify other chemical constituents such as chlorophyll, nitrogen, lignin, and cellulose to better understand their roles in ecosystem processes and biogeochemical cycles (Kokaly et al., 2009; Schimel, 1995; Wessman et al., 1998). In fact, the correlation scalogram includes a whole set of features characterized by wavelength and scale in the wavelet domain. Here I used a tropical data set to label the features sensitive to leaf water content. The next step could be to identify and label the features sensitive to all other leaf

chemical constituents used in the literature. This scalogram with labeling of wavelet features has the potential to provide improved estimation of leaf chemistry and valuable knowledge about the control of individual constituents on leaf spectral properties.

5.4. References

Ahern, F. J. (1988). The effects of bark beetle stress on the foliar spectral reflectance of lodgepole pine. *International Journal of Remote Sensing, 9,* 1451-1468.

Asner, G. P., & Martin, R. E. (2008). Spectral and chemical analysis of tropical forests: Scaling from leaf to canopy levels. *Remote Sensing of Environment, 112,* 3958-3970.

Blackburn, G. A., & Ferwerda, J. G. (2008). Retrieval of chlorophyll concentration from leaf reflectance spectra using wavelet analysis. *Remote Sensing of Environment, 112,* 1614-1632.

Bruce, L. M., Morgan, C., & Larsen, S. (2001). Automated detection of subpixel hyperspectral targets with continuous and discrete wavelet transforms. *IEEE Transactions on Geoscience and Remote Sensing, 39,* 2217-2226.

Castro-Esau, K. L., Sánchez-Azofeifa, G. A., Rivard, B., Wright, S. J., & Quesada, M. (2006). Variability in leaf optical properties of mesoamerican trees and the potential for species classification. *American Journal of Botany, 93,* 517-530.

Danson, F. M., & Bowyer, P. (2004). Estimating live fuel moisture content from remotely sensed reflectance. *Remote Sensing of Environment, 92,* 309-321.

Daughtry, C. S. T., Walthall, C. L., Kim, M. S., De Colstoun, E. B., & McMurtrey III, J. E. (2000). Estimating corn leaf chlorophyll concentration from leaf and canopy reflectance. *Remote Sensing of Environment, 74,* 229-239.

Ferwerda, J. G., & Jones, S. (2006). Continuous wavelet transformations for hyperspectral feature detection. *Proceedings of the 12th International Symposium on Spatial Data Handling,* 12-14 July, University of Vienna, Austria.

Koger, C. H., Bruce, L. M., Shaw, D. R., & Reddy, K. N. (2003). Wavelet analysis of hyperspectral reflectance data for detecting pitted morningglory (*Ipomoea lacunosa*) in soybean (*Glycine max*). *Remote Sensing of Environment, 86,* 108-119.

Kokaly, R. F., Asner, G. P., Ollinger, S. V., Martin, M. E., & Wessman, C. A. (2009). Characterizing canopy biochemistry from imaging spectroscopy and its application to ecosystem studies. *Remote Sensing of Environment, 113,* S78-S91.

Kokaly, R. F., & Clark, R. N. (1999). Spectroscopic determination of leaf biochemistry using band-depth analysis of absorption features and stepwise multiple linear regression. *Remote Sensing of Environment, 67,* 267-287.

Martin, M. E., Plourde, L. C., Ollinger, S. V., Smith, M. -L., & McNeil, B. E. (2008). A generalizable method for remote sensing of canopy nitrogen across a wide range of forest ecosystems. *Remote Sensing of Environment, 112*, 3511-3519.

Pu, R., & Gong, P. (2004). Wavelet transform applied to EO-1 hyperspectral data for forest LAI and crown closure mapping. *Remote Sensing of Environment, 91*, 212-224.

Rivard, B., Feng, J., Gallie, A., & Sánchez-Azofeifa, A. (2008). Continuous wavelets for the improved use of spectral libraries and hyperspectral data. *Remote Sensing of Environment, 112*, 2850-2862.

Runesson, U. T. (1991). *Considerations for early remote detection of mountain pine beetle in green-foliaged lodgepole pine.* PhD Dissertation. University of British Columbia, Canada.

Sánchez-Azofeifa, G. A., & Castro-Esau, K. (2006). Canopy observations on the hyperspectral properties of a community of tropical dry forest lianas and their host trees. *International Journal of Remote Sensing, 27*, 2101-2109.

Sánchez-Azofeifa, G. A., Castro, K., Wright, S. J., Gamon, J., Kalacska, M., Rivard, B., Schnitzer, S. A. & Feng, J. L. (2009). Differences in leaf traits, leaf internal structure, and spectral reflectance between two communities of lianas and trees: Implications for remote sensing in tropical environments. *Remote Sensing of Environment, 113*, 2076-2088.

Schimel, D. S. (1995). Terrestrial biogeochemical cycles: Global estimates with remote sensing. *Remote Sensing of Environment, 51*, 49-56.

Sims, D. A., & Gamon, J. A. (2002). Relationships between leaf pigment content and spectral reflectance across a wide range of species, leaf structures and developmental stages. *Remote Sensing of Environment, 81*, 337-354.

Sims, D. A., & Gamon, J. A. (2003). Estimation of vegetation water content and photosynthetic tissue area from spectral reflectance: A comparison of indices based on liquid water and chlorophyll absorption features. *Remote Sensing of Environment, 84*, 526-537.

Smith, M. -L., Martin, M. E., Plourde, L., & Ollinger, S. V. (2003). Analysis of hyperspectral data for estimation of temperate forest canopy nitrogen concentration: Comparison between an airborne (AVIRIS) and a spaceborne (Hyperion) sensor. *IEEE Transactions on Geoscience and Remote Sensing, 41*, 1332-1337.

Smith, M. -L., Ollinger, S. V., Martin, M. E., Aber, J. D., Hallett, R. A., & Goodale, C. L. (2002). Direct estimation of aboveground forest productivity through hyperspectral remote sensing of canopy nitrogen. *Ecological Applications, 12*, 1286-1302.

Tian, Q., Tong, Q., Pu, R., Guo, X., & Zhao, C. (2001). Spectroscopic determination of wheat water status using 1650-1850 nm spectral absorption features. *International Journal of Remote Sensing, 22*, 2329-2338.

Wessman, C. A., Aber, J. D., Peterson, D. L., & Melillo, J. M. (1988). Remote sensing of canopy chemistry and nitrogen cycling in temperate forest ecosystems. *Nature, 335*, 154-156.

White, J. C., Coops, N. C., Hilker, T., Wulder, M. A., & Carroll, A. L. (2007). Detecting mountain pine beetle red attack damage with EO-1 Hyperion moisture indices. *International Journal of Remote Sensing, 28*, 2111-2121.

Wulder, M. A., Dymond, C. C., White, J. C., Leckie, D. G., & Carroll, A. L. (2006). Surveying mountain pine beetle damage of forests: A review of remote sensing opportunities. *Forest Ecology and Management, 221*, 27-41.

APPENDIX

Appendix 1. Continuous wavelet transform of a reflectance spectrum

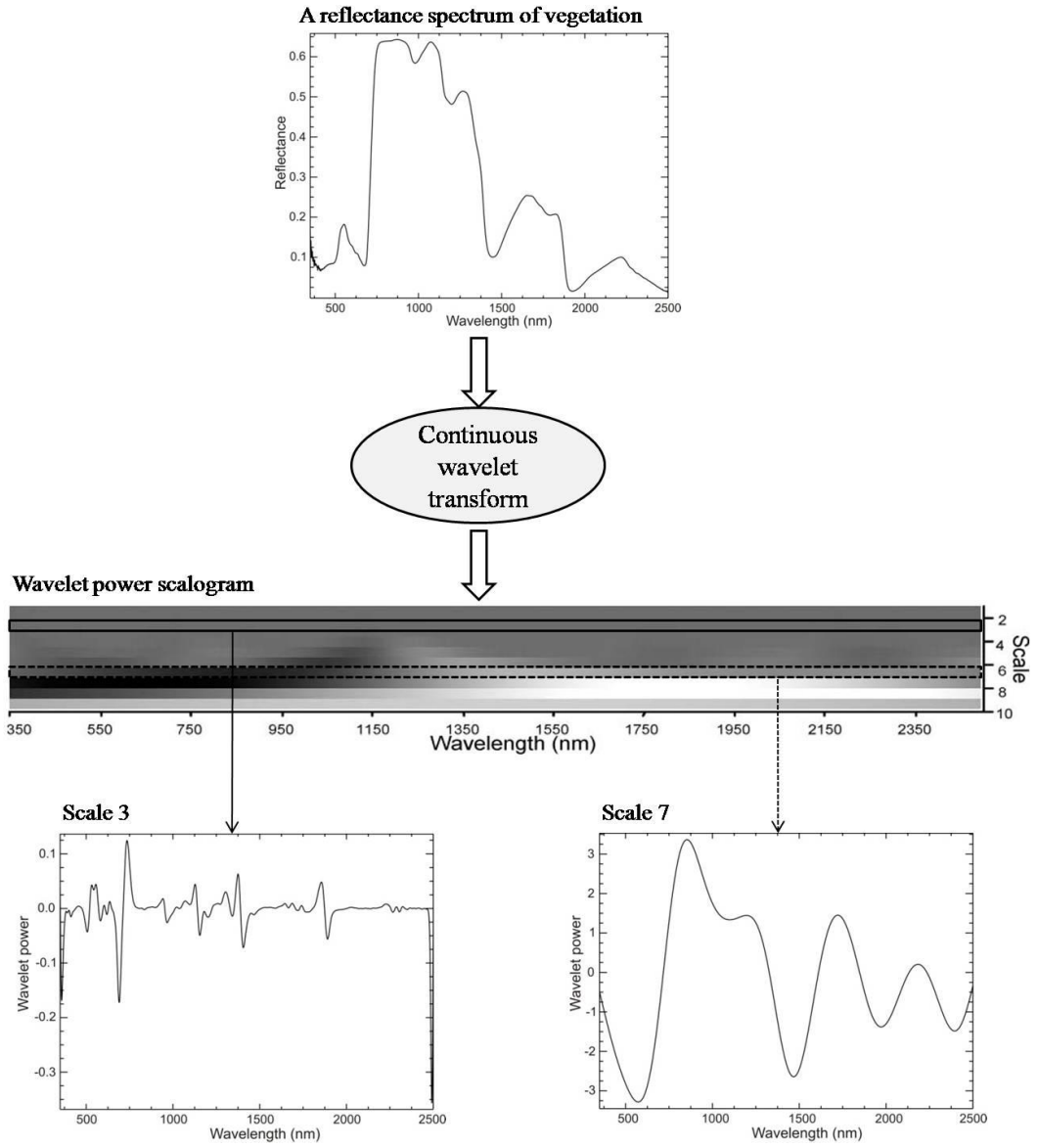

Fig. A-1. Schematic representation of the continuous wavelet transform workflow.

Each reflectance spectrum in data sets used in this thesis is an input to the continuous wavelet transform function implemented in a professional software (IDL). The output for each input is a wavelet power scalogram showing wavelet power (magnitude of a wavelet coefficient) as a function of wavelength and scale.

Two of the ten scale components are extracted from the wavelet power scalogram and displayed at the bottom of Fig. A-1 as a *Scale 3* spectrum and a *Scale 7* spectrum. Both can be compared to the reflectance spectrum. The *Scale 3* spectrum captures various absorption features and the *Scale 7* spectrum captures the overall shape of the reflectance spectrum.

Appendix 2. Workflow of the wavelet-based methodology

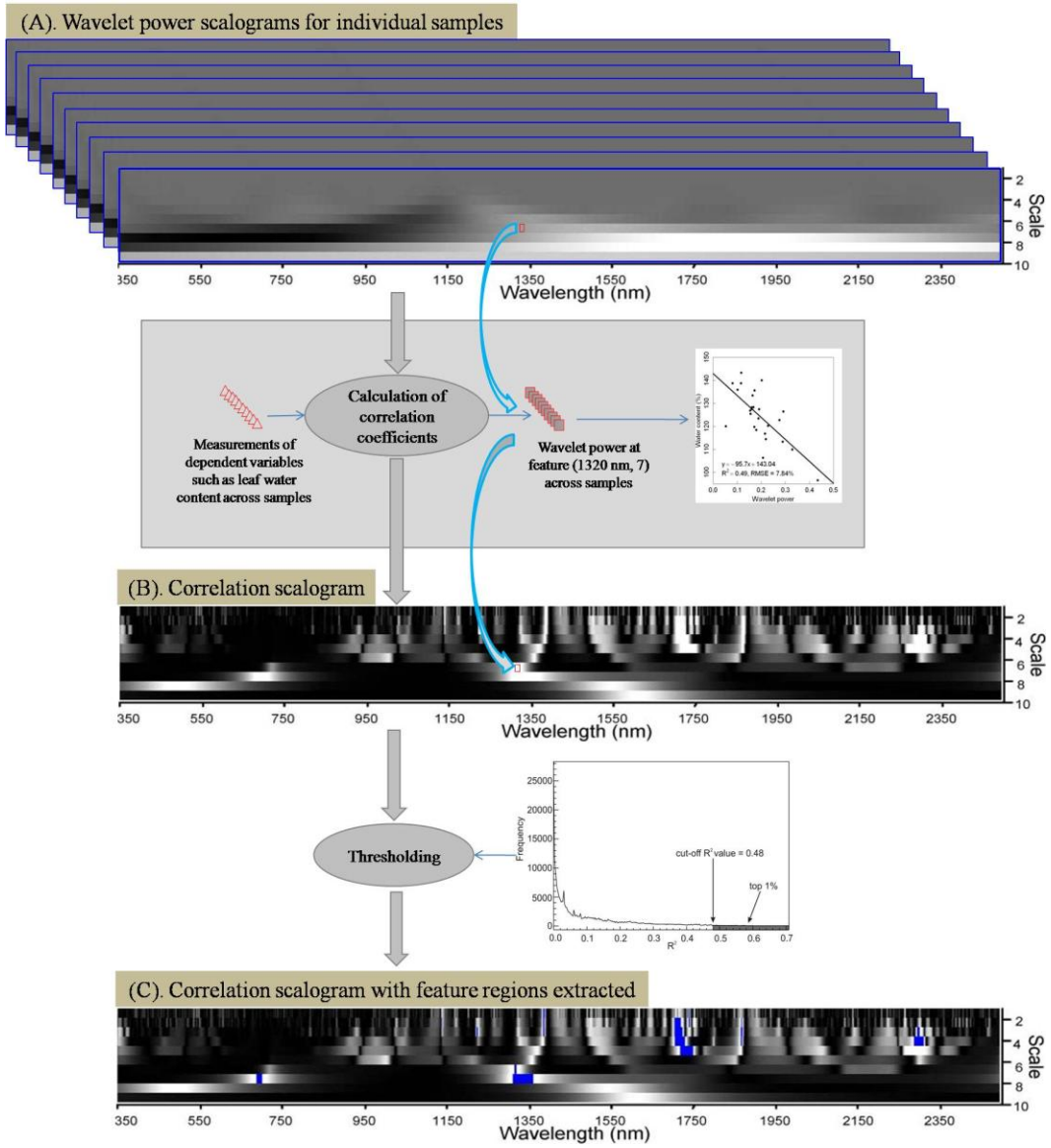

Fig. A-2. Workflow of the wavelet-based methodology.

The general procedures of the wavelet-based methodology developed in this thesis are the same for stress detection and water content estimation:

1. CWT is applied to each reflectance spectrum to calculate the wavelet power as a function of wavelength and scale as displayed in Fig. A-1. Each reflectance spectrum is transformed to a wavelet power

scalogram and the outcome of this step is a series of wavelet power scalograms for the samples in a data set (Fig. A-2A).

2. A correlation scalogram (Fig. A-2B) was constructed by establishing the Pearson's linear correlations between each element of the wavelet power scalograms and a dependent variable (i.e., chlorophyll concentration, water content, or class ID) across all samples. The correlation scalogram reports a squared correlation coefficient (R^2), ranging in magnitude from 0 to 1, at each wavelength and scale. Each element of the correlation scalogram represents a feature that could be selected.
3. The features where R^2 is not statistically significant (p>=0.05) are masked. The remaining features are then sorted in descending order of R^2, and a threshold R^2 value is applied to delineate the top 1% features that most strongly correlate with the dependent variable. These features delineated by the threshold form a number of scattered feature regions on the correlation scalogram (Fig. A-2C).

If the user is satisfied with the feature regions, the methodology terminates here. Otherwise, an additional step is required to select the most representative feature for each feature region because each region may carry redundant spectral information across consecutive wavelengths and scales. This can be done by determining a feature with the maximum R^2 within each region and the feature is expressed as (*wavelength* in nm, *scale*). Under this circumstance, the ultimate output of the wavelet-based methodology is a small number of wavelet features sparsely distributed on the correlation scalogram.